OPTIMAL FAULT-DETECTION FILTER DESIGN FOR STEER-BY-WIRE VEHICLES

A DISSERTATION
SUBMITTED TO THE DEPARTMENT OF ELECTRICAL ENGINEERING
AND THE COMMITTEE ON GRADUATE STUDIES
OF STANFORD UNIVERSITY
IN PARTIAL FULFILLMENT OF THE REQUIREMENTS
FOR THE DEGREE OF
DOCTOR OF PHILOSOPHY

Christopher David Gadda
December 2008

I certify that I have read this dissertation and that, in my opinion, it is fully adequate in scope and quality as a dissertation for the degree of Doctor of Philosophy.

(J. Christian Gerdes) Principal Adviser

I certify that I have read this dissertation and that, in my opinion, it is fully adequate in scope and quality as a dissertation for the degree of Doctor of Philosophy.

(Stephen P. Boyd)

I certify that I have read this dissertation and that, in my opinion, it is fully adequate in scope and quality as a dissertation for the degree of Doctor of Philosophy.

(Sanjay Lall)

Approved for the University Committee on Graduate Studies.

In memory of my grandfather

Abstract

Steer-by-wire technology promises to deliver numerous benets, both to auto manufacturers and end customers, making cars that are safer, more ecient, easier to design and manufacture, and more fun to drive. One of the most compelling aspects of steer-by-wire is the potential to improve the safety of vehicles. While the nominal role of a steering system is to reproduce the driver's steering command at the road wheels, a steer-by-wire system provides the opportunity for a software layer to intervene on behalf of the driver in dangerous driving situations. The simplest example of this is a car that could automatically counter-steer when starting to skid on wet or icy pavement, in order to prevent loss of control of the vehicle. In the case of higher-center of gravity vehicles, such as passenger vans and SUVs, where vehicle rollover becomes a significant safety issue, a steer-by-wire system could prevent the driver from executing a maneuver that would result in rollover.

Despite all of the benefits of steer-by-wire, there are no production vehicles with steer-by-wire on the road today. The potentially catastrophic nature of a steering system failure requires that any replacement for a conventional steering system be extremely reliable. One approach for achieving the necessary level of reliability relies upon a diagnostic system that can quickly and accurately detect and isolate a fault. This information is then used to switch over to a redundant component or a modified control law that can accommodate the fault. This strategy significantly relaxes the reliability requirements of the individual components in the system, without reducing the overall reliability of the system.

The research presented here demonstrates how a model-based diagnostic system can detect a wide range of potential steering system failures without the need for

redundant sensors. In many cases the diagnostic system can detect a steering system fault at a level well below that of driver perception. The performance of this system is demonstrated experimentally on a full-scale steer-by-wire research vehicle, developed here at Stanford.

The task of diagnostic filter design can be posed as an optimization problem, using channel capacity as measure of diagnostic performance. This eliminates the need for hand-tuning and allows design and evaluation of the diagnostic system to precede final construction of the system to be diagnosed. The usefulness of channel capacity as a diagnostic performance metric is experimentally demonstrated, as it can differentiate filter designs that provide good spectral separation of fault information and noise, from those that do not, unlike existing diagnostic performance metrics.

Acknowledgments

When you spend as long as I have in graduate school, you inevitably are the beneficiary of the some of the hard work, friendship, dedication, brilliance, devotion, insight, and patience of those around you. I'd like to take just a moment to acknowledge some of the people who have contributed to my research and to my happiness over the past seven years.

First of all, I would like to thank my advisor, Chris Gerdes for inviting me to join his lab and providing me an opportunity to work on such an exciting project. Chris possesses the rare ability to provide guidance when needed, such as when I try to write something, and a willingness to stay out of the way when you have things under control. You cannot find better academic mentor than my advisor.

I would also like to thank my defense committee members. Jean-Claude Latombe was kind enough to offer his time to chair my committee, despite having never met me before. Dave Beach contributed his time, camera equipment, and videography skills on numerous occasions, in addition to serving on my committee. He also was willing to experiment with the addition of a research project to his Product Realization Laboratory, a collaboration without which this research would not have been possible. I would like to thank Stephen Boyd and Sanjay Lall for taking the time to read this dissertation and for providing useful feedback on my research.

I would like to acknowledge Nissan Motor Corporation for sponsoring research in diagnostic systems for steer-by-wire vehicles, with special thanks to Toshimi Abo, Kazutaka Adachi, Takeshi Mitamura, Dr. Kimio Kanai, Tomoko Inoue, and Masaharu Asano for their support of this project.

The design and construction of P1 took many hands: Chris Gerdes, Craig Milroy,

Scott Kohn, Will Krump, Shad Laws, Dave Baggeror, Carrie Bobier, Craig Beal, Rami Hindiyeh, RK MacLean and Judy Hsu. I hope I have not forgotten anyone. I would like to thank Shad and Carrie in particular for their work understanding and redesigning the suspension. Also instrumental in the development of P1 was Denise Curti, who helped me navigate the intricacies of procurement on numerous occasions, not to mention helping straighten out some aspect of my funding pretty much every quarter I was in the lab.

One of the most important sources of support during my time at Stanford has been from my friends and family, whom I will not attempt to enumerate, lest I inadvertently omit someone important to me. I have been fortunate enough to have a group of friends who are kind and supportive and fun-loving and adventurous. My parents have been extremely supportive of my education over the years, encouraging me while I lived at home and funding my undoubtedly expensive undergraduate education. My father demonstrated either the utmost respect for advance degrees or great restraint when learning I was going to quit my paying job and return school after only three years of gainful employment. It is wonderful to have parents who were willing to fly out just to see my defense, even though I warned them that it would be dull.

I would especially like to thank my E205 TA, in part for her excellent review sessions, but also for introducing me to sailing in the San Francisco Bay, taking me on numerous backpacking trips, learning not just to ski but to actually enjoying skiing despite her hatred of the cold, and for eventually agreeing to marry me. Teresa has been unconditionally supportive of my efforts to get a Ph.D. She is my best friend, and without her encouragement I don't know if I would have found the determination to finish what I started.

Lastly, I would like to thank my daughter, Geneva Christine, the cutest little baby girl I have ever laid eyes on, for letting me get a good night's sleep before my defense (mostly).

Contents

List of Tables

List of Figures

Chapter 1

Introduction

1.1 Steer-by-wire

Steer-by-wire technology promises to deliver numerous benefits, both to auto manufacturers and end customers, making cars that are safer, more efficient, easier to design and manufacture, and more fun to drive [58][54][8]. In a vehicle with a steer-by-wire system, there is no longer a mechanical linkage between the steering wheel and wheels on the road. Rather, a sensor on the steering wheel generates a signal, which is fed to a steering controller, which controls an electric motor that turns the road wheels to steer the vehicle. An additional electric motor is attached the steering wheel, in order to reproduce the forces that a driver would feel in a car with a conventional steering system.

One of the most compelling aspects of steer-by-wire is the potential to improve the safety of vehicles. While the nominal role of a steering system is to reproduce the driver's steering command at the road wheels, a steer-by-wire system provides the opportunity for a software layer to intervene on behalf of the driver in dangerous driving situations. The simplest example of this would be a car that can automatically counter-steer when starting to skid on wet or icy pavement, in order to prevent loss of control of the vehicle. In the case of higher-center of gravity vehicles, such as passenger vans and SUVs, where vehicle rollover becomes a significant safety issue, a steer-by-wire system could prevent the driver from executing a maneuver that would result

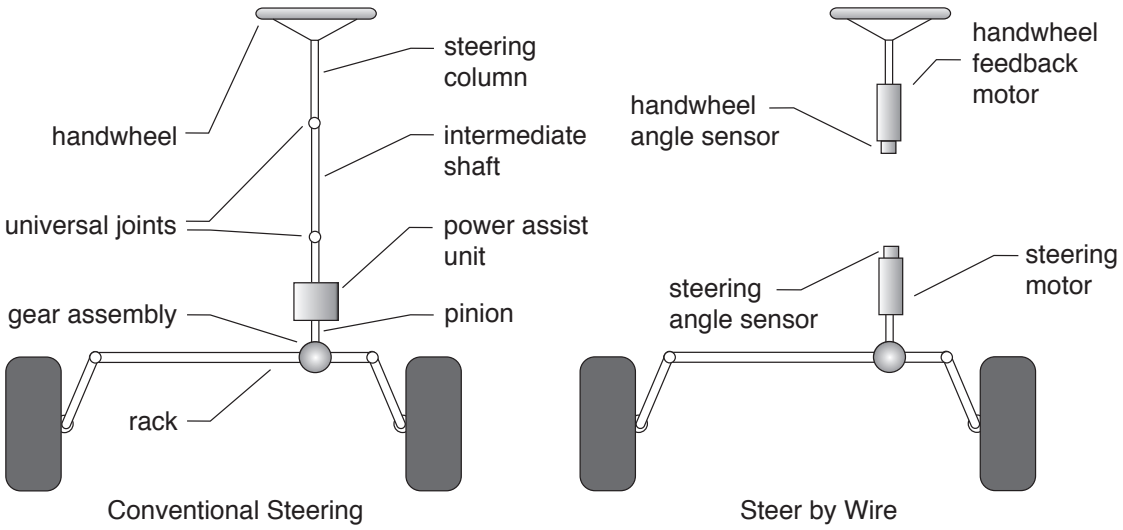

Figure 1.1: Conventional steering system and steer-by-wire system

in rollover[9]. More advanced safety systems such as collision avoidance systems and lane-keeping assistance systems are also made possible and/or more effective through the use of steer-by-wire[52][8].

Naturally, there may be some concern about the wisdom of having software intervening between what the driver commands the vehicle to do and what the vehicle actually does. However, the safety benefits of both anti-lock braking systems and vehicle stability control systems have been clearly established[25][17]. While the professional driver may be able to outperform vehicle control software in certain situations, most of us are not professional drivers, and the performance gap between vehicle control software and a skilled driver is steadily closing.

In the area of efficiency, steer-by-wire enables the possibility of a car that maintains its own wheel alignment. This reduces fuel consumption and improves tire wear. Most vehicles are designed to have a small amount of toe angle, when properly aligned, to improve handling characteristics. A steer-by-wire vehicle could vary its own toe angle dynamically, improving efficiency in situations such as freeway driving by reducing toe angle, while maintaining its handling abilities when cornering.

In a conventional steering system, there has to be a clear mechanical pathway

between the steering wheel and the road wheels. In a vehicle with steer-by-wire there is no need for this, which provides automotive designers a great deal of flexibility. For example, when a vehicle is sold in both left-hand drive and right-hand drive configurations, the engine compartment typically requires extensive redesign to make room for a steering column on the other side of the vehicle. Use of steer-by-wire eliminates this problem completely.

Lastly, steer-by-wire promises to change the way drivers think about vehicle handling. Currently, vehicle handling characteristics are a function of the mechanical design of the vehicle, and can only be changed at great expense and inconvenience. With steer-by-wire, handling characteristics become a software feature, easily customizable to suit the preferences of the driver. A car can be switched from handling like a sports car, with a tight steering ratio and fast steering response, to handling like a large luxury vehicle, with a smooth and stable feel, simply at the press of button.

While the potential benefits of steer-by-wire are numerous, there are no production vehicles offering steer-by-wire yet. There are, however, a number of a vehicles on the road today with systems that represent incremental progress toward a true steer-by-wire system.

The first of these is electric power steering. Electric power steering is a direct replacement for hydraulic power steering but consumes significantly less energy during operation [37]. Hydraulic power steering uses a mechanical torque sensor to measure the torque applied to the steering wheel by the driver. The torque sensor is coupled to a valve, which directs hydraulic fluid so as to amplify this applied torque. Electric power steering works on the same principle, however an electronic torque sensor is used to measure the steering wheel torque, and a motor is used to apply additional torque to the steering rack. Electric power steering realizes its energy savings by only consuming electricity when actively assisting the driver, whereas with hydraulic power steering the hydraulic power steering pump runs continuously, drawing roughly the same amount of power all the time, regardless of whether it is needed or not. Electric power steering is especially attractive in hybrid vehicles, where the engine may or may not be running, resulting in an intermittent source of mechanical power to run a hydraulic pump, but a continuous and plentiful source of electrical power.

A more significant development in steering systems was introduced by BMW in 2002 under the name of Active Steering. Developed by ZF Lenksysteme GmbH, Active Steering uses a conventional hydraulic power steering system, but interrupts the steering column with a planetary gearbox coupled to an electric motor. The motor and planetary gearbox allow software to establish an offset between the steering wheel angle, which the driver controls, and the angle of the wheels at the road. Active Steering is currently used for speed-dependent steering ratio, providing convenient maneuvering at low speeds and a more stable feel at higher speeds. It is also used by the vehicle stability control system in conjunction with differential braking to prevent loss of vehicle control [1].

While they represent important development along the way to steer-by-wire, neither electric power steering nor Active Steering offer the flexibility of a true steer-by-wire system [52]. Steer-by-wire is a topic of considerable interest in recent years in the academic world, with the majority of work examining either ways to ensure reliability of steer-by-wire systems, such as in Hammett and Babcock [24] and Isermann [30], or looking at advanced vehicle control strategies that steer-by-wire will enable, such as in Switkes [52], Andreasson et al. [4], and Huh et al. [29]. There is also significant interest at major auto manufacturers such as General Motors, with their well-known concept car, the Hy-Wire, Daimler, with concept vehicles such as the F400, and Nissan, who has graciously funded this research. There is also considerable interest among tier one suppliers, such as Delphi and ZF, both of whom offer complete steer-by-wire systems for research purposes.

1.2 Diagnostic Systems

Despite all of the excitement surrounding steer-by-wire and the benefits it offers, there are no production vehicles with steer-by-wire on the road today. The potentially catastrophic nature of a steering system failure requires that any replacement for a conventional steering system be extremely reliable. One approach for achieving the necessary level of reliability relies upon a diagnostic system that can quickly and accurately detect and isolate a fault. This information is then used to switch

over to a redundant component or a modified control law that can accommodate the fault. This strategy significantly relaxes the reliability requirements of the individual components in the system, without reducing the overall reliability of the system. Rather than attempting to design components that never fail, a diagnostic system can detect or even predict when a component is about to fail and accommodate this failure or impending failure before it creates a hazardous situation.

This use of diagnostic systems to maintain high system reliability has been used successfully for decades in the aerospace industry. A probabilistic analysis of the failure rates of steer-by-wire systems using various forms of redundancy coupled with diagnostic techniques described in Hammett and Babcock [24], shows that steer-by-wire systems can be designed to have an overall reliability rate of 10^{-9} failures/hour, the same as imposed on the aviation industry. However, diagnostic systems for aircraft have certain design freedoms that are not available to those for ground vehicles. In particular, the expense of triply redundant sensors, actuators, and controllers, all common practices in fly-by-wire designs, are prohibitive in production automobiles.

1.2.1 Scope

There are many aspects to the problem of fault detection. Generally speaking the problem can be broken down into a series of stages: residual generation, fault detection, fault isolation, and system reconfiguration, as shown in Figure 1.2. Residual generation is concerned with taking available data from the system and producing a collection of signals that are close to zero when the system is working correctly, and non-zero when there is a fault. Fault detection is the step that evaluates the residuals to determine whether or not a fault is present. The simplest form of detection simply compares a residual to a fixed threshold. Fault isolation seeks to determine the cause of the fault and is often combined with the detection step. The last step, system reconfiguration, is responsible for modifying the control laws to accommodate the fault, possibly by switching over to a backup component. This thesis will focus primarily on the problem of residual generation.

The magnitude of a fault can be used to classify it, determining the difficulty of

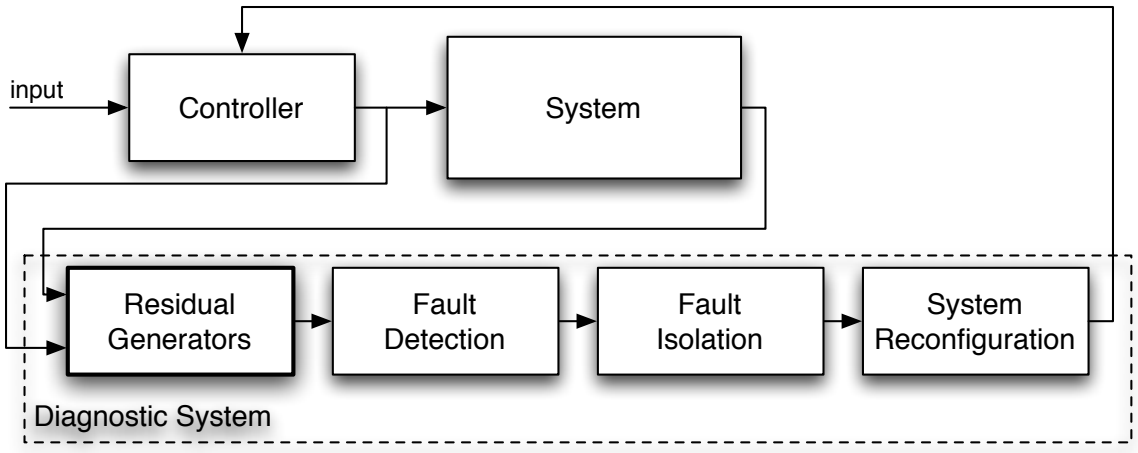

Figure 1.2: Block diagram of system and diagostic system

detection and the hazard it presents. Large-magnitude faults, such as the catastrophic failure of an actuator, present a serious hazard and require immediate attention, but are also easy to detect. Faults that are small in magnitude, such as an increase in friction in a linkage or a slight sensor bias are harder to detect, but generally do not present the immediate hazard that the sudden and complete loss of an actuator or sensor does. In many cases, however, such a minor fault is indicative of a fundamental problem that will worsen with time, providing a strong indication of a more serious impending failure. So by being able to detect small faults and remove the failing component from service, it may be possible to prevent catrastrophic failures from occurring. This thesis is primarily concerned with the challenges presented by these small, hard-to-detect faults.

1.3 Previous Work

Some of the earliest work on observer-based fault detection methods is attributable to Beard and Jones. These researchers first presented the idea of designing a Luenberger observer which diagonalizes the transfer matrix from input faults to output residuals in Beard [5] and Jones [35]. This approach simultaneously solves the problems of fault detection and isolation, but relies on precise knowledge of system to be diagnosed, in

order to exactly decouple the response to one fault from that of any other. This issue of robustness is a problem for a number diagnostic techniques and was first addressed in Chow and Willsky [11], where model uncertainty was explicity accounted for with a set of bounded parameters, and in Emami-Naeini and Rock [16], where a 2-norm bounded uncertainty block was used to represent model uncertainty.

Another observer-based approach, first described in Clark et al. [12] uses a bank of Kalman filters, each designed for the system with a particular fault condition. When operating, the Kalman filter with the smallest innovation stream is deemed to be the closest match to the actual system, and thus establishes the diagnosis. This approach requires one Kalman filter for each fault to be diagnosed, which makes it computationally more expensive than most other diagnostic techniques.

Neural networks have been used successfully for fault-detection applications, and are primarily attractive for systems with significant nonlinearities, where frequency-domain techniques aren't applicable [44][2]. Neural network methods, however, typically require access to training data and provide no analytic performance guarantees, which limits their usefulness for many applications. Fuzzy logic methods are similarly well-suited to nonlinear systems without requiring training data, but still typically provide no performance guarantees [42][3].

More recently, a number of researchers have examined ways to optimize the design of a diagnostic filter, using fault sensitivity as a performance measure. In Chen and Patton [10] the ratio of ∞-norm of the noise response to ∞-norm of the fault response is minimized:

$$J = \frac{||G(s)_d||_\infty}{||G(s)_f||_\infty}. \tag{1.1}$$

This cost function can lead to filter designs that are only particularly sensitive to faults at a narrow range of frequencies. In Ding and Guo [14] this issue is addressed by using the minimum fault response over all frequencies in place of the ∞-norm:

$$J = \frac{||G(s)_d||_\infty}{||G(s)_f||_-}, \tag{1.2}$$

where $||\cdot||_-$ denotes the infimum of the minimum singular value of the transfer matrix

over all frequencies:

$$||G(s)||_- \equiv \inf_{\omega} \sigma_{min}(G(j\omega)). \tag{1.3}$$

Note that despite the notation, $||\cdot||_-$ is not a norm, as it satisfies neither the positivity requirement of norms, nor the triangle inequality. In Rank and Niemann [47] and Ding et al. [13] the definition of $||\cdot||_-$ is adapted to only include non-zero singular values, and in number of studies, such as Wang et al. [55], the infimum is restricted to a bounded range of frequencies. Some work (e.g Ding et al. [13] and Wang et al. [55]) has also explored cost functions of the form:

$$J = ||G(s)_d||_\infty - ||G(s)_f||_- \tag{1.4}$$

or

$$J = ||G(s)_d||_\infty^2 - ||G(s)_f||_-^2 \tag{1.5}$$

where a difference replaces the ratio, highlighting the multi-objective nature of these optimization problems.

A similar approach divides the design process into two steps as seen in Zhong et al. [62]. In this work an ∞-norm ratio cost function is used to design an ideal diagnostic filter assuming a perfect system model, which is then used with robust H_∞ model matching techniques to produce the final, robust diagnostic filter. This two-stage approach avoids a computationally inefficient search for an filter that is optimal over all possible modeling errors, while still providing some degree of robustness.

1.3.1 Limitations of Existing Methods

Unfortunately, none of these diagostic cost functions explicitly address the fundamental tradeoffs between sensitivity, robustness, and speed of response, focusing only on sensitivity and robustness. For the application of a steer-by-wire diagnostic system, speed of response is of critical importance, which motivates the search for a diagnostic cost function that explicitly measures both the sensitivity and the usable bandwidth of a diagnostic filter.

Another limitation of the existing cost functions used for diagnostic filter design is

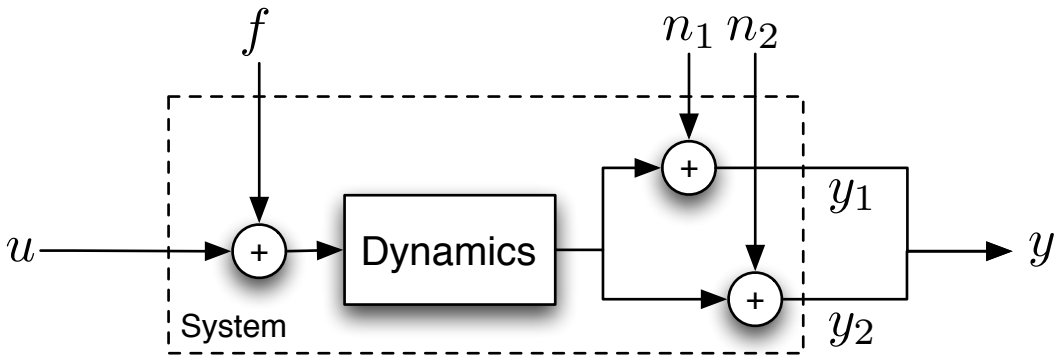

Figure 1.3: Example system illustrating the importance of spectral separation.

their insensitivity to spectral separation of the fault signal from noise and interference. This stems from a common aspect of existing diagnostic functions: the fault response is measured separately from the noise and interference response, then their ratio or difference is used as the cost function. This overlooks the inherent value of having a large signal-to-noise ratio at some frequencies where fault information dominates and a poor signal-to-noise ratio at other frequencies, where noise and interference dominate, but can be easily filtered away.

This is most clearly illustrated in the following example. Consider the system represented by the block diagram in Figure 1.3. The system to be diagnosed has a single input u, which is subject to a possible actuator fault, represented by the fault signal f. The system has a low-pass response to its input and therefore also has a low-pass response to the fault signal. It has a pair of sensors that measure the same output, but are affected by two different sources of noise, n_1 and n_2. Sensor 1 has a noise spectrum that is dominated by high-frequency noise, while sensor 2 has a noise spectrum that is dominated by low-frequency noise, as shown in Figure 1.4. These noise sources are each produced by filtering white Gaussian noise through one of two linear filters. These two filters have been chosen such that they have identical 2-norms and ∞-norms; they differ only in frequency response.

For this example we employ a very simple diagnostic system, which uses a model of the plant to generate a predicted output value which is then subtracted from each of the measured outputs. This creates a pair of residuals which, assuming no modeling

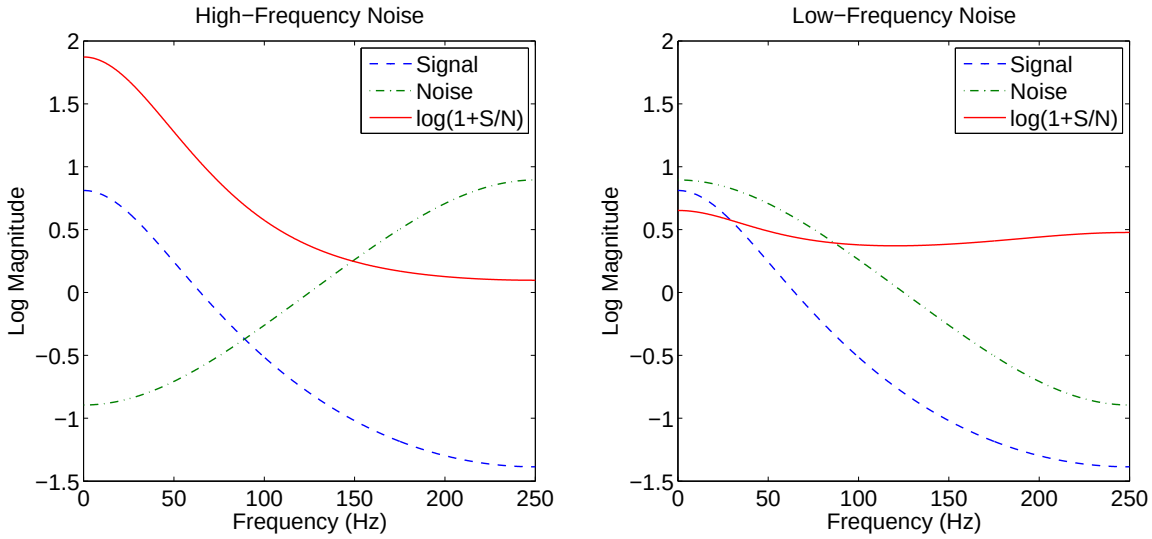

Figure 1.4: Signal and noise power spectral densities of two possible filter designs

uncertainty, should each track the fault signal filtered by the dynamics of the system, plus the noise due to their respective sensors. This diagnostic system is shown in Figure 1.5.

The fault signal is the same in both residuals, and the noise response has the same 2-norm and ∞-norm in both residuals. So by cost functions such as (1.1), (1.2), (1.4), or (1.5), these two residuals are of equal diagnostic value. A time domain simulation of this system is shown in Figure 1.6, where it is difficult to see much distinction between the two residuals. It is tempting to conclude that these two residuals are of equivalent diagnostic value, as would any of the cost functions discussed so far, but this overlooks an important difference between these two residuals: in one case the signal and noise lie in the same portion of the frequency spectrum and in the other case they do not.

In Figure 1.7 the same two residuals are shown after processing with a simple linear filter, which can easily separate fault signal from noise if they occupy different portions of the frequency spectrum. The benefits of spectral separation are clear, as the residual based on sensor 1 provides a clear diagnosis, while the residual based on sensor 2 does not. Unfortunately, despite its obvious value, none of these existing

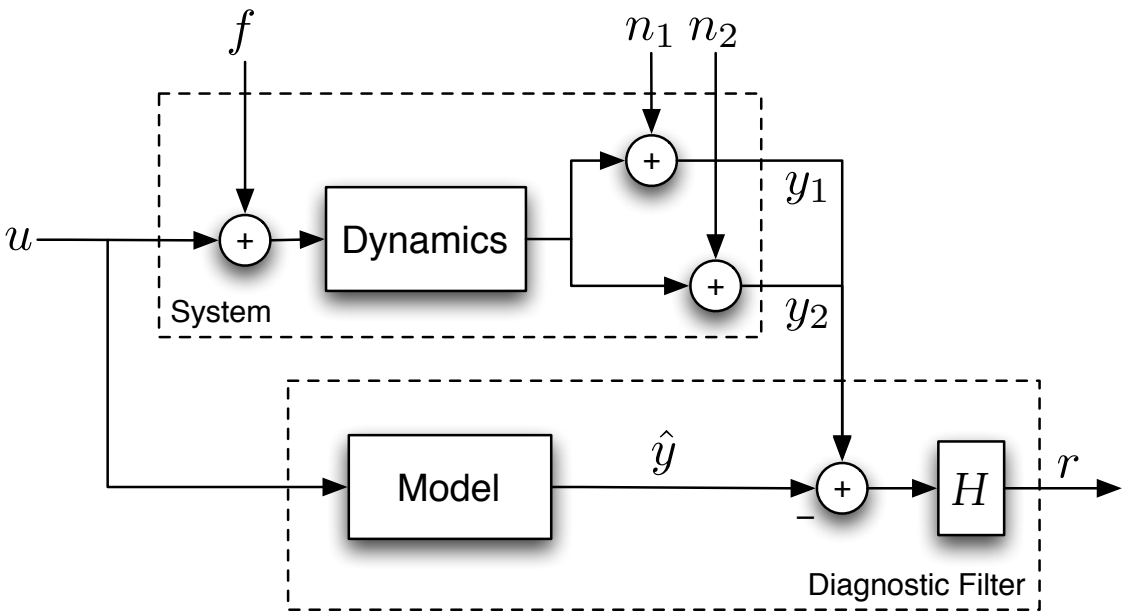

Figure 1.5: Example system and simple diagnostic filter

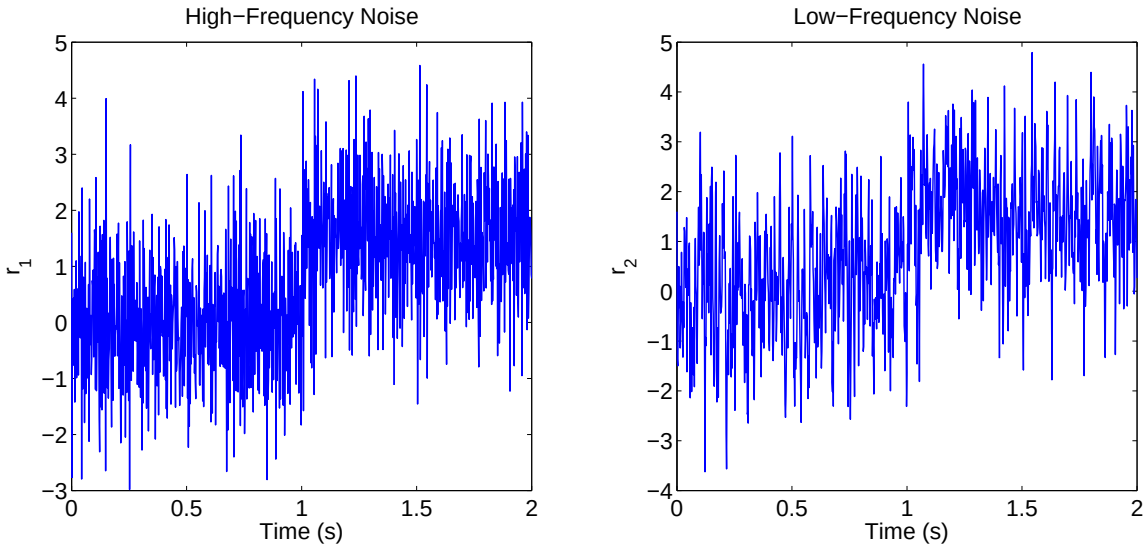

Figure 1.6: Simulated fault response of two possible diagnostic filters

cost functions are sensitive to spectral separation, hence the need for a new way of measuring the diagnostic performance of a residual.

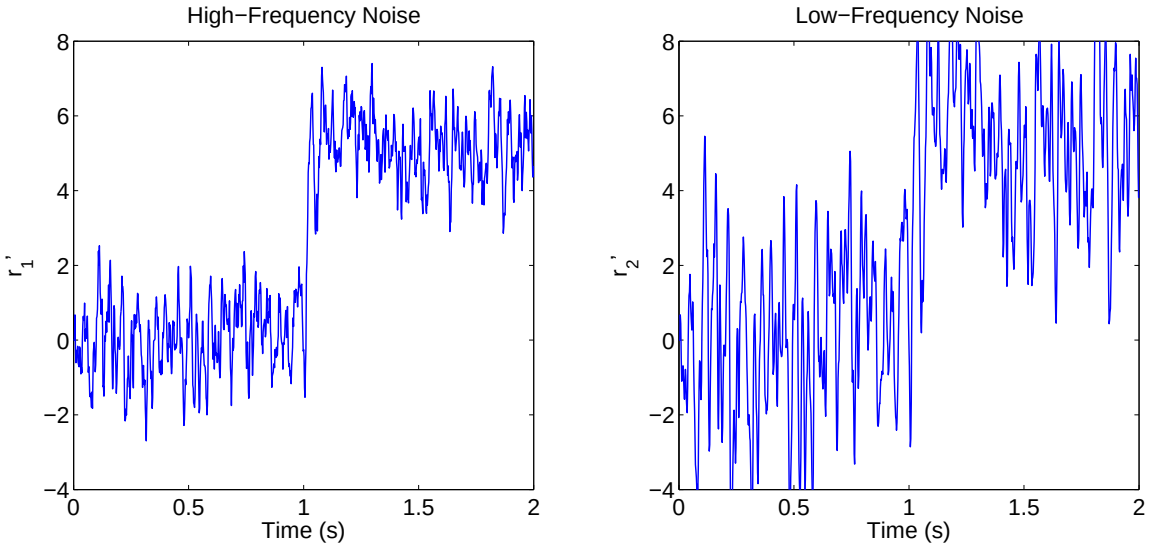

Figure 1.7: Simulated fault response of two possible diagnostic filters after post-filtering

1.4 Contributions

The research presented in this thesis makes several contributions to the design of diagnostic systems for steer-by-wire vehicles, as well as to the problem of diagnostic system design in general. The research presented here resulted in the following contributions:

- A full-scale steer-by-wire research vehicle, with independent front steering and independent rear traction was designed and constructed. This vehicle is the basis for all of the experimental results presented in this thesis, as well as numerous other experiments performed by colleagues in the Dynamic Design Laboratory.

- A model-based diagnostic system for use with steer-by-wire vehicles, which can detect and isolate faults without the need for redundant sensors, was developed.
- The effectiveness of this diagnostic system was demonstrated experimentally, showing that faults can be detected at or below the level of driver perception, using only automotive grade sensors.
- The diagnostic filter design problem was posed as an optimization problem, using channel capacity as measure of diagnostic performance. This eliminates the need for hand-tuning and allows diagnostic system design and performance evaluation to precede final construction of the system to be diagnosed.
- The usefulness of channel capacity as a diagnostic performance metric was experimentally demonstrated, as it can differentiate filter designs that provide good spectral separation of signal and noise from those that do not. Existing diagnostic performance metrics are insensitive to spectral separation.

1.5 Outline

Chapter 2 describes the steer-by-wire vehicle, known as "P1", developed in the course of this research. The models described in this chapter capture the relevant dynamics of the vehicle and steering system, and are used in the subsequent chapters in the design of a diagnostic system.

Chapter 3 describes how to design a model-based diagnostic system that can detect and isolate a wide variety of steering system faults, using only measurements from sensors already present in the steering system.

Chapter 4 describes a novel diagnostic filter performance metric: the capacity of the communication channel between the fault signal and the diagnostic residual signal, as established by the system and diagnostic filter. This chapter also illustrates how to optimize diagnostic filter design using this proposed performance metric, using the steer-by-wire system as an example problem, with experimental results.

Chapter 5 describes some of the properties of channel capacity as a diagnostic performance metric, and the impact these have on its use in designing diagnostic filters. In particular, the channel capacity of a diagnostic residual is invariant under linear filtering, a property which decouples the design of a diagnostic filter from the design of post-processing filters. Additionally, the channel capacity of a diagnostic residual based on a Luenberger observer is invariant over all choices of observer gain when the observer only has access to a single measurement of the system. This property establishes the triviality of single-measurement observer design for diagnostic systems.

Chapter 6 presents some concluding remarks and a discussion of possible directions in which this research could continue in the future.

Appendix A contains a detailed proof of Shannon's limit on capacity of a noisy channel. This proof is not a contribution by the author; it is merely included for completeness, as many of the results in Chapters 3 and 4 are based on the measurement of channel capacity.

Appendix B contains a detailed derivation of the recursive least-square algorithm, which is used in Chapter 3 for real-time estimation of various motor parameters.

Chapter 2

Modeling of a Steer-by-wire Electric Vehicle

2.1 Introduction

This chapter serves to orient the reader to the steer-by-wire research vehicle, P1, by describing its basic characteristics and highlighting some of its more distinctive capabilities. A thorough discussion of the dynamic models of P1 follows, focusing on the dynamics of the vehicle chassis, the dynamics of the steering systems, and the electrical dynamics of the steering motors and data acquisition circuitry. These models are the basis for all of the diagnostic techniques presented in this thesis.

It should be noted that the development of P1 was a large project, requiring the effort of many individuals over the span of several years. Some of the people who have helped make P1 what it is today include: Scott Kohn, Will Crump, Paul Yih, Chris Gerdes, Craig Milroy, Josh Switkes, Shad Laws, Carrie Bobier, RK MacLean, Rami Hindiyeh, Judy Hsu, Craig Beal, and Kirstin Talvala.

2.1.1 Vehicle Description

P1 was designed to be a flexible research vehicle, allowing for easy changes to hardware configuration and control software. It also needed to have performance and

Figure 2.1: Steer-by-Wire Testbed Vehicle

handling characteristics like those of a typical production vehicle in order to get relevant experimental results, and it needed to have a by-wire steering system. Notably absent from these design criteria are aesthetics, ergonomics, and efficiency.

The use of an electric powertrain eliminated many of the mechanical complexities associated with components typically found in vehicles with an internal combustion engine. P1 has no need for a multi-speed transmission or clutch, as the drive motors can provide full torque at zero speed and can operate as high as 9000 RPM. By using a separate drive motor for each rear wheel, P1 has no need for a differential, and has the unique ability to precisely control the torque applied by each drive wheel independently. The drive motors and corresponding power electronics are far more efficient than an internal combustion engine, so for similar power and torque capabilities, there is significantly less waste heat produced, which simplified the design of the cooling system.

The body of a vehicle serves a number of purposes: it reduces drag, it protects the occupants from the elements, and it (usually) provides an aesthetically pleasing

exterior. For a research vehicle, these features are of secondary importance. A bare chassis provides convenience and flexibility in terms of being able to rapidly reconfigure the vehicle for new experiments. This outweighs the traditional benefits of a body, and as such, P1 was designed without one.

One of the most striking features of P1 is the independent steer-by-wire system. Mechanically, the left and right front wheels are linked only by their contact with the road surface. This provides a unique degree of freedom for control of the steering system, enabling a variety of control techniques not possible with a traditional, coupled steering system. These range from simple control strategies such as software-defined steering geometry or speed-dependent steering geometry, to more advanced algorithms designed to maximize cornering forces at each wheel, to truly bizarre techniques such as braking by "snow-plowing". This additional degree of freedom incurs a modest increase in modeling complexity, as compared to a vehicle with a conventional steering system. This is addressed in detail later in this chapter.

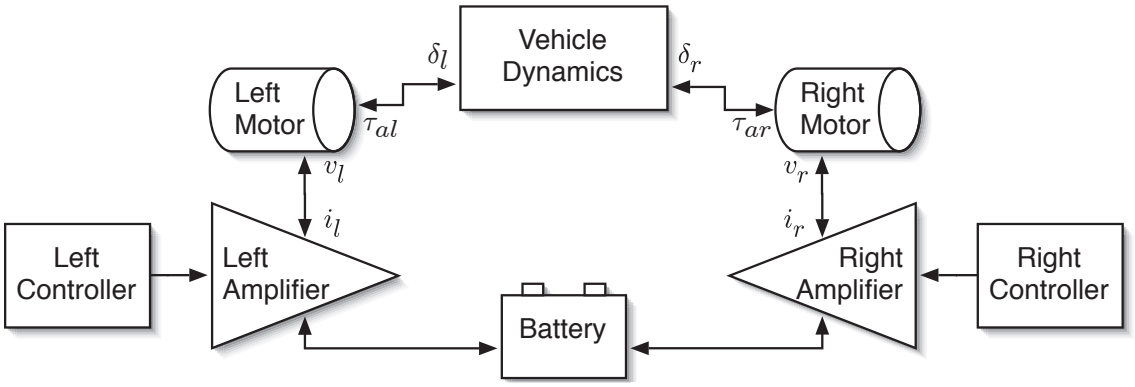

Figure 2.2: Vehicle steering system block diagram

2.2 Planar Vehicle Dynamics

The vehicle model used is the simple, linear bicycle model modified to include relaxation length and two independent front wheels. This is a simple extension of the model developed in Yih [59]. The linear bicycle model can be decomposed into the following three components:

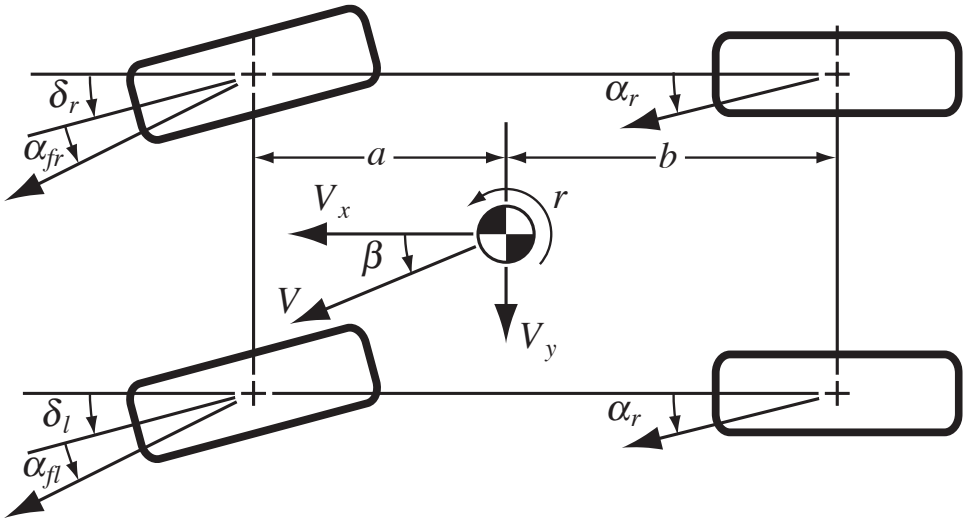

Figure 2.3: Vehicle schematic and nomenclature

- Vehicle kinematics, which map the vehicle sideslip angle, β, and yaw rate, r, to tire slip angles α_{fl}, α_{fr}, and α_r.
- Vehicle dynamics, which map the lateral forces F_{yfl}, F_{yfr}, and F_{yr} to the vehicle state derivatives $\dot{\beta}$ and $\dot{r}$. α_r to lateral forces F_{yfl}, F_{yfr}, and F_{yr}.
- Tire model, which maps the tire slip angles α_{fl}, α_{fr}, and α_r to lateral forces F_{yfl}, F_{yfr}, and F_{yr}.

2.2.1 Vehicle Kinematics

The vehicle kinematics and dynamics components used are very similar to the traditional bicycle model. The only difference is that the front slip angles and lateral forces are considered independently. This kinematic relationship between β and r and α_{fl}, α_{fr}, and α_r is given by:

$$\alpha_{fl} = \beta + \frac{a}{V}r - \delta_\ell \tag{2.1}$$

$$\alpha_{fr} = \beta + \frac{a}{V}r - \delta_r \tag{2.2}$$

$$\alpha_r = \beta - \frac{b}{V}r \tag{2.3}$$

where a and b are the distances from the center of gravity to the front and rear axles, respectively, r is the yaw rate of the vehicle, β is the sideslip angle of the vehicle, V is the speed of the vehicle, and δ_ℓ and δ_r are the left and right steer angles. The left and right front tire slip angles are denoted by α_{fl} and α_{fr}, and α_r is the rear tire slip angle.

2.2.2 Vehicle Dynamics

The dynamic relationship between lateral tire forces and the vehicle states is given by the following differential equations:

$$\dot{\beta} = -r + \frac{1}{mV}F_{yfl} + \frac{1}{mV}F_{yfr} + \frac{1}{mV}F_{yr} \tag{2.4}$$

$$\dot{r} = \frac{a}{I_z}F_{yfl} + \frac{a}{I_z}F_{yfr} - \frac{b}{I_z}F_{yr} \tag{2.5}$$

where m is the vehicle mass, I_z is the vehicle yaw moment of inertia, and F_{yfr}, F_{yfl}, and F_{yr} are the lateral forces generated by the front left tire, front right tire, and the combined lateral force generated by the rear tires.

2.2.3 Tire Model

In many tire models, the relationship between tire slip angle and lateral force is assumed to be static. This assumption works reasonably well when the characteristic frequency of the tire dynamics is sufficiently above the characteristic frequency of the overall vehicle dynamics. In the case of P1, however, which has an atypically low yaw moment of inertia, the tire dynamics are not of significantly higher frequency than the vehicle dynamics, and their effect can be seen in the vehicle response. For a thorough discussion of vehicles with a low yaw moment of inertia see Bobier et al. [6]. In order to capture these dynamics, a linear first-order tire relaxation length model is used. Conceptually, this model says that a tire cannot begin producing lateral force instantaneously. Rather, the tire must roll through a small distance, during which time the lateral force builds up. In the following equation C_α represents the cornering stiffness of the tire, α represents the actual tire slip angle, $\bar{\alpha}$ represents the effective

slip angle, and σ represents the tire relaxation length:

$$\dot{\bar{\alpha}} = \frac{V_x}{\sigma}(\alpha - \bar{\alpha}) \tag{2.6}$$

$$F_y = -C_\alpha \bar{\alpha} \tag{2.7}$$

Note that the time constant of this relationship between α and $\bar{\alpha}$ decreases with speed. This means that while notable at lower speeds, at higher speeds the effect of relaxation length diminishes.

Combining the kinematic and dynamic vehicle equations with the equations for the tire dynamics results in a five-state model of the planar dynamics of the vehicle, given by the following:

$$\dot{x}_v = A_v x_v + B_v \begin{bmatrix} \delta_\ell & \delta_r \end{bmatrix}^T \tag{2.8}$$

$$y_v = C_v x_v \tag{2.9}$$

where

$$x_v = \begin{bmatrix} \beta & r & \bar{\alpha}_{fl} & \bar{\alpha}_{fr} & \bar{\alpha}_r \end{bmatrix}^T \tag{2.10}$$

$$A_v = \begin{bmatrix} 0 & -1 & -\frac{C_{\alpha fl}}{mV_x} & -\frac{C_{\alpha fr}}{mV_x} & -\frac{C_{\alpha r}}{mV_x} \\ 0 & 0 & -\frac{aC_{\alpha fl}}{I_z} & -\frac{aC_{\alpha fr}}{I_z} & \frac{bC_{\alpha r}}{I_z} \\ \frac{V_x}{\sigma_f} & \frac{a}{\sigma_f} & -\frac{V_x}{\sigma_f} & 0 & 0 \\ \frac{V_x}{\sigma_f} & \frac{a}{\sigma_f} & 0 & -\frac{V_x}{\sigma_f} & 0 \\ \frac{V_x}{\sigma_r} & -\frac{b}{\sigma_r} & 0 & 0 & -\frac{V_x}{\sigma_r} \end{bmatrix} \tag{2.11}$$

$$B_v = \begin{bmatrix} 0 & 0 & -\frac{V_x}{\sigma_f} & 0 & 0 \\ 0 & 0 & 0 & -\frac{V_x}{\sigma_f} & 0 \end{bmatrix}^T \tag{2.12}$$

$$C_v = [\, 0\ 1\ 0\ 0\ 0 \,]. \tag{2.13}$$

This model is then discretized using a zero-order-hold approximation to get the final A, B, C, and D matrices. The data acquisition system in P1 runs at 500 Hz, so the discretization is performed using a 2 ms sample time.

The values of the parameters of this vehicle model of P1 are listed in Table 2.1.

Table 2.1: Vehicle model parameters for P1

Parameter	Symbol	Value
Front axle to c.g.	a	1.35 m
Rear axle to c.g.	b	1.15 m
Total vehicle mass	m	1724 kg
Yaw moment of inertia	I_z	1300 kg·m^2
Front, left cornering stiffness	$C_{\alpha fl}$	45000 N/rad
Front, left cornering stiffness	$C_{\alpha fr}$	45000 N/rad
Combined rear cornering stiffness	$C_{\alpha r}$[1]	138000 N/rad
Front, left relaxation length	σ_{fl}	0.3 m
Front, right relaxation length	σ_{fr}	0.3 m
Rear relaxation length	σ_r	0.55 m

2.3 Steering System Dynamics

The basic model for each of the front wheels is given by:

$$\tau = J_{eff}\ddot{\delta} + b_{eff}\dot{\delta} \tag{2.14}$$

where τ is the total torque about the wheel's steer axis, J_{eff} is the effective inertia about the wheel's steer axis, b_{eff} is the effective damping about the wheel's steer axis, and δ is the steer angle measured about the wheel's steer axis.

The steering motors transmit torque to the wheels through a constant gear ratio n_g and a non-constant linkage ratio n_l. The linkage ratio is defined by the kinematics of the steering system, namely the pitman arm, tie rod, and steering knuckle. This mechanism translates the angle of the gearbox output θ to the steering angle of the wheel δ. It can be defined as a function of steer angle:

$$n_l(\delta) = \frac{d\theta(\delta)}{d\delta} \tag{2.15}$$

[1]Note that the lumped rear axle cornering stiffness $C_{\alpha r}$ is twice that of a single rear tire, whereas $C_{\alpha fl}$ and $C_{\alpha fr}$ are each for a single tire. The same cannot be said for rear tire relaxation length, σ_r; it is the same value as that of a single tire.

The effective inertia and damping are functions of this linkage ratio:

$$J_{eff} = J_w + n_l^2(\delta) J_m \tag{2.16}$$

$$b_{eff} = b_w + n_l^2(\delta) b_m \tag{2.17}$$

where J_m and b_m are the inertia and damping of the motor and gearbox felt at the gearbox output shaft and J_w and b_w are the inertia and damping of the steering knuckle and wheel assembly felt at the wheel's steer axis.

There are five dominant sources of torque about the steering axis: the torque due to lateral tire forces, τ_a; the torque due to vertical tire forces, τ_j; the torque due to longitudinal tire forces, τ_s; the torque applied by the steering motor, τ_m; and the torque due to internal forces within the tire, τ_t.

$$\tau = \tau_a + \tau_j + \tau_s + \tau_t + \tau_m \tag{2.18}$$

The last two of these terms are comparatively easy to model, but the first three terms require a model of the steering knuckle geometry.

2.3.1 Steering Knuckle Geometry

The following expression establishes the steer axis (or kingpin axis) vector, $\hat{k}$, as a function of the caster angle, θ_c, and the kingpin inclination angle, θ_k:

$$k = \frac{1}{\sqrt{\tan^2\theta_c + \tan^2\theta_k + 1}} \begin{bmatrix} -\tan\theta_c \\ -\tan\theta_k \\ 1 \end{bmatrix} \tag{2.19}$$

$$\hat{k} = [\hat{x} \;\; \hat{y} \;\; \hat{z}]\, k \tag{2.20}$$

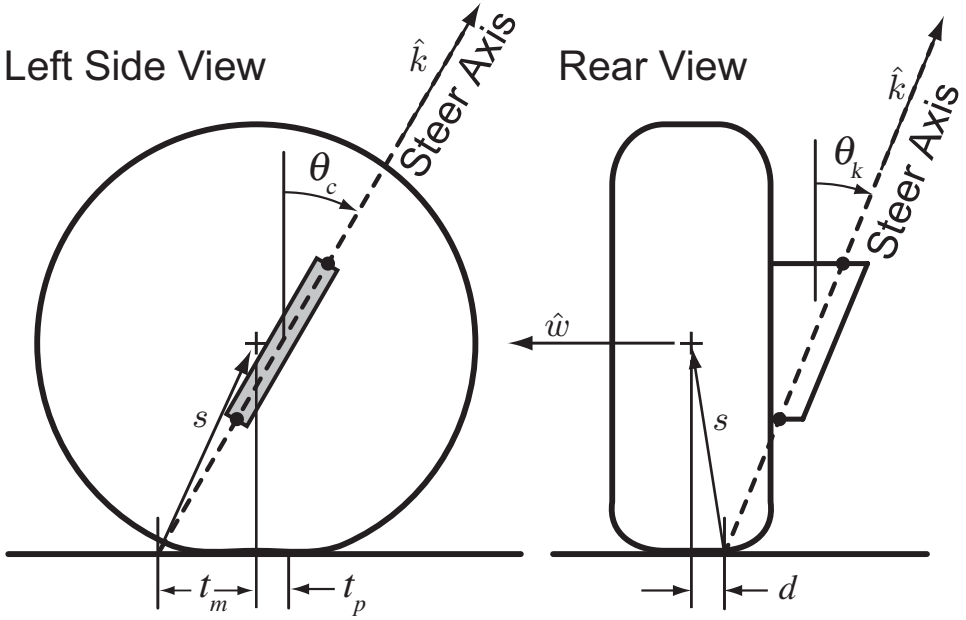

Figure 2.4: Left and rear views of the left-hand wheel

This leads to the following expression for the rotation matrix, P, which rotates about the steer axis by an angle δ:

$$P = (1-\cos\delta)kk^T + \begin{bmatrix} \cos\delta & k_3\sin\delta & -k_2\sin\delta \\ -k_3\sin\delta & \cos\delta & k_1\sin\delta \\ k_2\sin\delta & -k_1\sin\delta & \cos\delta \end{bmatrix} \tag{2.21}$$

The orientation of the wheel is represented by $\hat{w}$ in (2.23). The location of the center of the wheel and the location of the center of the contact patch, both relative to the nominal intersection of the steering axis with the ground, are given by $\vec{s}$ and $\vec{l}$ in (2.22) and (2.26). Vectors $\hat{k}$, $\hat{w}$, and $\vec{s}$ are illustrated in Figure 2.4. The vectors $\hat{x}'$ and $\hat{y}'$ represent a set of coordinates that rotate with the wheel, but which lie in the

same plane as $\hat{x}$ and $\hat{y}$.

$$\vec{s} = [\hat{x} \;\; \hat{y} \;\; \hat{z}]\, P\, [-R_l \tan\theta_c \;\; d \;\; R_l]^T \tag{2.22}$$

$$\hat{w} = [\hat{x} \;\; \hat{y} \;\; \hat{z}]\, P\, [0 \;\; 1 \;\; 0]^T \tag{2.23}$$

$$\hat{x}' = \frac{\hat{w} \times \hat{z}}{||\hat{w} \times \hat{z}||} \tag{2.24}$$

$$\hat{y}' = \hat{z} \times \hat{x}' \tag{2.25}$$

$$\vec{l} = \vec{s} - R_l(\hat{x}' \times \hat{w}) \tag{2.26}$$

Table 2.2: Steering Knuckle Parameters

Parameter	Symbol	Value
Wheel Radius	R_l	320 mm
Caster Angle	θ_c	5.5°
Kingpin Inclination Angle	θ_k	13.2°
Scrub Radius	d	50.5 mm
Mechanical Trail	t_m	28 mm

2.3.2 Jacking Torque

As the wheel turns in and out, it lowers and raises the car. Suspension jacking is the torque felt about the steer axis as a result of this motion. Jacking torque is simply the torque about the steer axis that results from vertical tire forces.

Jacking torque, τ_j, as a function of steer angle, δ, and normal force, F_z, is given by (2.19, 2.21, 2.22, 2.23, 2.20, 2.26) and the equation below:

$$\tau_j = \hat{k} \cdot (\vec{l} \times F_z \hat{z}) \tag{2.27}$$

Figure 2.5 illustrates the jacking torque effect on P1. The jacking torque tends to be large only when turning out at high steer angles. When the wheels are linked together in a traditional steering system, the jacking torques of each wheel nearly cancel at low steer angles. At high steer angles, the jacking torque of the wheel that

is turning out dominates, resulting in a return-to-center feel. This is less important at high speeds since, for a given amount of steer angle, the torque due to lateral tire forces becomes much larger than jacking torque.

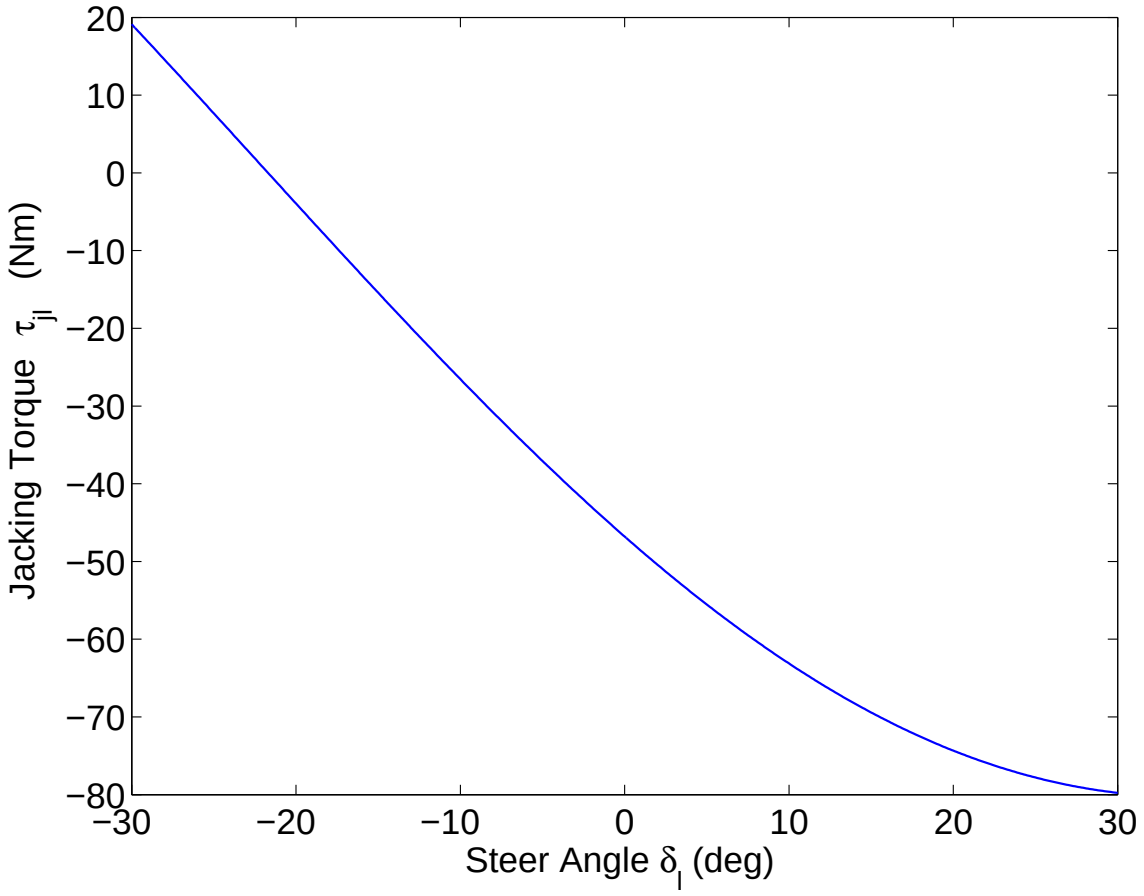

Figure 2.5: Jacking torque on the left wheel as a function of steer angle

2.3.3 Aligning Torque

The aligning moment τ_a is the product of the total trail (the effective moment arm of the lateral force about the steer axis), t_t, and the lateral force felt by the steering system F_y. The total trail is the sum of mechanical trail, t_m, which is due to steering system geometry, and pneumatic trail, t_p, which is due to the non-uniform distribution of lateral force along the length of the contact patch (see Figure 2.4). Mechanical trail

is a function of steer angle. Pneumatic trail is a function of tire slip angle, roughly constant in the linear region of handling and tapering off to zero as the tire reaches saturation. Since this model is designed for the linear region of handling, pneumatic trail is assumed constant. This gives the following equation:

$$\tau_a = -t_t(\delta)F_y \tag{2.28}$$

$$t_t(\delta) = t_m(\delta) + t_p \tag{2.29}$$

where F_y is the effective lateral tire force given by:

$$F_y = -C_\alpha \bar{\alpha} \tag{2.30}$$

where C_α is the linear cornering stiffness of the corresponding tire, and $\bar{\alpha}$ is the effective tire slip angle.

The following equation provides an analytic expression for mechanical trail, t_m, for the left wheel as a function of steer angle, δ:

$$t_m(\delta) = \hat{k} \cdot (\hat{y}' \times \vec{l}) \tag{2.31}$$

A plot of mechanical trail for P1 is given in Figure 2.6.

2.3.4 Scrub Radius Torque

Longitudinal tire forces, due to braking or accelerating, also produce a torque about the steer axis. In the case of braking, where the tire force is due to a torque applied by the brake calipers, the torque about the steering axis is given by:

$$\tau_s = -F_x d \tag{2.32}$$

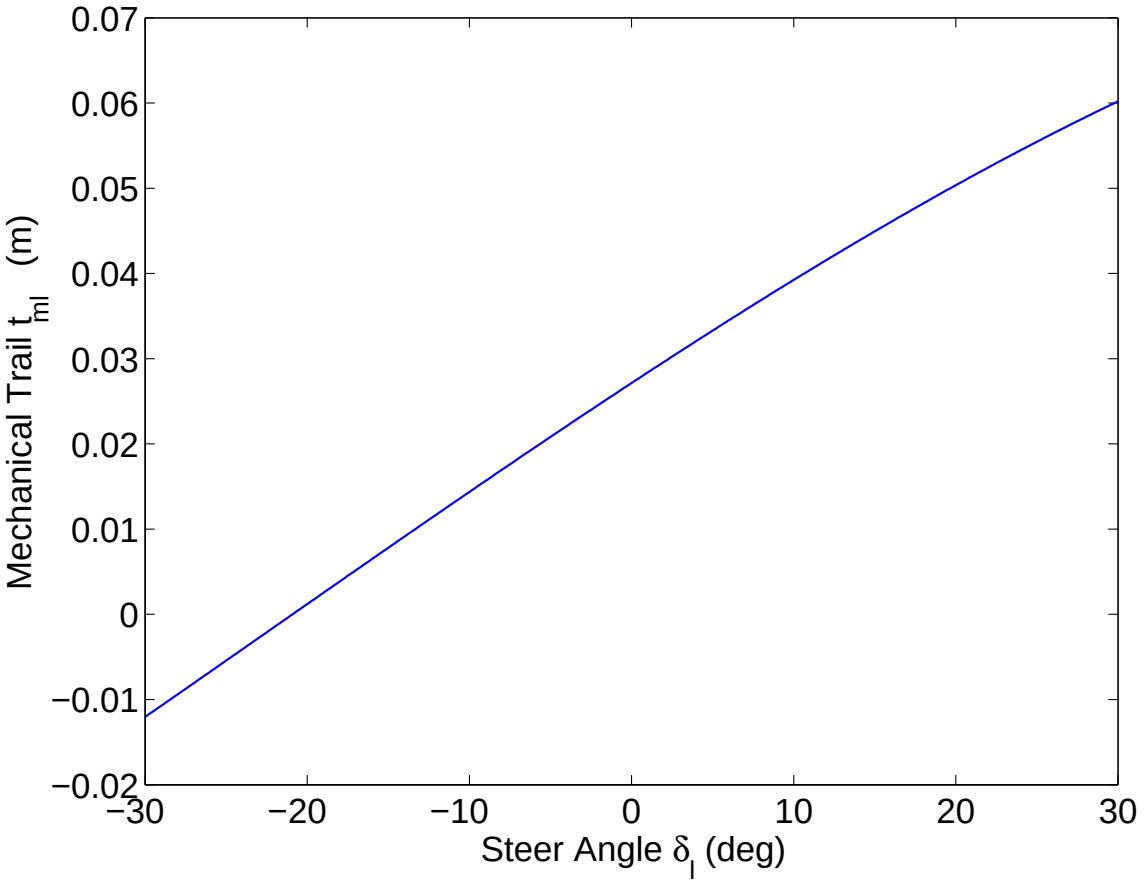

Figure 2.6: Mechanical trail change on the left wheel as a function of steer angle

where d is the scrub radius (see Figure 2.6), which exhibits only a slight dependence on steer angle:

$$d = \hat{k} \cdot (\hat{x}' \times \vec{l}) \tag{2.33}$$

In the case of accelerating, the tire force is due to a torque applied by the drive shaft, which (unlike the brake calipers) is a source of torque that is external to the steering knuckle and must be accounted for separately. This results in an additional

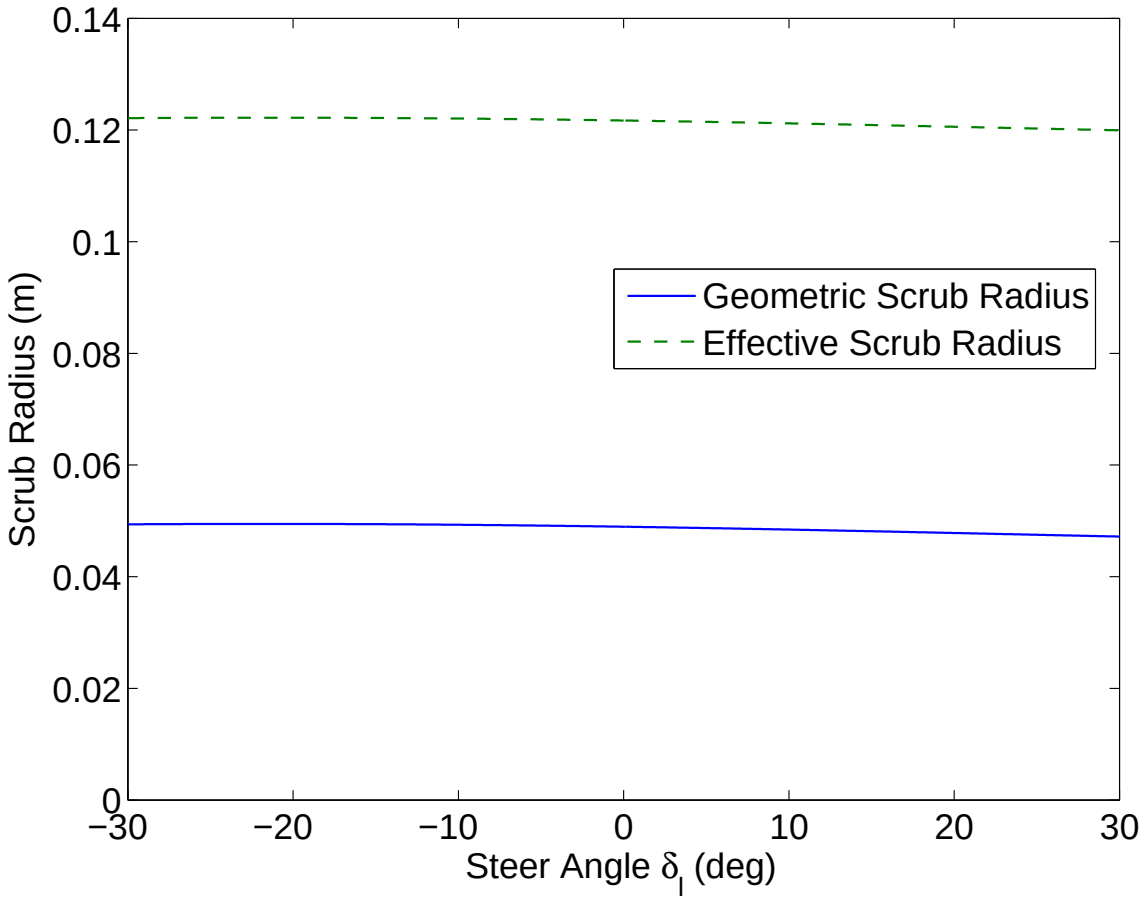

Figure 2.7: Geometric and effective scrub radius on the left wheel as a function of steer angle

term in the equation for scrub radius torque:

$$\tau_s = -F_x d + F_x R_l \hat{w} \cdot \hat{k} \tag{2.34}$$

$$= -F_x (d - R_l \hat{w} \cdot \hat{k}) \tag{2.35}$$

By factoring $-F_x$ out of each term, as in (2.35), the contribution of this additional torque can be regarded as a constant offset to the scrub radius. This leads to the notion of a pair of scrub radii, the geometric scrub radius for tire forces due to the brakes, and an effective scrub radius for tire forces due to the engine. Figure 2.7 shows both of these scrub radii for the steering system on P1.

As P1 is a rear-wheel drive vehicle, braking is the only significant source of longitudinal tire forces on the front wheels. For the sake of simplicity, τ_s is assumed to be zero. This simplification means the model developed here is only strictly valid when the driver is not applying the brakes, hence the torque due to braking forces is considered to be a disturbance.

2.3.5 Torsional Tire Stiffness Torque

The tire presents a resistance to turning about the steering axis until the tire has rolled far enough for the rubber in the contact patch to align itself with the angle of the wheel. This effect can modeled as a torsional spring:

$$\tau_t = C_t(\bar{\alpha} - \alpha) \tag{2.36}$$

where $\bar{\alpha}$ is the effective tire slip angle, and α is the tire slip angle. Their difference represents the amount of twist in the tire between the contact patch and the rim of the wheel, hence it proportional relationship to torque, τ_t.

2.3.6 Motor Torque

Each steering motor generates a torque given by the product of the motor constant, k_m, and the input current, i. The torque at the output shaft of the gearbox τ_g is this torque modified by the gearbox's gear ratio n_g, coulomb friction f_m, and efficiency η:

$$\tau_g = (n_g k_m i - f_m)\eta \tag{2.37}$$

The net actuator torque felt at the steer axis τ_m is this torque modified by linkage ratio n_l and coulomb friction from the steering knuckle and wheel assembly f_w:

$$\tau_m = (n_g k_m i - f_m)\eta n_l(\delta) - f_w \tag{2.38}$$

Both of these coulomb friction terms act to oppose movement. Therefore, their sign depends on the steer axis's direction of rotation.

2.3.7 Complete Steering System Model

The net actuator torque and aligning moment can be put together to form the total torque on the wheel:

$$\begin{aligned} \tau &= [(n_g k_m i - f_m)\eta n_l(\delta) - f_w + \tau_j(\delta)] \\ &\quad + t_t(\delta) C_\alpha \bar{\alpha} - C_t(\bar{\alpha} - \alpha) \end{aligned} \tag{2.39}$$

Note that the last term is a function of vehicle states. The expression in the brackets can be considered an effective input to our system, which can be called τ_{eff}. This can be combined with our original differential equation to get:

$$J_{eff}(\delta)\ddot{\delta} = t_t(\delta) C_\alpha \bar{\alpha} - C_t(\bar{\alpha} - \alpha) - b_{eff}(\delta)\dot{\delta} + \tau_{eff} \tag{2.40}$$

$$\tau_{eff} = (n_g k_m i - f_m)\eta n_l(\delta) - f_w + \tau_j(\delta) \tag{2.41}$$

The nominal values of parameters for the model of the steering system on P1 are provided in Table 2.3.

Table 2.3: Steering system model parameters for P1

Parameter	Symbol	Value
Gearbox ratio	n	160
Gearbox efficiency	η	0.95
Wheel & steering linkage inertia	J_w	1.2 Nms^2/rad
Wheel & steering linkage damping	b_w	9 Nms/rad
Wheel & steering linkage friction	f_w	7 Nm
Left motor inertia	$J_{m,l}$	8.6 Nms^2/rad
Right motor inertia	$J_{m,r}$	8.7 Nms^2/rad
Left motor damping	$b_{m,l}$	20 Nms/rad
Right motor damping	$b_{m,r}$	26 Nms/rad
Left motor friction	$f_{m,l}$	14 Nm
Right motor friction	$f_{m,r}$	18.5 Nm
Pneumatic trail	t_p	0.023 m
Motor constant	k_m	0.128 Nm/A

2.3.8 Motor Electrical Model

The steering motors used in this vehicle are DC permanent magnet motors and as such, their electrical properties can be reasonably modeled as the series connection of a resistor, an inductor, and a voltage source representing the back-EMF produced by the motor. This results in the following $i - v$ relationship at the motor terminals:

$$v = L\frac{di}{dt} + iR + k\omega \tag{2.42}$$

where L is the motor inductance, R is the motor resistance, k is the motor constant, and ω is the angular velocity of the motor shaft. This equation has no dependence on the torque applied to the motor by the steering system, which provides a convenient decoupling between the electrical and mechanical dynamics of the motor. The nominal values for L, R, and k for the steering motors on P1 are given in Table 2.4.

Table 2.4: Nominal electrical parameters for steering motors

Parameter	Symbol	Value
Resistance	R	0.55 Ω
Motor constant	k	0.128 V·s/rad
Inductance	L	1.1 mH

The steering motors are each driven by a PWM current amplifier with switching frequency of 32 kHz. This is more than an order of magnitude faster than the electrical time constant of the motors ($L/R = 2$ ms) hence this PWM signal can be regarded as an analog current input.

2.4 Stochastic Modeling

2.4.1 Sensor Noise Modeling

In the absence of noise and modeling uncertainty, fault detection becomes a trivial problem. Therefore, accurate models of noise sources are critical to being able to predict diagnostic performance.

To develop stochastic models of the noise source, n, and the driver, u, experimental was data collected. A sixth-order model of the power spectral density of the noise on the yaw rate sensor found by hand-fitting is shown in Figure 2.8. Most of the frequency spectrum for this sensor is fairly white, with the exception of the two spikes in frequency content, one around 0.3–0.6 Hz and one around 230 Hz.

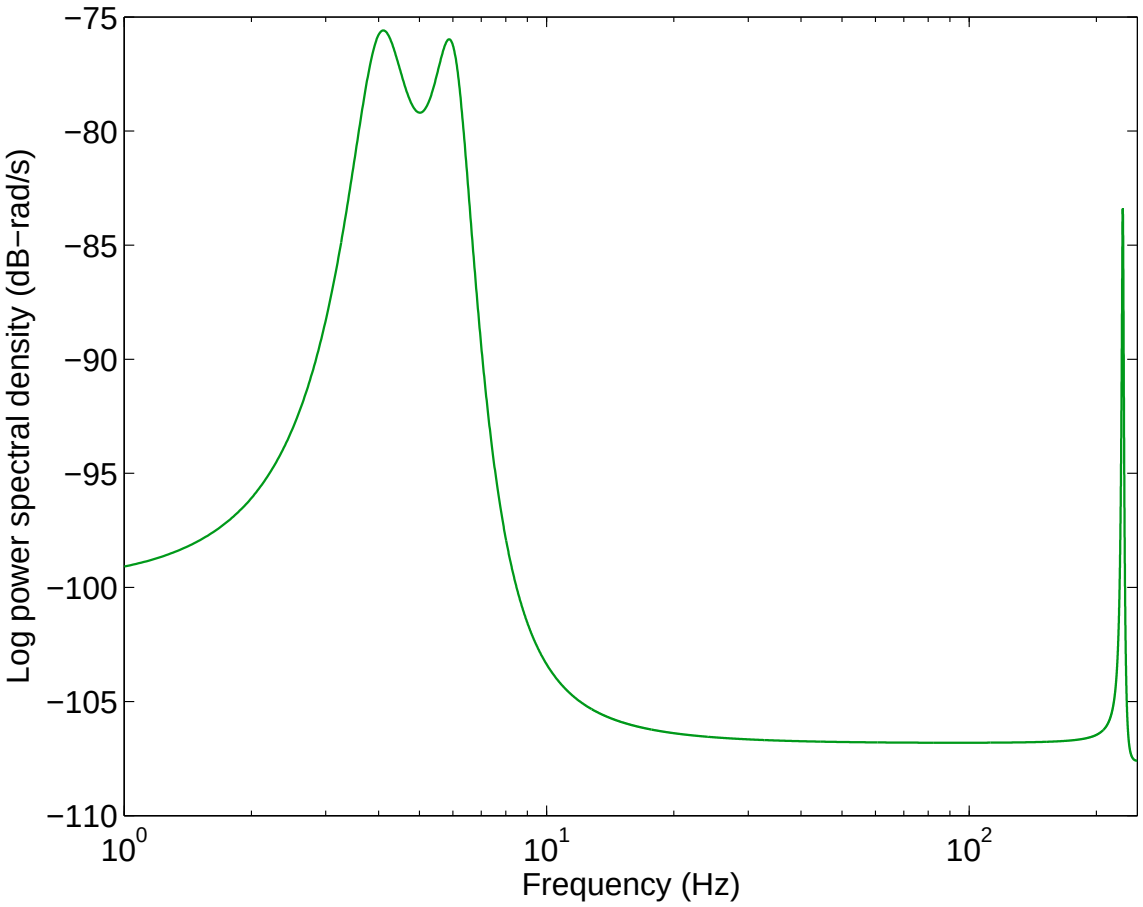

Figure 2.8: Power Spectral Density of the Yaw Rate Sensor Noise Model

2.4.2 Stochastic Driver Model

Although there exist numerous studies (such as Hess and Modjtahedzadeh [27], Kramer and Rohr [38], or Modjtahedzadeh and Hess [40]) that have focused on the development of dynamic models of humans as pilots or drivers, for the purposes of the work

presented here a stochastic model of driver input is used instead. Typical dynamic driver models require some knowledge of the environment surrounding the driver and vehicle, such as a view of the road and other nearby vehicles, or a measure of the offset between the vehicle and center of the lane. This sort of information is unavailable to a diagnostic system, thus deterministic driver models are not applicable. Rather, a stochastic model of typical driver steering input is used.

The driver input signal was hand-fit with a fourth-order model, shown in Figure 2.9. This model shows a sharp roll-off above 1 Hz, which fits intuition about typical driver commands.

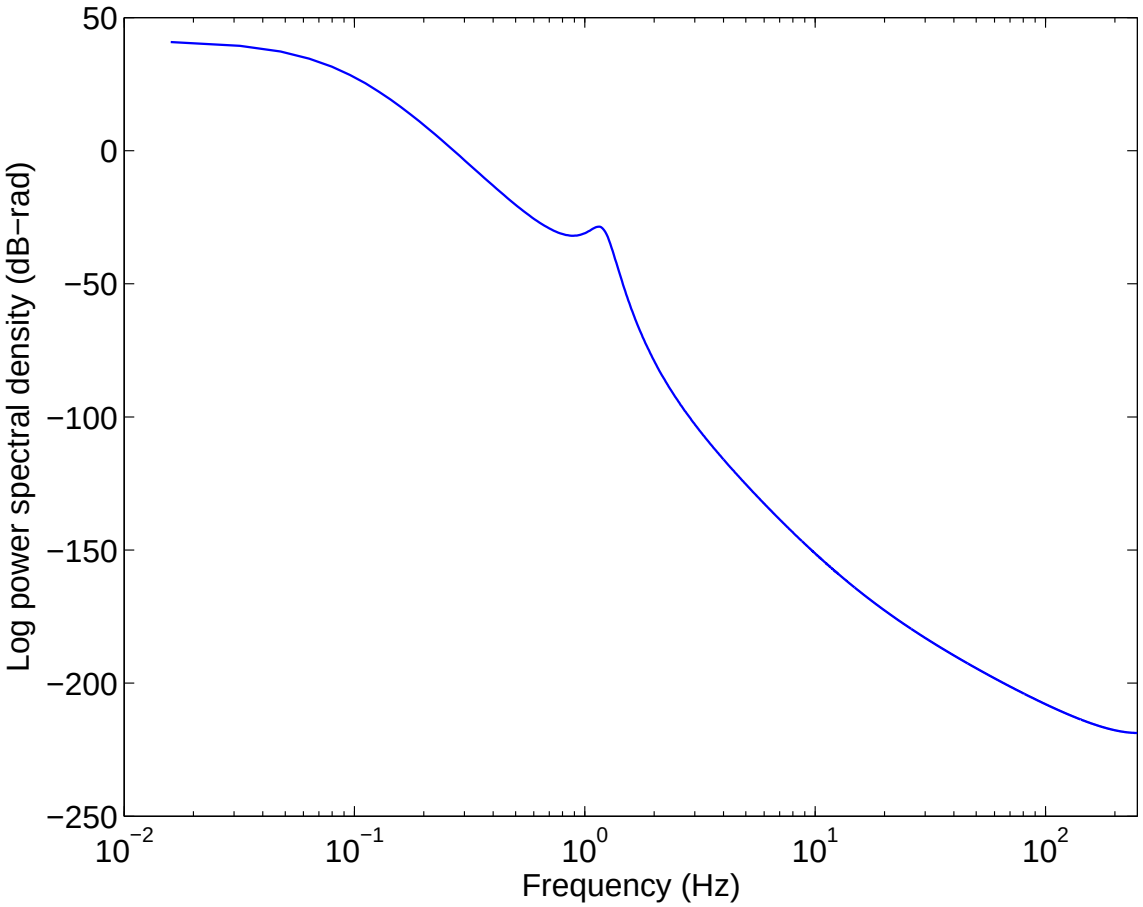

Figure 2.9: Power Spectral Density of the Stochastic Driver Model

2.5 Experimental Validation

While no model is perfect, in order to be useful a model must show reasonable agreement with experimental data. For diagnostic systems in particular, it is important to characterize the limitations of the model. In this section, time-domain plots of modeled vehicle and steering system behavior are compared to experimental results, showing how well the models developed in this chapter match experimental results.

Two different driving maneuvers are used here for model validation. The first is a double step-steer maneuver, where both front wheels are turned 2.5° to the right for three seconds, then back to center for three seconds, then turned 2.5° to the left for three seconds, and then back to center again. The second maneuver is a chirp input, sweeping from .25 Hz to 6 Hz over the course of 15 seconds, with an amplitude 5° peak-to-peak. Both maneuvers were generated in software and superimposed onto the driver's input signal. This was done to provide a consistent, repeatable test signal while still maintaining the driver's ability to control the vehicle for safety reasons. Both maneuvers were performed at approximately 16 m/s.

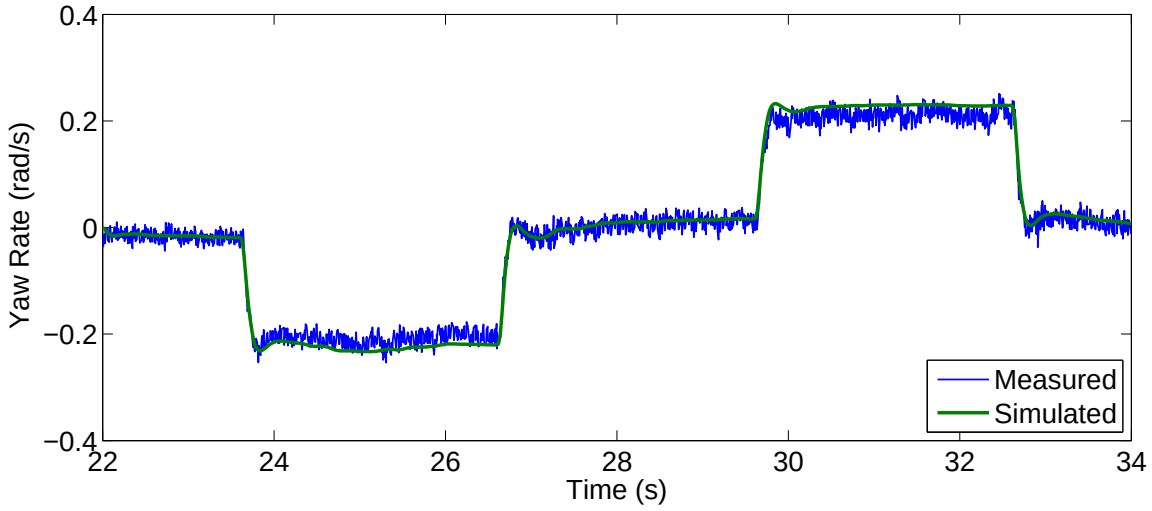

Figure 2.10: Comparison of vehicle dynamics model with experimental results for a step input

Figure 2.10 shows the response of the vehicle model, given by (2.8) and (2.9), to

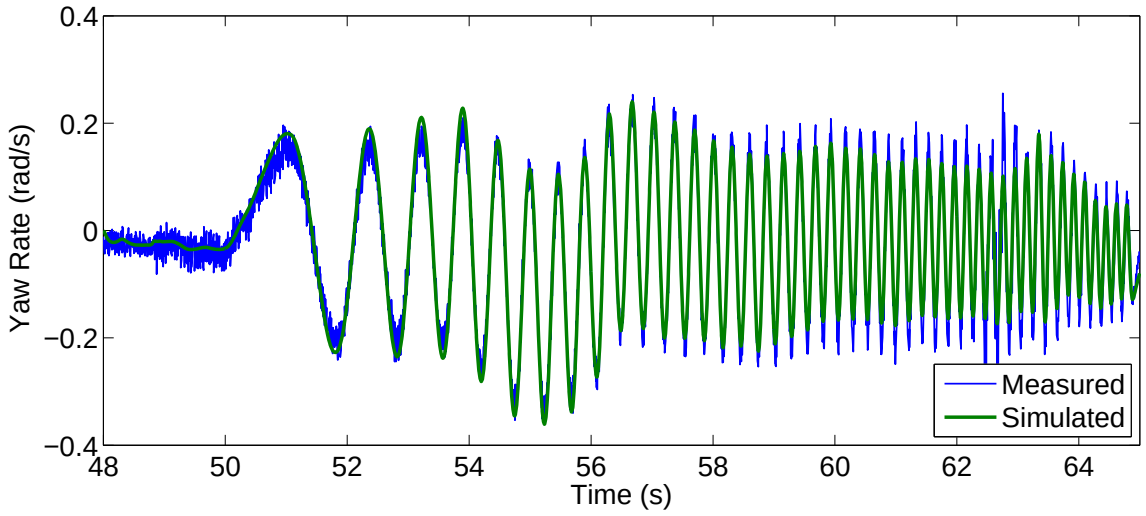

Figure 2.11: Comparison of vehicle dynamics model with experimental results for a chirp input

the double step-steer input. The inputs to this model are the two steer angles, δ_ℓ and δ_r, and the output is the yaw rate, r. This is plotted over the actual response of the vehicle, as measured by the yaw rate sensor. The model shows good agreement both in steady-state and in its transient response. Figure 2.11 shows the same comparison, only this time using the chirp maneuver instead of the double step-steer. Again the model agrees with the experimental results very well, although at frequencies above about 3Hz, a slight discrepancy in amplitude begins to emerge.

Figure 2.12 shows the double step-steer response of the steering system model, given by (2.40) and (2.41), combined with the vehicle model. The inputs to this combined model are the left and right motor currents, i_ℓ and i_r, and the output is the yaw rate. Again, there is very good agreement between the model and the experimental results, although not as good as with the vehicle model alone, since there are more sources of uncertainty in this combined model. Figure 2.13 shows a comparison of the combined model with experimental results for the chirp maneuver. Here the amplitude mismatch begins to manifest itself at around 2 Hz, but shows good agreement at lower frequencies.

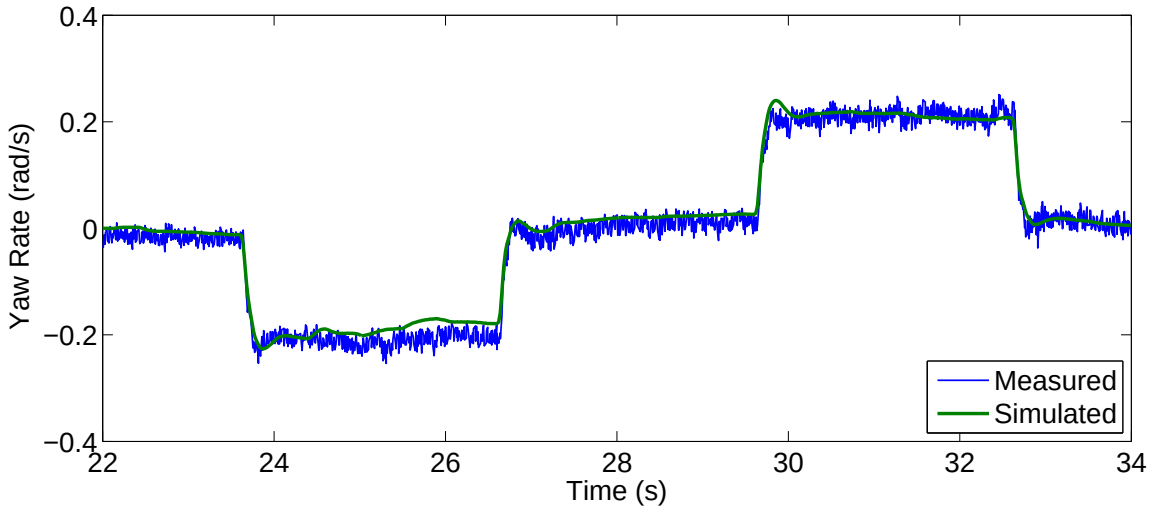

Figure 2.12: Comparison of steering system model with experimental results for a step input

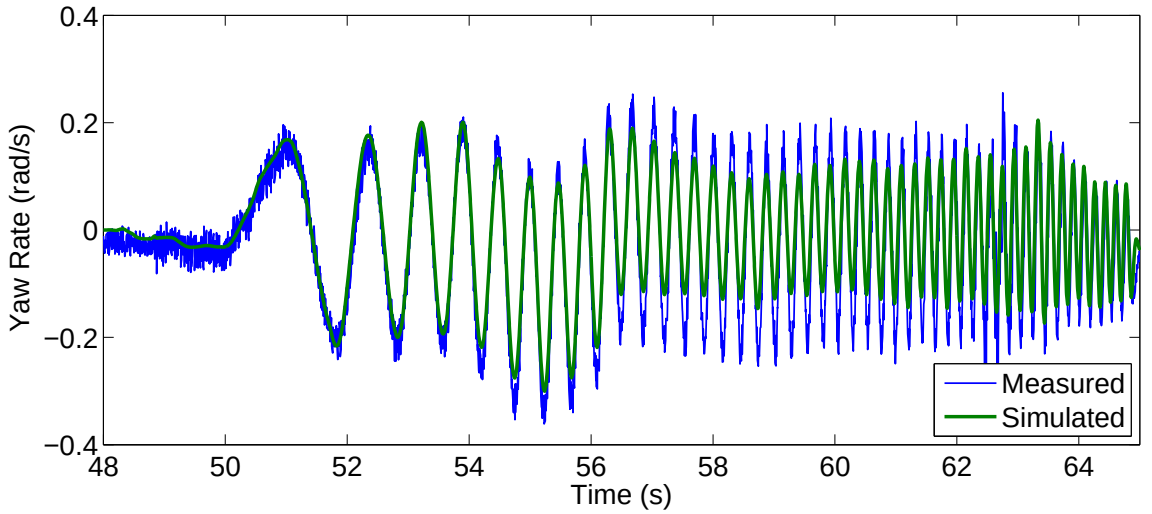

Figure 2.13: Comparison of steering system model with experimental results for a chirp input

2.6 Conclusion

This chapter described the experimental steer-by-wire vehicle developed in the course of this research. Detailed mathematical models were developed from first principles for the steering system and the vehicle dynamics. These models were validated against experimental data collected from the vehicle under a variety of driving maneuvers. Subsequent chapters willl use these models in the design of diagnostic filters for the steer-by-wire system.

Chapter 3

Analytic Redundancy for Sensor Reduction

3.1 Introduction

Steer-by-wire remains unavailable on production vehicles today, despite the numerous benefits it will provide, due to the expense of high-reliability designs. Model-based fault detection techniques can eliminate the need for redundant sensors in steer-by-wire vehicles, lowering costs without compromising reliability. Using the models developed in the previous chapter, this chapter presents the fault detection filter design techniques used to construct a set of diagnostic residuals. Based only on measurements from sensors already present in a steer-by-wire system, these residuals are suitable for detecting and isolating a wide variety of steering system faults. These diagnostic residuals are sensitive enough to detect faults at a magnitude well below where they would impact the driver's ability to control the vehicle, and in many cases below the level of driver perception. This chapter concludes with experimental results from P1 demonstrating this sensitivity.

An important component of such a diagnostic system is the collection of diagnostic residuals, which are used to detect and then isolate a fault. A common approach in fly-by-wire systems for aircraft relies on triply-redundant sensors to produce these residuals, so many steer-by-wire studies propose the same principle [19][26]. For

steer-by-wire vehicles this is a prohibitively expensive approach, so steer-by-wire has yet to find its way into a production vehicle. Through the use of analytic redundancy, however, it is possible to produce diagnostic residuals without the need for redundant sensors [36][20]. This chapter presents a set of residuals for a steer-by-wire system based on only measurements available from sensors that would already be have to be present in the steering system—encoders used for control of steer angle, current and voltage sensors for used for control of motor current—and a yaw rate sensor, commonly found in stability control systems.

The techniques presented here rely on relatively simple models of the steering system and vehicle dynamics, and the diagnostic residuals are formed using very straightforward parameter and state estimation techniques: recursive least-squares estimators and extended Kalman filters. Despite the comparative simplicity of the models and filtering techniques used, the methods presented here provide residuals that are both highly sensitive to faults and able to distinguish a wide variety of different fault conditions. In addition to a description of the models and filters used, this chapter discusses a number of the technical details that require attention in order to get good diagnostic performance.

It is natural in designing a diagnostic system to focus on a particular component, such as a steering motor, with the aim of developing a residual that will indicate when the particular component is malfunctioning, repeating this process for each component in the system. This approach, however, neglects both the interactions between various components, and the inherent decoupling that is present in many systems. This results in a diagnostic system that requires additional sensors, or suffers from poor sensitivity to faults. In contrast to this approach, the diagnostic residuals in this chapter are based on a model of the entire steering system and vehicle dynamics. Each residual is sensitive to a number of different possible fault conditions as decoupling occurs not along component boundaries, but where the models suggest there exists an inherent independence. For example, the model of a steering motor shows that the angular position of the output shaft has a strong dependence on the external torques being applied to it by the steering linkage, so no attempt is made to model the motor independently from the steering linkage to which it is connected.

At the same time, the electrical characteristics of a motor can be written such that they have no dependence on the mechanical properties of the motor, and this natural decoupling is used to an advantage in designing the diagnostic filters presented here.

This approach results in a set of diagnostic residuals with two important characteristics. The first of these is their sensitivity: in many cases it is possible to detect faults that are too subtle for the driver to notice. This presents the possibility of a system where faults can be detected and accommodated before they ever adversely affect the handling of the vehicle. The second characteristic is that each residual is sensitive to only a limited set of possible faults such that, in general, each fault condition excites a unique set of the residuals, making it possible to isolate the source of the fault. As there are a variety of methods available for the processing of these residuals, such as simple fixed or adaptive thresholds or the Bayesian network-based approach of Schwall [48], the remainder of this chapter focuses on the design of these diagnostic residuals, rather than on how to make a final diagnosis.

3.2 Steer-by-wire Diagnostic System Overview

The steer-by-wire diagnostic system presented here has been designed for use with the steering system used on the P1 experimental steer-by-wire vehicle, although the techniques presented here are quite general and ought to apply to variety of steer-by-wire systems designs. Table 3.1 shows a list of possible faults and the collection of residuals that can be used to detect and isolate these faults. The first four residuals, denoted R_{Rl}, R_{Rr}, R_{kl}, and R_{kr}, are based on a comparison of nominal and estimated motor parameters. These are described in section 3.3. The next three residuals, R_r, $R_{\delta l}$, and $R_{\delta r}$ are based on the model of the steering system and vehicle dynamics. These are described in section 3.4. The last four residuals, R_{Il}, R_{Ir}, R_{el}, and R_{er}, are simply the tracking error in the left and right motor current loops and the left and right steer angle loops. This collection of eleven residuals makes it possible to detect and isolate a wide variety of steering system faults.

Table 3.1: Fault isolation logic

Fault	R_{Rl}	R_{Rr}	R_{kl}	R_{kr}	R_r	$R_{\delta l}$	$R_{\delta r}$	R_{Il}	R_{Ir}	R_{el}	R_{er}
Left current sensor	•		•			•		•			
Right current sensor		•		•			•		•		
Left voltage sensor	•		•								
Right voltage sensor		•		•							
Left steer angle sensor					•	•					
Right steer angle sensor					•		•				
Yaw rate sensor					•	•	•				
Left motor resistance change	•										
Right motor resistance change		•									
Left motor constant change			•			•					
Right motor constant change				•			•				
Left motor friction change						•					
Right motor friction change							•				
$C_{\alpha fl}$ change					•	•					
$C_{\alpha fr}$ change					•		•				
Left amplifier failure								•		•	
Right amplifier failure									•		•
Left steering controller failure										•	
Right steering controller failure											•
Battery failure						•	•			•	•

3.3 Motor Parameter Estimation

One approach for diagnosing faults in the electrical portion of the steering motors is to use a real-time recursive least-squares estimator to estimate continuously the electrical resistance and motor constant of the steering motors. By modeling the back-EMF produced by the motors, these parameter estimates can be formed without having to consider the load on the motors. This approach is similar to the technique used in [41], however, in that work the effects of motor inductance are ignored and the motor being diagnosed is a three-phase, brushless DC motor.

3.3.1 Theory

In order to apply a least-squares estimation approach, the problem needs to be rewritten in the form of $y = Ax$, where A and y are either known or directly measurable and the parameters to be estimated are contained in x. The model given by (2.42) can be written in this form, with $y = v - L\frac{di}{dt}$, $A = [i\ \omega]$, and $x = [R\ k]^T$. This requires that we be able to directly measure motor terminal voltage, v, motor current, i, and its first derivative, and angular velocity, ω. Note that there are a number of ways this problem could be cast as a least-squares estimation problem. Here we choose to estimate only resistance and motor constant, although using this approach a filter could be designed to estimate any combination of motor inductance, motor resistance, motor constant, and aggregate sensor bias.

In order for a recursive least-squares estimator to detect changes in either the motor constant or the electrical resistance of the motor and wiring harness, the estimator must have some way of emphasizing newer data, and disregarding older data. Otherwise, the estimator would eventually become largely insensitive to new data and would only detect changes in motor parameters after they had been present for a long time, which is not useful. One simple and common way to accomplish this is by applying an exponential weighting to the data as it becomes available, increasing the importance of the most recent data, and decreasing the importance data as it becomes older. This introduces an adjustable parameter, λ, commonly referred to as the "forgetting factor", which controls the rate at which older data is de-emphasized.

Setting λ to 1 corresponds to standard least-squares, where all data is considered equally important and there is no exponential weighting. Setting λ to 0 results in a filter which has no memory of past data at all (which in general presents numerical problems). Typical values for λ are between 0.9 and 1.

The standard algorithm for recursive least-squares estimation with exponential weighting is as follows:

```
Initialization
 x   :=  x_0
 P   :=  P_0

At each time step
 k   :=  Pa / (λ + a^T P a)
 P   :=  (1/λ)(I − k a^T) P
 x   :=  x + k(y − a^T x)
```

3.3.2 Implementation Considerations

There are a number of practical considerations that need to be taken into account in order to make this diagnostic technique work well. Recursive least-square algorithms have persistence of excitation requirements which must be accommodated. In the case of P1, there is no direct measurement of angular rate, and existing motor current data is very noisy. When sampling continuous-time signals, antialiasing filters are often required, and when used, the dynamics of these filters need to be accounted for. Lastly, an appropriate value for λ must be selected, such that the filter both rejects noise on the measurements and responds quickly enough to changes in parameter value.

Persistence of Excitation

There are a number of techniques for dealing with the need for persistence of excitation. In this implementation we have chosen to simply halt the filter whenever either the current or the angular rate are too close to zero (within 0.01 A or 0.01 rad/s). This prevents the internal state of the filter from diverging when driving in a straight

line, which is the most common cause of a lack of excitation in this application. While it is possible for non-zero inputs to still lack sufficient excitation, such as if the current and angular rate were to vary but in a fixed ratio, on the P1 steering system this has not been observed.

Derivative Signals

Although there are no angular rate sensors on the steering motors on P1, the motor shaft angle measurements are provided by reasonably high-resolution optical encoders. Since these measurements are essentially noise-free, and have only a very small amount of quantization error present, it is possible to just differentiate numerically to find an estimate of the angular rate. This same approach is also used for di/dt, and although this results in a relatively noisy signal, in practice the benefits of accurately modeling the effects of motor inductance outweigh the penalty of this additional noise.

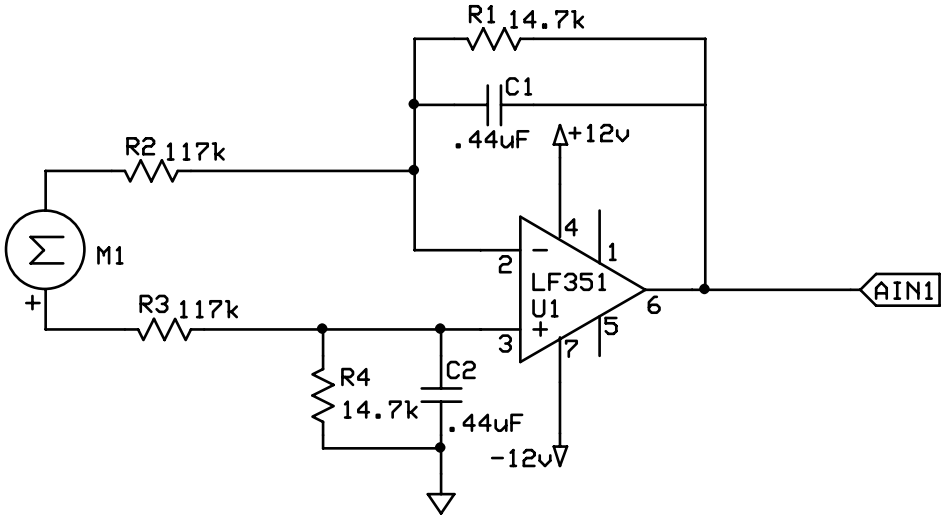

Figure 3.1: Motor voltage signal conditioning circuitry

Antialiasing

The voltage applied to the motor terminals is pulse-width modulated by the amplifier at frequency of 32 kHz, which far exceeds the sampling frequency of 500 Hz, thus

analog antialiasing filters are required. The circuitry used to provide this filtering is shown in Figure 3.1. This differential amplifier circuit provides roughly 80 dB of attenuation at the switching frequency. It also scales the motor terminal voltage down by a factor of 8 so that the output can be fed directly to the A/D converter. However this is largely transparent as the signal is scaled back up by the hardware interface layer of the software. Effectively, the transfer function for this filter is given by:

$$H(s) = \frac{174}{s + 174} \tag{3.1}$$

If the estimates of ω, i, and di/dt are not passed through this same filter, the simple algebraic relationship given by (2.42) no longer holds, and not surprisingly, the quality of the parameter estimates will suffer, particularly when v is changing quickly. One simple solution to this problem is to filter ω, i, and di/dt in software using a discrete-time approximation of this filter. The simulations and experimental results presented here all use this technique.

Filter Tuning

As λ is the only free parameter, tuning the recursive least-squares estimator is not a difficult procedure, however, it is best to have access to some actual data. The value for λ must be strictly less than 1, or the filter will not be able to detect faults. Reasonable values for λ tend to range from 0.9 to 0.9999. Larger values result in a filter which is responds to noise less, but detects faults more slowly, while smaller values give a quicker response time, with more noise sensitivity.

For a given sampling period, T_s, the effective time constant of the filter can be determined by the following:

$$\tau = -\frac{T_s}{\ln(\lambda)} \tag{3.2}$$

where τ is the effective time constant in seconds. This can be used to aid in the selection of λ if there are specific detection time goals. Note that the actual time required to detect a fault will depend not only on the values of τ but on the level of filter excitation when the fault occurs, the magnitude of the fault, and the fault

detection threshold. In all of the experimental and simulated results presented here, $\lambda = 0.995$ and the sampling period is 2 ms, providing an effective filter time constant of about 0.4 seconds.

3.3.3 Experimental Results

The following figures were generated by passing data collected from P1 to the same recursive least-squares estimators as were used in the previous section. The data was collected while driving at approximately 10 m/s with a 1 Hz slalom of 6° steering angle, as measured at the road wheels.

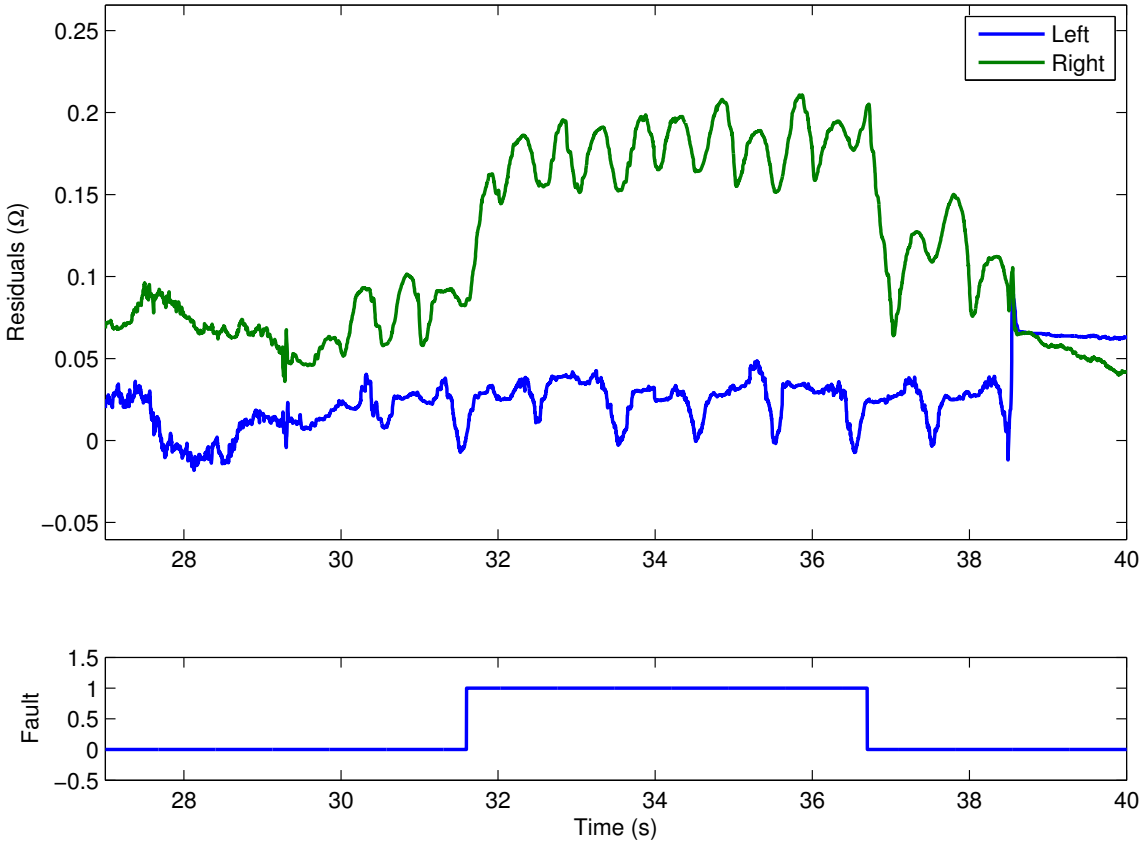

Figure 3.2: Recursive least-squares resistance residuals responding to a fault of 0.1 Ω increase in motor resistance

In Figure 3.2 a 0.1 Ω (roughly 20%) increase in right motor resistance is introduced at approximately $t = 31.5$ s and then removed at $t = 36.5$ s. (These times are approximate, as P1's data collection system does not record exactly when the fault is introduced.) This fault is introduced by opening a bypass relay and forcing motor current to pass through a 0.1 Ω power resistor in series with the motor raising the combined resistance by the same amount.

In response to this fault, the residual rises as expected by roughly 0.1 Ω. Note that the residual for the right motor is approximately 0.075 Ω higher than expected both when the fault is present and when it is not. This may be due to additional resistance in the fault simulation circuitry or perhaps an inherent difference in nominal motor resistance. This effect can be seen throughout the test results presented here.

In Figure 3.3 a 3° left steer angle sensor bias is introduced at $t = 44$ s and then removed at $t = 48$ s. This fault is introduced by changing the value returned by the sensor in software at run-time. The steering controller tries to correct for this fault while the test is being conducted.

In Figure 3.4 an 8 A left current sensor bias is introduced at $t = 26.5$ s and removed at $t = 31.5$ s. This fault is introduced in software at run-time, as with the steering angle sensor fault. However, this fault is not applied to an input, but rather to the commanded current output. The reason for this is that the amplifier has its own internal feedback loop controlling the current, so an actual fault in the current sensor should cause the amplifier to drive a different current through the steering motors. In order to achieve this effect through software, the current command is modified so that the amplifier will behave as though its own current sensor has the fault. Since the commanded current is used as a proxy for measured current in these diagnostic filters, this simulated fault will also affect the residuals generated by the recursive least-squares estimator, just as an actual current sensor bias would. This can clearly be seen in Figure 3.4.

Note that these parameter estimation residuals are sensitive not just to changes in the parameter they are designed to estimate, but also to sensor faults on which those estimates are based. This may seem like a flaw in the design of these filters, but keep in mind that precise decoupling of one fault from another by any single residual is

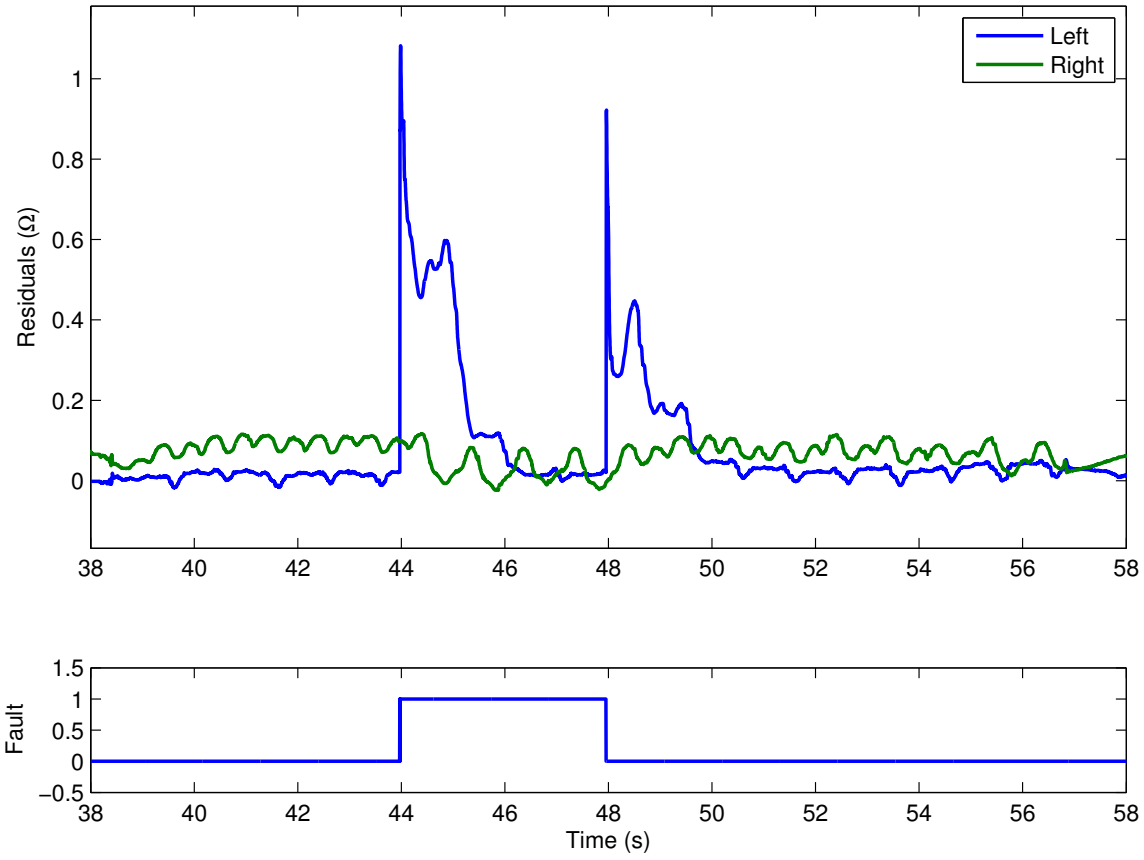

Figure 3.3: Recursive least-squares resistance residuals responding to a 3 steer angle sensor bias

not a requirement of this diagnostic system. It is only required that each fault have a unique combination of residuals that are sensitive to it.

3.4 Vehicle and Steering System Dynamics

There are three residuals based on models of vehicle dynamics and steering system dynamics: a yaw rate estimator residual, R_r, a left steer angle estimator residual, $R_{\delta l}$, and a right steer angle estimator residual, $R_{\delta r}$. The first of these uses only a model of vehicle dynamics, generating an estimate of vehicle yaw rate based on measurements of both steer angles. The second and third each use a model of vehicle dynamics and

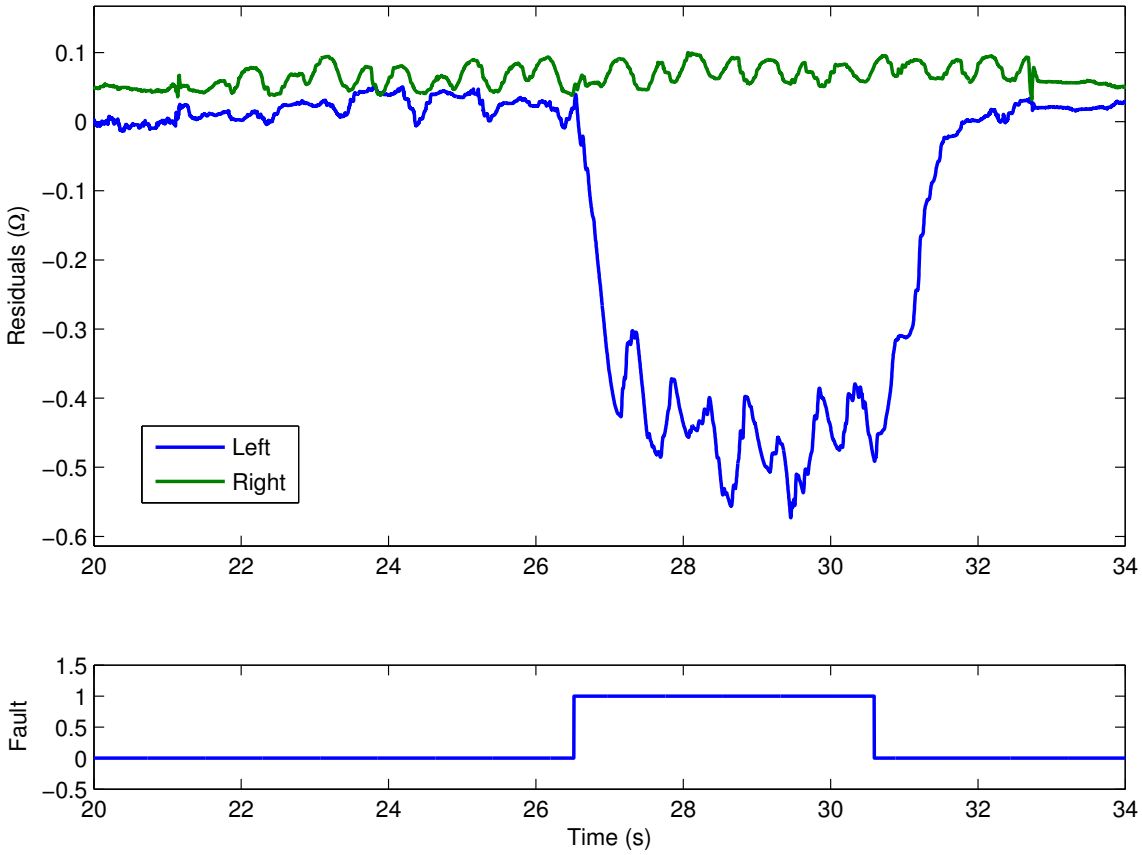

Figure 3.4: Recursive least-squares resistance residuals responding to an 8 A current sensor bias

a model of either the left or right steering system to generate an estimate of the left or right steer angle, based on measurements of yaw rate, the current in one steering motor and the steer angle of the opposite steering motor.

3.4.1 Theory

Yaw Rate Estimator Residual

The yaw rate estimator residual uses the five-state bicycle model developed in the preceding chapter to generate an estimate of the vehicle yaw rate, using measured left and right steer angles as input. This estimated yaw rate is compared to the measured

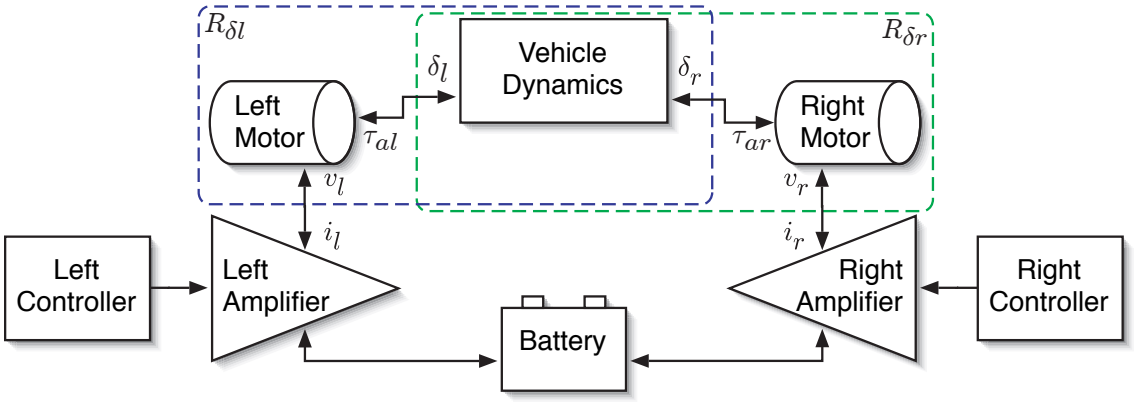

Figure 3.5: P1 steer-by-wire system block diagram

yaw rate to form the residual. Thus R_r is computed by the following:

$$\hat{x}[k+1] = A\hat{x}[k] + B \begin{bmatrix} \delta_\ell[k] & \delta_r[k] \end{bmatrix}^T \tag{3.3}$$

$$\hat{r}[k] = C\hat{x}[k] \tag{3.4}$$

$$R_r[k] = r[k] - \hat{r}[k] \tag{3.5}$$

where (3.3) and (3.4) are the discretized versions of (2.8) and (2.9).

The A and B matrices in (3.3) both depend on the vehicle speed, so this model is not LTI. Since the speed of the vehicle is largely independent of state of the planar dynamics, the speed can be regarded as an independent input, making this an LTV system.

Left Steer Angle Estimator Residual

The left steer angle estimator residual uses the model of planar vehicle dynamics, given by (2.8) and (2.9), in combination with the model of just the left steering system, given by (2.40) and (2.41). The steer angle, δ_ℓ, output by the steering model is connected to the corresponding input of the vehicle dynamics model, which in turn calculates a the torque applied about the steering motor, τ_ℓ which is then fed back to the corresponding input to the steering model, as shown in Figure 3.6. This results in a seven-state model described by the following:

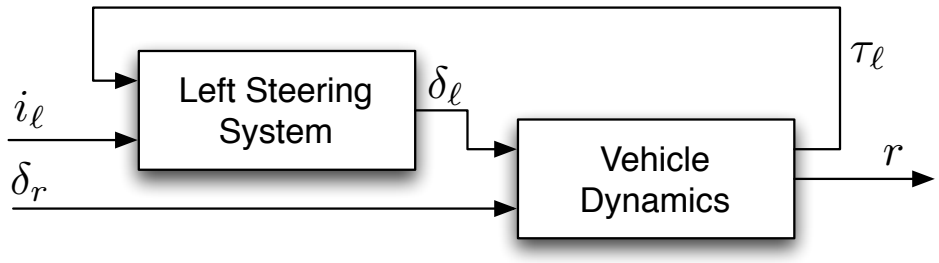

Figure 3.6: System model for left steer angle residual

$$\dot{x} = A_c x + B_c \begin{bmatrix} \tau_{eff,l} & \delta_r \end{bmatrix}^T \tag{3.6}$$

$$\begin{bmatrix} r & \delta_\ell \end{bmatrix}^T = C_c x \tag{3.7}$$

where

$$x = \begin{bmatrix} x_v^T & \delta_l & \dot{\delta}_l \end{bmatrix}^T \tag{3.8}$$

$$A_c = \begin{bmatrix} & & A_v & & & & B_{v1} & 0 \\ & & & & & & & \\ 0 & & 0 & 0 & 0 & 0 & 0 & 1 \\ \frac{C_{\alpha f l} t_t(\delta)}{J_{eff}(\delta)} & & \frac{a C_{\alpha f l} t_t(\delta)}{J_{eff}(\delta) V_x} & 0 & 0 & 0 & \frac{C_{\alpha f l} t_t(\delta)}{J_{eff}(\delta)} & -\frac{b_{eff}(\delta)}{J_{eff}(\delta)} \end{bmatrix} \tag{3.9}$$

$$B_c = \begin{bmatrix} 0 & B_{v2} \\ 0 & 0 \\ \frac{1}{J_{eff}(\delta)} & 0 \end{bmatrix} \tag{3.10}$$

$$C_c = \begin{bmatrix} 0 & 1 & 0 & 0 & 0 & 0 & 0 \\ 0 & 0 & 0 & 0 & 0 & 1 & 0 \end{bmatrix}, \tag{3.11}$$

and B_{v1} and B_{v2} denote the first and second columns of B_v, which is defined in (2.12).

This model is then discretized using a forward-Euler approximation with a sample

time of 2 ms. This leads to the following discretized model:

$$x[k+1] = (I + T_s A_c)x[k] + T_s B_c \begin{bmatrix} \tau_{eff,l}[k] & \delta_r[k] \end{bmatrix}^T \quad (3.12)$$

$$\begin{bmatrix} r[k] & \delta_l[k] \end{bmatrix}^T = C_c x[k] \quad (3.13)$$

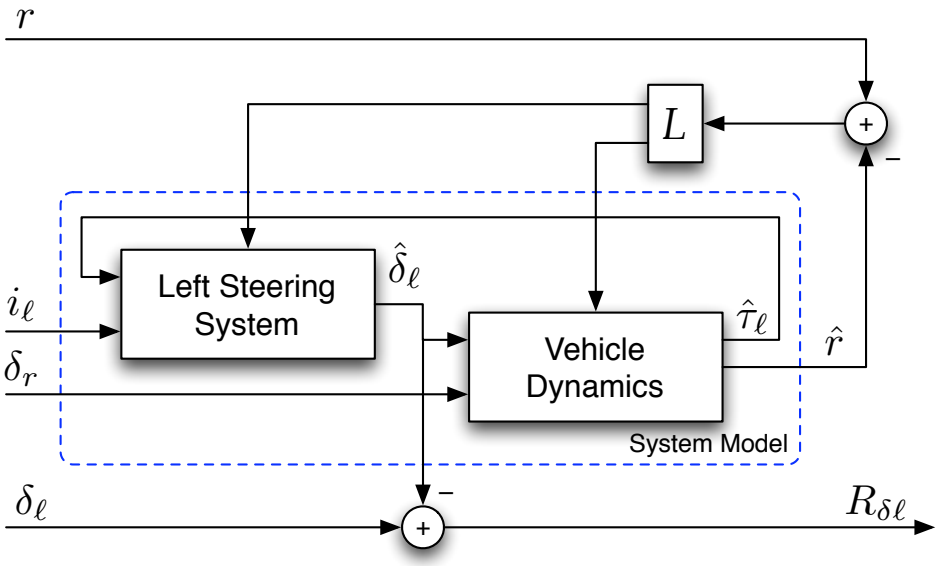

Figure 3.7: Structure of the diagnostic filter for left steer angle residual

In order to incorporate information provided by the yaw rate sensor into a diagnostic filter based on this model, a Luenberger observer structure is required. The right steer angle and the left motor current are both inputs to this model, but the yaw rate is only an output, so without a feedback path provided by an observer structure, there would be no way to include yaw rate measurements. This is illustrated in Figure 3.7, which shows the structure of the Luenberger observer used for this diagnostic filter. The observer generates an estimate of the left steer angle, $\hat{\delta}_\ell$, which

is compared to the measured value of the left steer angle, δ_ℓ, to form this residual:

$$\hat{x}[k+1] = (I + T_s A_c - LC_{c1})\hat{x}[k] + T_s B_c \begin{bmatrix} \tau_{eff,l}[k] & \delta_r[k] \end{bmatrix}^T + Lr[k] \quad (3.14)$$

$$\hat{\delta}_\ell[k] = C_{c2}\hat{x}[k] \quad (3.15)$$

$$R_{\delta\ell}[k] = \delta_\ell[k] - \hat{\delta}_\ell[k]. \quad (3.16)$$

Unlike the yaw rate residual in the preceding section, which used a simple, open-loop model, with this residual there are design variables which need to be selected. The observer gains, L, determine how sensitive the residual is to various types of faults. For example, in the case of $L = 0$, the residual will be completely insensitive to yaw rate sensor faults.

Unfortunately, $L \in \mathbb{R}^7$, which is a large enough space that it becomes difficult to manually choose an appropriate value for L. Many choices of L result in a filter that is unstable and useless for diagnostic purposes. There are a couple of standard techniques that make selecting a set of observer gains easier. The simplest of these is pole placement, wherein you can directly select the eigenvalues of $(I + T_s A_c) - LC_{c1}$, then solve for the appropriate value of L. This immediately avoids the problem of unstable filter designs (as one can simply refrain from placing poles outside the unit circle), but still lacks any intuitive relationship between filter pole locations and the sensitivity of the filter to various fault conditions.

Another technique for selecting observer gains is the steady-state Kalman filter. The Kalman filter is the optimal (minimum mean square error) state estimator for a linear system subject to Gaussian noise. It can be shown that, independent of its input, the Kalman filter's state error covariance matrix converges to a steady-state value, at which point the filter is identical in structure to a Luenberger observer. The observer gains can be computed by solving an algebraic Riccati equation, using the system matrices and the covariance matrices of the various noise sources. In the case of this diagnostic filter, an optimal state estimate is of no interest, but a set of observer gains is precisely what is needed. Designing a hypothetical Kalman filter turns the problem of choosing observer gains into choosing noise covariances, which have a much more natural interpretation: the larger the covariance associated with a

particular sensor, the less sensitive the resulting filter will be to the signal from that sensor.

In general, the Kalman filter equations require a pair of positive semi-definite matrices of process noise covariance, Q, and output sensor noise covariance, R, where $Q \in \mathbb{R}^{n \times n}$, $R \in \mathbb{R}^{m \times m}$, n is the number of states, and m is the number of outputs. For this particular diagnostic filter,

$$Q = B_c^T \begin{bmatrix} q & 0 \\ 0 & 0 \end{bmatrix} B_c \qquad q > 0, \tag{3.17}$$

and R is a scalar, since there is only one output sensor measurement. This reduces the observer gain selection problem down to the selection of just two values, R and q, with the simple interpretation that larger values of q reduce the sensitivity of the filter to current sensor measurements, and larger values of R reduce the sensitivity of the filter to yaw rate measurements.

Just as with the model for the yaw rate residual, the system matrices, A_c and B_c depend on the speed of the vehicle. This can be readily addressed through gain scheduling by designing a series of diagnostic observer gains, spread over the range of speeds at which the vehicle is designed to operate, then choosing at run-time the most appropriate set of gains for the vehicle's current speed. Additionally, the A_c and B_c matrices now have a number of steer angle-dependent entries, $J_{eff}(\delta)$, $b_{eff}(\delta)$, and $t_t(\delta)$ which introduce slight non-linearities into this model. In order to use a steady-state Kalman filter-based design method, the model can be linearized about a steer angle of 0.

Right Steer Angle Estimator Residual

The right steer angle estimator residual uses the same structure as that of the left, described in the preceding section. The only difference is that the estimator uses a model of the right steering system instead of the left, and relies on measurements of right motor current and left steer angle. The Luenberger observer structure remains the same.

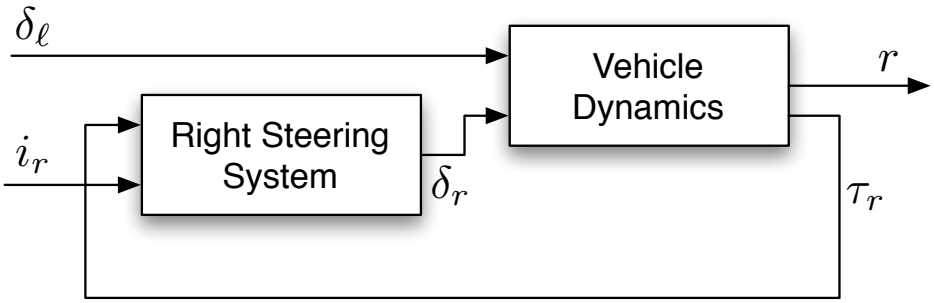

Figure 3.8: System model for right steer angle residual

3.4.2 Implementation Considerations

Sensors

An accurate measure of steer angle is essential. As the harmonic drive gearboxes have essentially no backlash, the steer motor encoder measurement (once translated through the gearbox and the steer linkage) can be used as a noise-free, high-resolution steer angle measurement. Vehicle velocity is taken from front wheel speed sensors, which is low-pass filtered to smooth the signal out.

The yaw rate measurement is based on an automotive-grade yaw gyro. As automotive gyros tend suffer a very low-frequency bias, for the results presented here, this sensor bias is measured when the vehicle is not in motion and then subtracted off to provide a measurement of yaw rate that is largely free of bias. In practice this same effect could be achieved by high-pass filtering the yaw rate signal with a very low cutoff frequency, or by using a Kalman filter to estimate sensor bias.

The diagnostic filters use the amplifier current commands as current inputs, because the P1 test vehicle does not provide a clean measurement of motor current. There is effectively no difference between the commanded current and the actual motor current, since the bandwidth of the amplifiers is much higher than the speed at which these diagnostic filters operate.

3.4.3 Experimental Results

In this section, the diagnostic filter's performance is shown in the presence of faults. The faults used are instantaneous biases on the left steer motor current, the left steer angle measurement, and the yaw rate measurement. The test maneuvers consist of straight driving and 1 Hz slaloms at approximately 15 m/s.

For steer angle residuals, the practical detection threshold depends on the speed of the vehicle. This is because the effect on yaw rate of a particular steer angle varies with vehicle speed. So at 10 m/s a steer angle error of 3° would result in an unintended yaw rate of roughly 6 deg/s. At 15 m/s, the vehicle yaw is rate is more sensitive to steer angle, and a steer angle error of just 2° will produce the same unintended yaw rate of ∼6 deg/s. The relationship between steady-state steer angle error, δ_{ss}, and steady-state yaw rate error, r_{ss}, is shown in Figure 3.9 and is given by the following:

$$\delta_{ss} = \frac{2(a+b+KV^2)}{V} r_{ss} \tag{3.18}$$

where K is the understeer gradient, given by:

$$K = \frac{m}{a+b}\left(\frac{b}{C_{\alpha fl}+C_{\alpha fr}} - \frac{a}{C_{\alpha r}}\right). \tag{3.19}$$

The practical implication of this is that while sensitivity to yaw rate sensor faults remains relatively constant as vehicle speed varies, the sensitivity to steer angle sensor faults varies significantly. Interestingly, the sensitivity to steer angle faults varies in the same fashion that a driver is able to notice a steer angle fault: at high speeds, a driver may notice a steer angle error of less than a degree, while at low speeds it takes a much larger steer angle error for a driver to be able tell that something is wrong. Having a diagnostic sensitivity that tracks driver sensitivity is convenient, since the ultimate criteria for a successful diagnostic system is one that can detect faults before they can adversely impact the driver's ability to steer the vehicle.

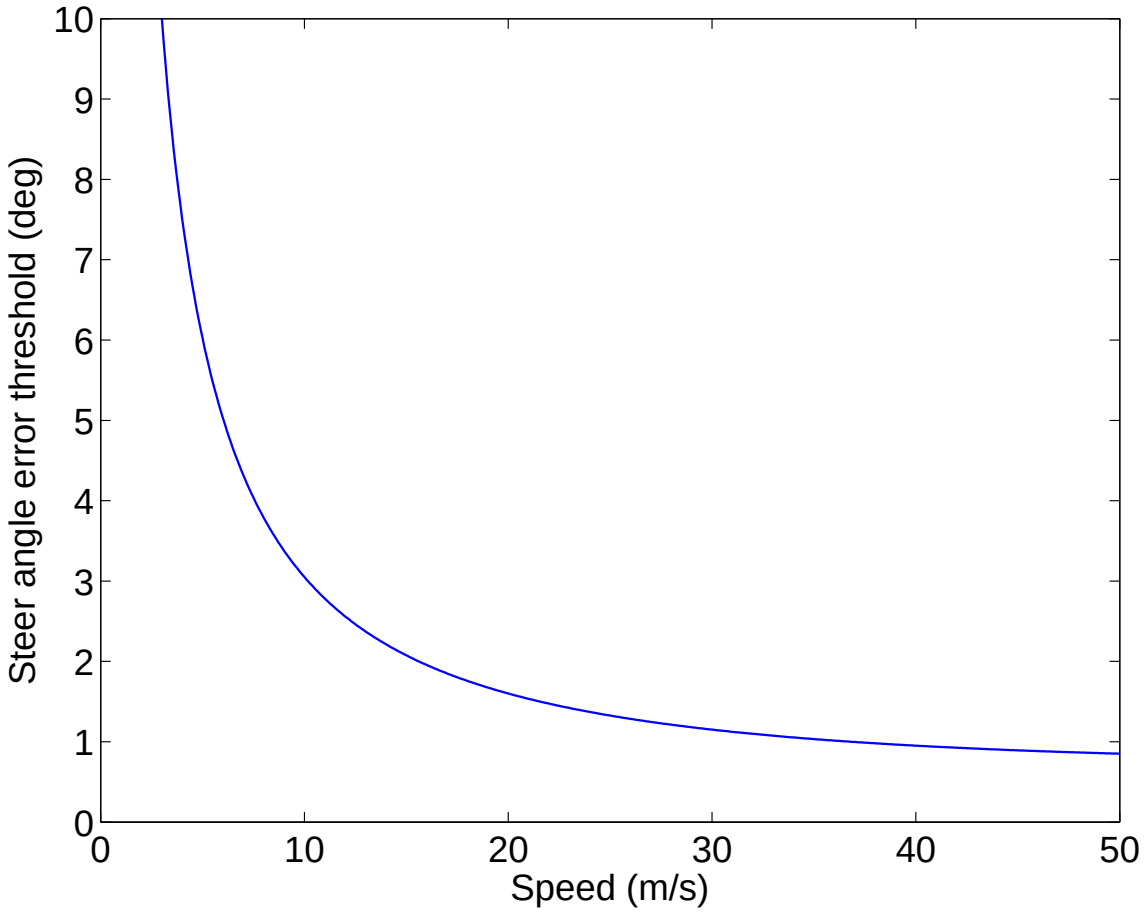

Figure 3.9: Steer angle fault sensitivity as a function of speed for a yaw rate fault sensitivity of 6 deg/s.

Yaw Rate Faults

Figures 3.10 and 3.11 show the experimental response to the sudden introduction of an 8 deg/s bias on the yaw rate sensor. Since the yaw rate measurement is subtracted directly from its estimate to form the residual, the fault appears after just one time step T_s in the residual. A yaw rate fault causes residuals to appear in all three signals. The reason that it appears as both a left and a right steer angle residual is because both of these filters rely on the yaw rate measurement, which is faulted. This signature of triggering all three residuals is unique to yaw rate faults.

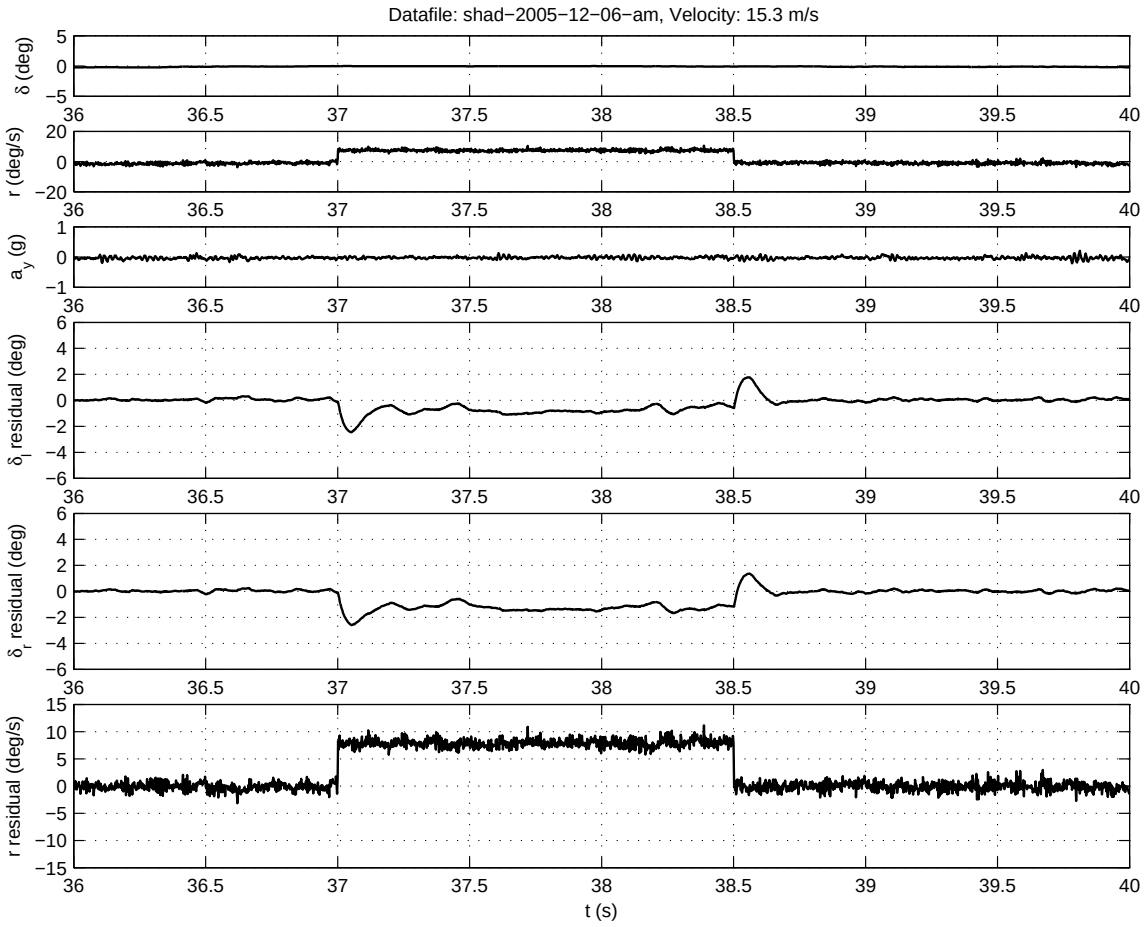

Figure 3.10: Experimental straight driving, 15 m/s, 8 deg/s yaw rate fault

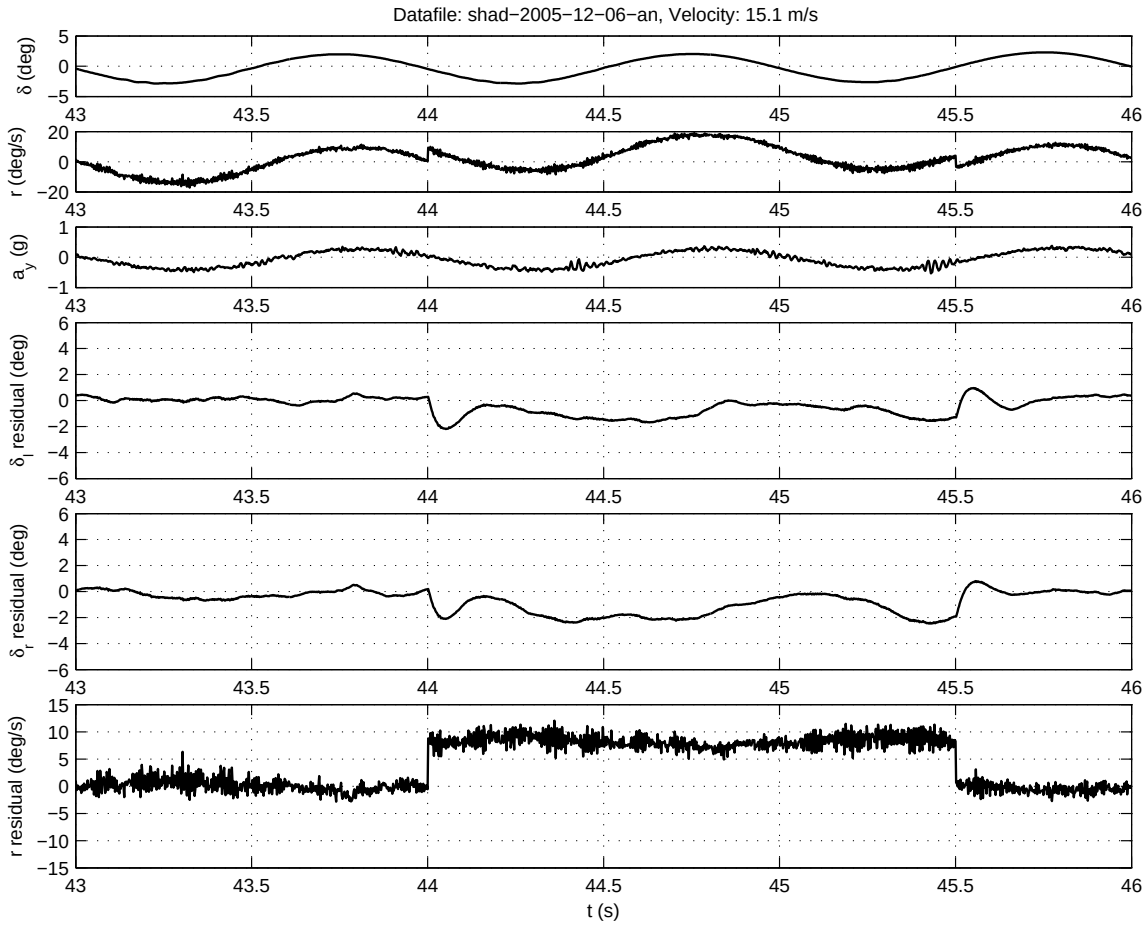

Figure 3.11: Experimental slalom, 1 Hz, 15 m/s, 8 deg/s yaw rate fault

Left Motor Current Faults

Figures 3.12 and 3.13 show the experimental results of an 8 A motor current sensor bias on the left current sensor. A motor current fault on the left wheel causes a residual on the left steer angle, but not on the right steer angle or yaw rate. This is because the left steer angle estimate is the only one that uses the left motor current as an input. The other two filters do not use the left motor current. This signature of triggering a residual only in one of the steer angles is unique to current faults. Right motor current faults look analogous to left motor current faults except on the opposite side, so plots are not shown for them.

Since current faults have to pass through the modeled steering system dynamics in the diagnostic filters, they do not appear instantaneously in the residuals. They take about 100-150 ms to appear.

In practice, there are other things that can also be interpreted as a current sensor fault. For example, excessive friction in the left gearbox or steering linkage would also generate a left steer angle residual without triggering either of the other two residuals. Perhaps a broader interpretation is that this type of fault is any effect that causes something not captured by the steering system model, i.e. some torque mismatch, which is the same as a scaled current mismatch.

Left Steer Angle Faults

Figures 3.14 and 3.15 show the results of experiments where a 3° bias is introduced suddenly on the left steer angle sensor. A left steer angle fault causes both left steer angle and yaw rate residuals. The reason that it appears as a yaw rate residual is because the yaw rate estimator uses it directly as an input. This signature of triggering just two residuals, the steer angle itself and the yaw rate, is unique to steer angle faults. Since the steer angle measurement is subtracted directly from its estimate to form the residual, the fault appears after just one time step T_s in the residual.

It should be noted that there is some small amount of residual generated in the right steer angle as well, particularly when switching on and off the fault, but its

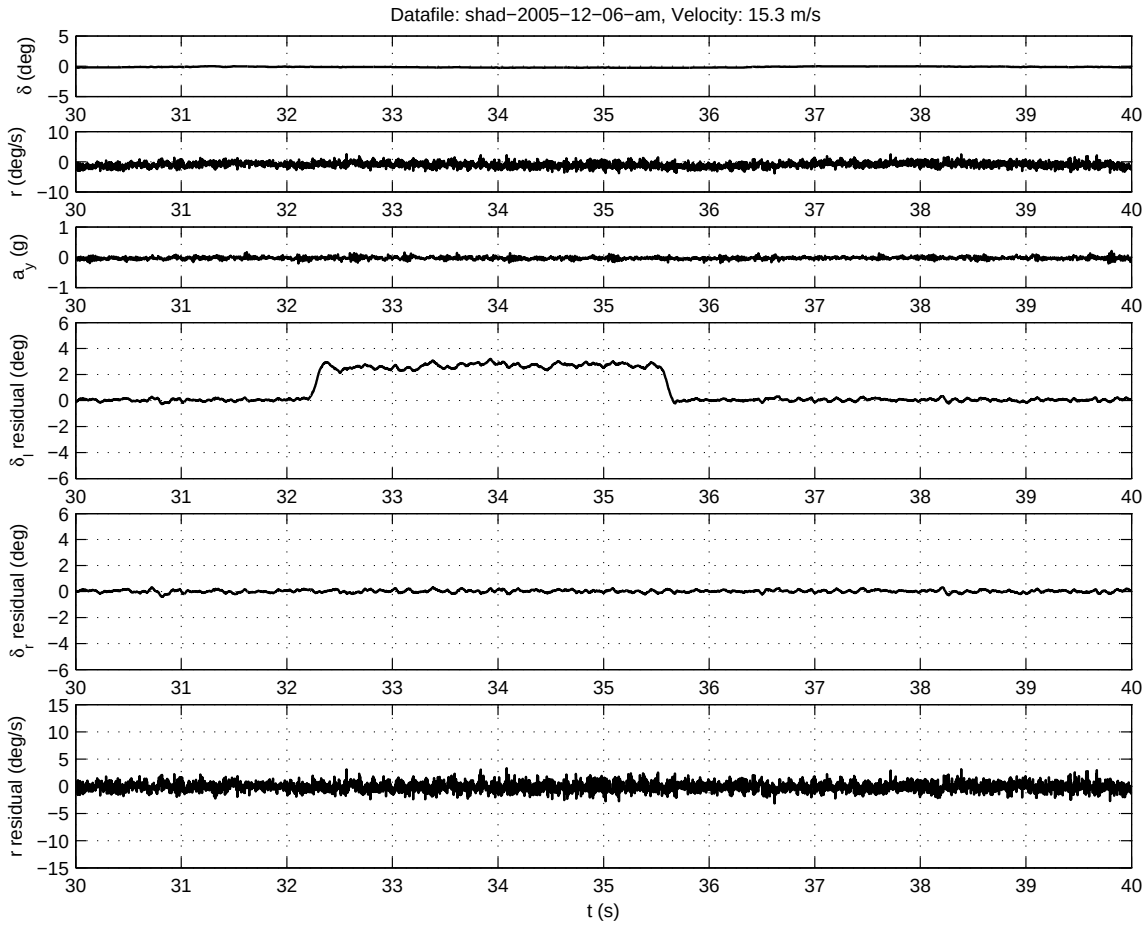

Figure 3.12: Experimental straight driving, 15 m/s, 8 A left motor current fault

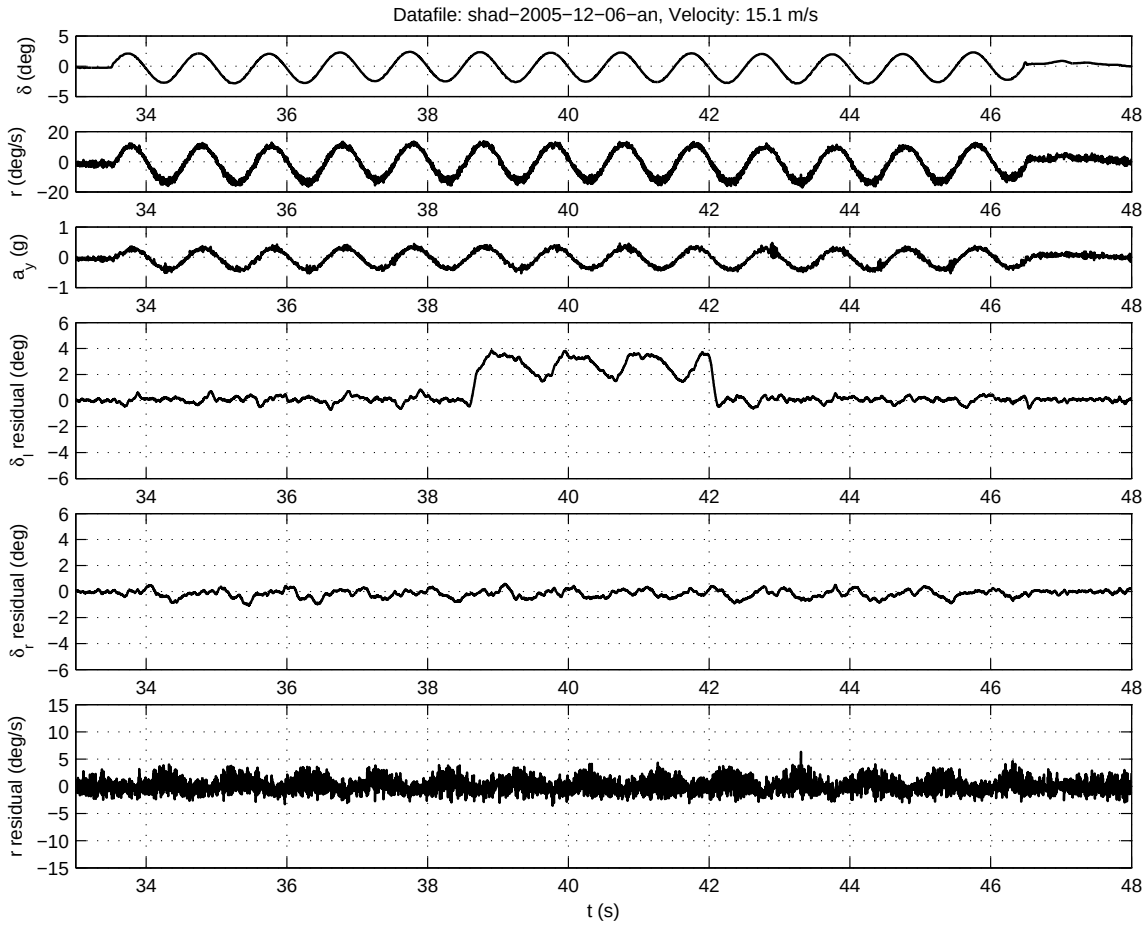

Figure 3.13: Experimental slalom, 1 Hz, 15 m/s, 8 A left motor current fault

magnitude is less than the residual of the left steer angle. In fact, the magnitude of this undesired residual can be controlled by varying the ratio between the two covariances used in the new filter structure. A lower yaw rate covariance will increase trust in the vehicle model, so the input left steer angle measurement into the right steer angle estimator will create a larger residual.

In practice, there are other things that could be interpreted as steer angle faults. Basically, anything that causes mismatch between the motor encoder measurement and the wheel angle is interpreted as a steer angle fault. This includes, but is not limited to, excessive gearbox backlash, worn out tie rod ends, and bent/broken linkage components.

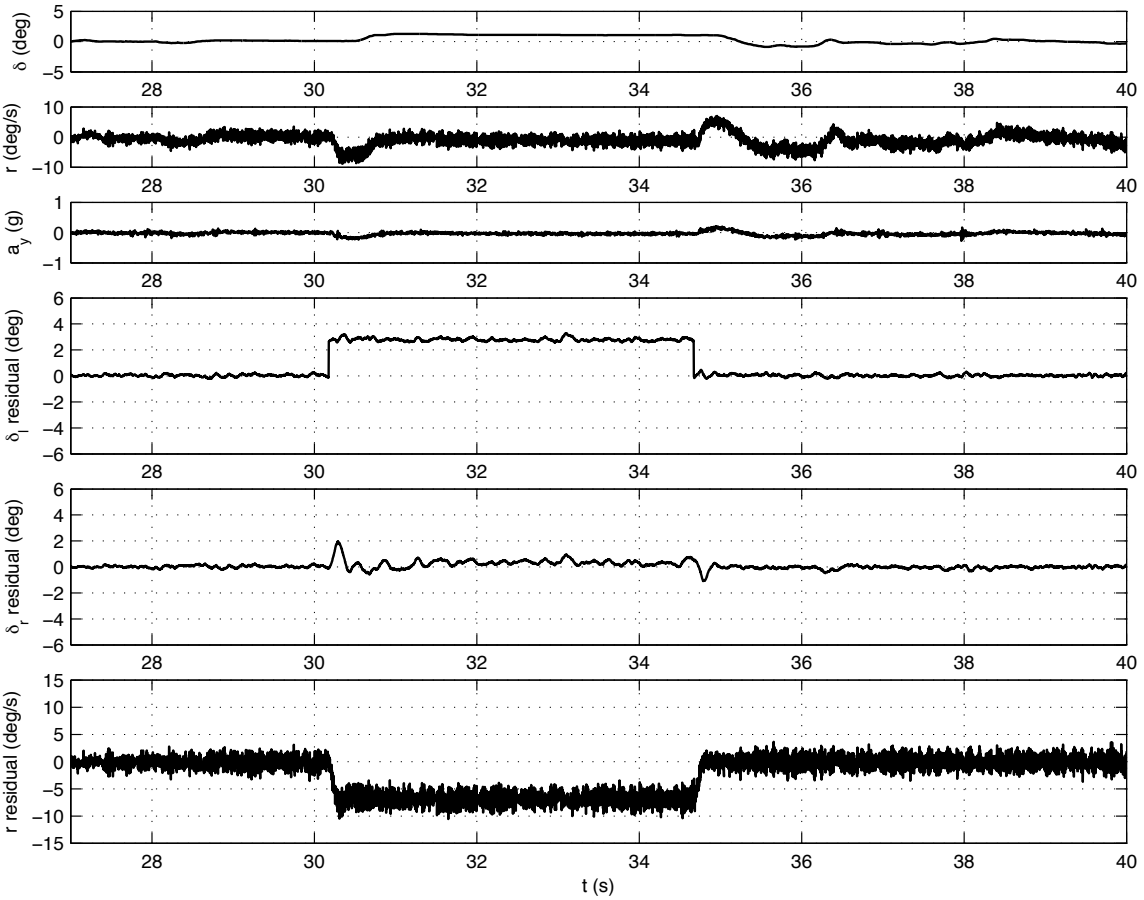

Figure 3.14: Experimental straight driving, 15 m/s, 3 deg left steer angle fault

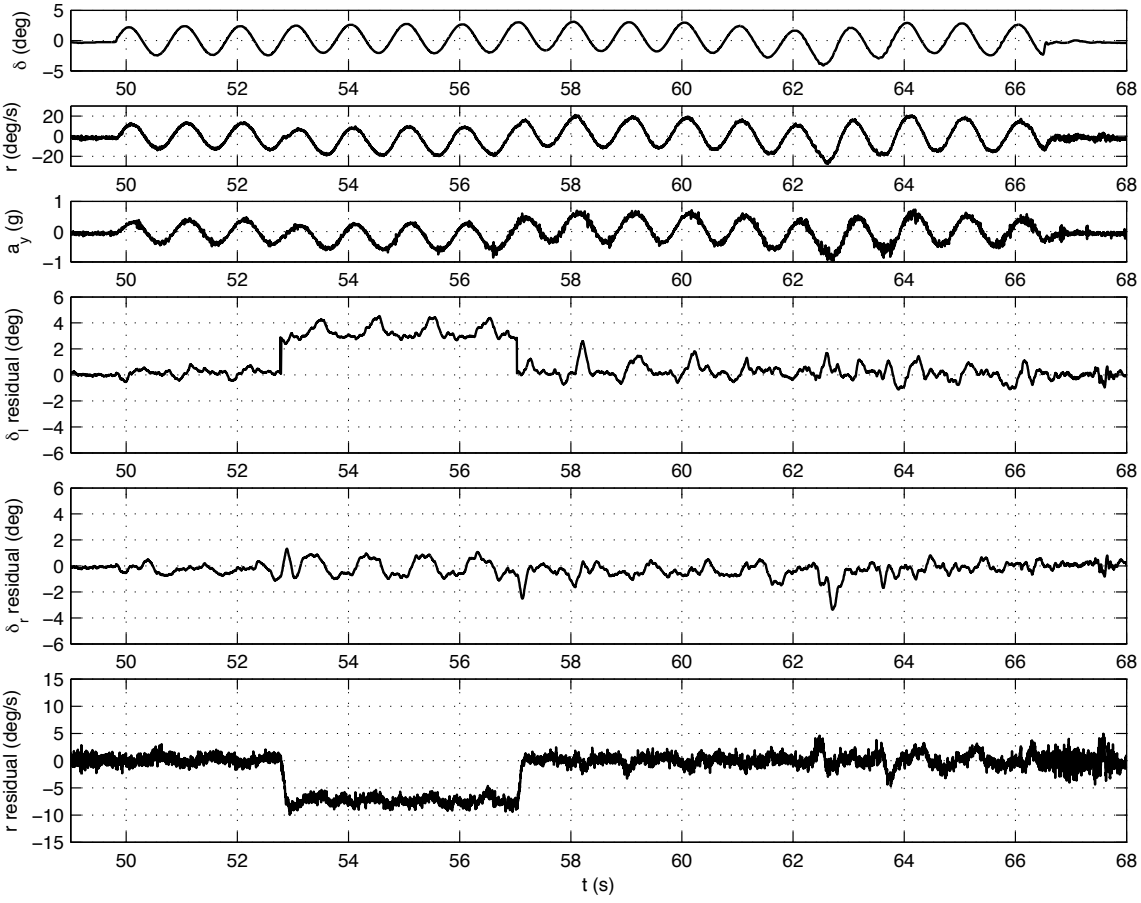

Figure 3.15: Experimental slalom, 1 Hz, 15 m/s, 3 deg left steer angle fault

3.5 Conclusion

The diagnostic residuals described here rely on relatively simple models of motors, steering system, and vehicle dynamics, yet offer the ability to detect faults of a magnitude so small they are often unnoticeable to the driver. Furthermore these residuals are each sensitive to a unique set of faults, making it possible to distinguish a variety of different faults, without the need for redundant steering system sensors. While such a fault detection system cannot relieve the burden of actuator or controller redundancy, by eliminating the need for redundant sensors, it can significantly reduce the cost of a steer-by-wire implementation, without compromising reliability.

Unfortunately, in order to achieve the level of diagnostic performance presented in this chapter, the diagnostic filters required extensive hand-tuning. Naturally this required access to experimental data, which means the filter tuning process could not be started until after the system to be diagnosed had been designed, built, and tested. While acceptible in a research environment, such a process is incompatible with the development cycle of a production automobile. The next chapter addresses this issue by presenting a method for designing diagnostic filters based on information available while the system is still being designed.

Chapter 4

Optimizing the Performance of Diagnostic Residuals

4.1 Introduction

The results from the preceding chapter illustrate how a model-based diagnostic system can be used to detect and isolate steering system faults in a steer-by-wire vehicle. Unfortunately, the existence of one working diagnostic system for a particular vehicle does not provide much guidance for someone hoping to design a diagnostic system for another vehicle. The diagnostic filters presented in the preceding chapter required a significant amount of tuning in order to get the desired level of performance. This is time consuming, requires access to experimental data, and it requires some skill and experience with filter tuning. This poses two significant problems: one, experimental data is often not available at the time when design decisions are being made; two, in cases where a hand-tuned filter does not provided an acceptable level of performance, the designer is left to wonder if they simply need to keep tuning, or they have reached a fundamental performance limit for the particular system. These issues lead to the desire for a automated design process, and to that end, a diagnostic performance metric is required.

This chapter presents a method for designing robust, model-based fault detection

filters for linear systems with stochastic inputs and bounded uncertainty. The approach maximizes the theoretical channel capacity of the system and diagnostic filter together, regarding the fault condition as an input to a hypothetical communication channel and the resulting residual as the output, with sensor noise, disturbances, and system input as sources of interference. This results in a robust residual that is both sensitive to faults and insensitive to noise and normal system variation. The effectiveness of the technique is demonstrated in the design of a fault detection filter for use with a diagnostic system for a steer-by-wire vehicle.

4.2 Diagnostic Cost Function

In order to design an optimal fault-detection filter, we must select an appropriate cost function. It is common to use H_∞-based cost functions, because of the well developed theory related to optimization over such cost functions. There are a number of variations on the basic H_∞ cost function which are designed to encourage sensitivity to faults while simultaneously rejecting noise and disturbances, either by a multi-objective cost function such as (1.4) or (1.5), or a ratio of H_∞ norms as in (1.1), or the ratio of an H_∞ norm and a minimum singular value as in (1.2) [62][13][55]. Unfortunately, these do not ensure that the resulting optimal filter is particularly well suited to fault detection, as they address only the issues of fault sensitivity and robustness, neglecting the matter of response time.

Here we take a different approach by starting with a cost function that measures the maximum rate at which usable information about a fault condition may be presented in the residual, referred to here as the *diagnostic capacity* of a residual. Without a direct way to compare the suitability of two diagnostic cost functions, it is not possible to prove the superiority of a particular cost function over all others, and the results presented here make no attempt to do so. Rather, it is simply noted that existing diagnostic cost functions found in literature all exhibit a common pair of limitations, an indifference to speed of response and an indifference to spectral separation, and that the use of diagnostic capacity as a cost function overcomes these limitations.

4.2.1 Shannon's Channel Capacity Limit

In order to select a cost function, we turn to a standard result from information theory, Shannon's noisy channel coding theorem[51], which places an upper bound on the rate at which information can pass through a communication channel:

$$C = \int_0^W \log_2 \left(1 + \frac{S(f)}{N(f)}\right) df \tag{4.1}$$

where W is the bandwidth of the communications channel in Hertz, $S(f)$ is the power spectral density of the signal containing the information to be communicated, and $N(f)$ is the power spectral density of a Gaussian noise source. C is the maximum rate of communication that can occur over such a channel, in bits per second. For a thorough derivation of this result see Appendix A. The remainder of this section provides a brief, conceptual basis for this result.

To begin with, consider a bandwidth-limited communication channel, as shown in Figure 4.1. A series of symbols, such as those shown in Figure 4.2, will be transmitted through the channel, using a rate and encoding scheme of our choosing, but will be corrupted by a noise source, n, which has zero mean and a uniform distribution between $-N$ and $+N$. Assume that maximum amplitude of the symbols sent is S. The channel has a limited bandwidth of W Hertz, so any frequency content above W will be completely eliminated before the signal arrives at the receiver.

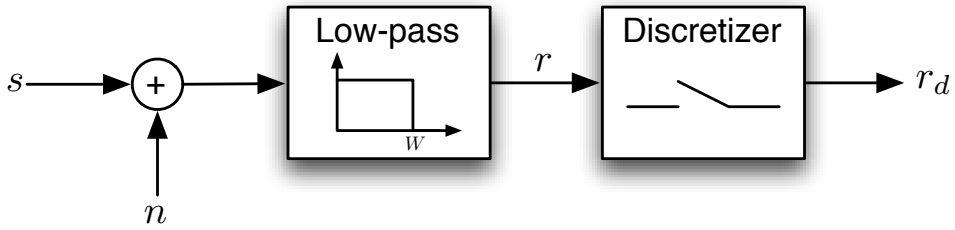

Figure 4.1: Diagram of Simple Communication Channel

In order for there to be no ambiguity at the receiver about which symbol has been sent, the minimum spacing between any two symbols must be larger than $2N$. With

the amplitude limit of S, the maximum number of unique symbols is given by:

$$M = \left\lfloor 1 + \frac{2S}{2N} \right\rfloor = \left\lfloor 1 + \frac{S}{N} \right\rfloor, \tag{4.2}$$

as illustrated by the example waveform shown in Figure 4.2 where $N = 1$ and $S = 3$.

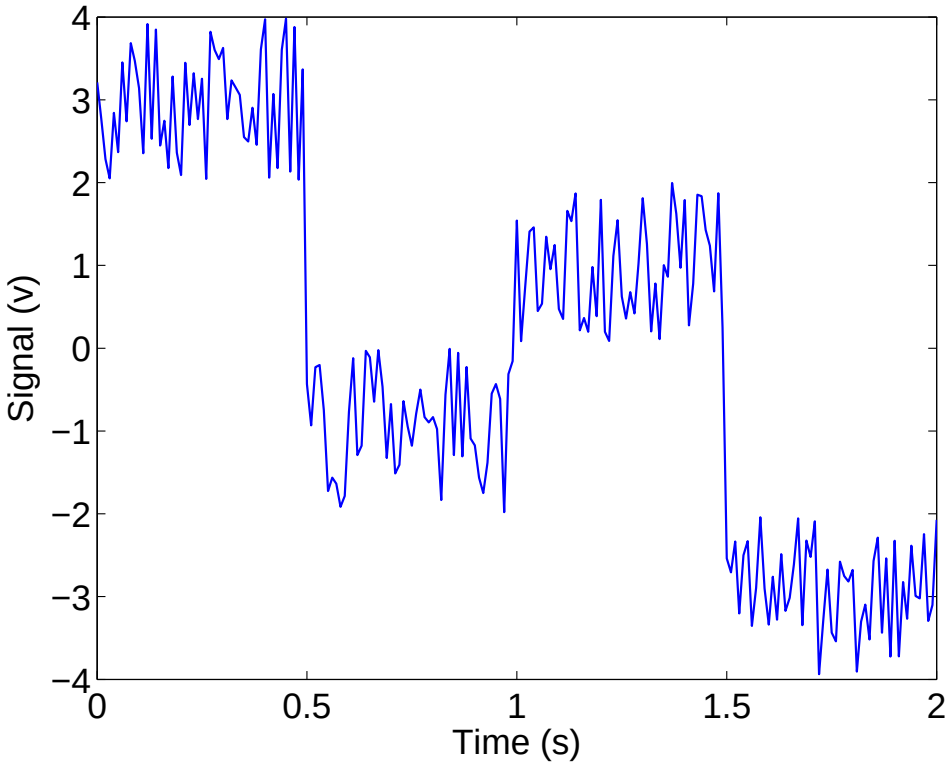

Figure 4.2: Example Waveform Showing 4 Distinct Symbols with Additive Noise

The amount of information, in bits, carried by a particular symbol is $\log_2 M$. This is easiest to see in the case where M is a power of two. For example, if $M = 256$, then each symbol carries eight bits of information. Combined with (4.2) the amount of information in bits per symbol is given by:

$$\log_2 \left\lfloor 1 + \frac{S}{N} \right\rfloor. \tag{4.3}$$

Having established the information content per symbol, it remains to examine the

rate at which these symbols can be sent. Nyquist's sampling theorem states that a bandwidth-limited signal need only be sampled at twice its bandwidth in order to preserve all of the information present in the original signal. If the signal at the receiver were to be sampled at at frequency of $2W$, there should be no loss of information, as the channel limits the bandwidth of the signal at the receiver to W. From this it is clear that we cannot send symbols at a rate higher than $2W$, which gives the following expression for maximum data rate:

$$2W \log_2 \left[1 + \frac{S}{N} \right]. \tag{4.4}$$

Lastly, consider the case where the available bandwidth is divided into K equally spaced communication channels operating in parallel, each with different amplitude and noise limits. The total maximum data rate for all of these separate channels is simply the sum of their independent data rates:

$$\sum_{i=1}^{K} \frac{2W}{K} \log_2 \left[1 + \frac{S_i}{N_i} \right]. \tag{4.5}$$

Taking the limit as $K \to \infty$ this summation becomes:

$$\int_0^W 2 \log_2 \left[1 + \frac{S(f)}{N(f)} \right] df. \tag{4.6}$$

This integral is clearly very similar to Shannon's result but differs slightly as there are a couple subtle differences in the assumptions made here. In particular, Shannon's theorem applies to a communication channel corrupted by a noise source with a Gaussian distribution, not a uniform distribution. Also, in this section $S(f)$ and $N(f)$ represented frequency-dependent amplitude limits, as opposed to power spectral densities. Also, we only examined the case of pulse code modulation as a coding method, whereas Shannon puts no restriction on coding strategy. These simplifying differences are made here so as to provide some intuition for the basis of Shannon's channel capacity limit.

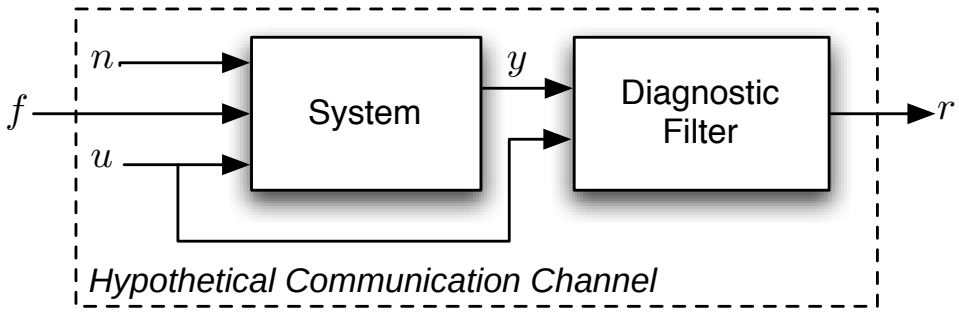

Figure 4.3: Block Diagram of System and Diagnostic Filter

4.2.2 Diagnostic Channel Capacity

In order to apply Shannon's noisy channel coding theorem to the problem of fault diagnosis, we consider the combination of the system to be diagnosed and the fault-detection filter to constitute a noisy communication channel, as shown in Figure 4.3. At the input of this communication channel the fault signal f is injected. Noise, n, and system input, u, corrupt this signal along the way. The output of the communication channel is the residual, r, which contains a filtered and corrupted version of the fault signal. Our objective is to design a fault-detection filter such that the capacity, in bits per second, of this hypothetical communication channel is maximized. This allows the maximum amount of useful information about the fault condition to be present in the residual.

Since most diagnostic systems are implemented digitally, it is practical to describe the diagnostic filter and system to be diagnosed as a discrete-time system. This leads to the following integral as a measure of the diagnostic capacity:

$$C = \int_0^{2\pi} \log_2 \left(1 + \frac{S(\omega)}{I(\omega)} \right) d\omega \tag{4.7}$$

where $S(\omega)$ represents the residual response to the fault signal and $I(\omega)$ represents the residual response to sources of interference. The transfer matrix (from n, f, and u to r) of the combination of the system and its diagnostic filter can be written as:

$$G(z) = [\ G_n(z) \ \ G_f(z) \ \ G_u(z)\ ]\,. \tag{4.8}$$

Note that f and r are scalars, while u and n in general are not. This means that $G(z)$ always has only a single row, i.e. $G(z) \in \mathbb{C}^{1\times m}$ for some m.

With this definition of $G(z)$, expressions for $S(\omega)$ and $I(\omega)$ can be written as:

$$\begin{aligned} S(\omega) &= G_f(z)G_f^*(z)\big|_{z=e^{j\omega}} \\ &= \left|G_f(e^{j\omega})\right|^2 \end{aligned} \tag{4.9}$$

$$I(\omega) = G_n(z)N(z)N^*(z)G_n^*(z) + G_u(z)U(z)U^*(z)G_u^*(z)\big|_{z=e^{j\omega}} \tag{4.10}$$

where $N(z)$ is the transfer matrix for the noise model, and $U(z)$ is the transfer matrix for a stochastic input model.

The definition for $S(\omega)$ inherently assumes there is no prior knowledge about the frequency distribution or magnitude of the fault signal. In cases where there is more information available about the particular type of fault signal to be detected, a stochastic frequency-domain model of the fault could be added to $S(\omega)$ in the same manner that the stochastic noise and input models are included in $I(\omega)$.

4.3 Additive Model Uncertainty

Since it is rarely the case that a system can be modeled exactly, any practical diagnostic design technique must address the issue of model uncertainty. Here an additive uncertainty block, with transfer matrix $\Delta(z)$, represents the difference between the nominal system and the actual system, as shown in Figure 4.4. This configuration readily accommodates a system that is well represented by a linear model but is subject to parametric uncertainty. It can also capture the effects of neglected higher-frequency linear dynamics, in cases where a reduced-order system model is being used. This configuration does not address situations where the system has significant nonlinearities, as both the nominal system and the uncertainty $\Delta(z)$ are assumed to be linear.

Since $\Delta(z)$ is used to represent the uncertainty in the system, it is by definition unknown. However, in order for this structure to be useful at all, there must be some

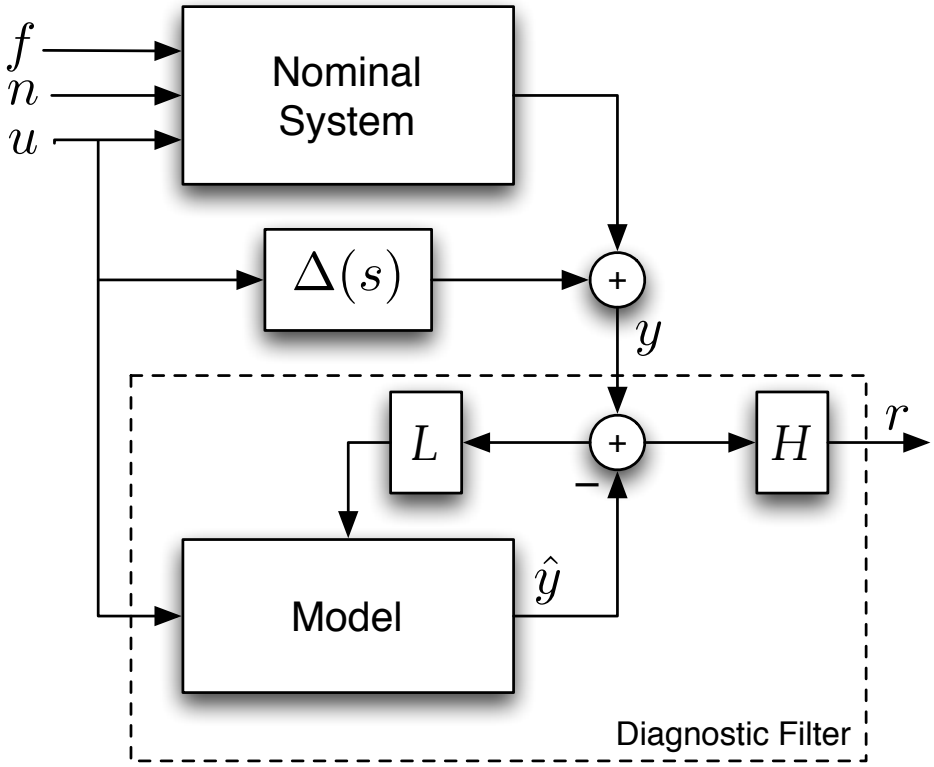

Figure 4.4: Block diagram of actual system represented by a nominal system model and an additive uncertainty block

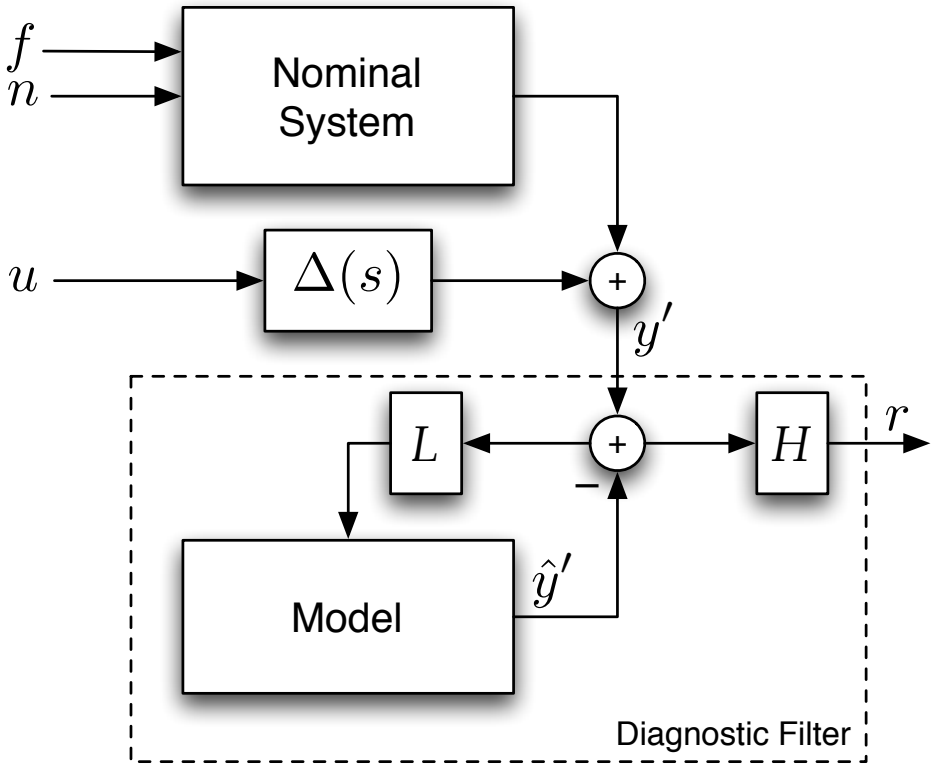

Figure 4.5: Simplifed block diagram of system with additive uncertainty

knowledge about the possible values $\Delta(z)$ could take on. Here it is assumed that we have a frequency-domain bound on the magnitude of each element of $\Delta(z)$, denoted by $\Delta_{wc}(\omega)$.

$$|\Delta(z)_{ik}|_{z=e^{j\omega}} \leq \Delta_{wc}(\omega)_{ik} \quad \forall \omega, i, k \tag{4.11}$$

For example, if the system had a single input and two outputs, $\Delta(z)$ would be a 2 by 1 transfer matrix, $\Delta(z) \in \mathbb{C}^{2\times 1}$, and $\Delta_{wc}(\omega)$ would be a 2 by 1 real matrix function of frequency, $\Delta_{wc}(\omega) \in \mathbb{R}^{2\times 1}$. In the simplest case, this bound on $\Delta(z)$ could be just an ∞-norm bound, although for most systems this would probably be overly conservative.

In Figure 4.5 the user input signal, u, is removed from both the model of the system and the nominal system, leaving $\Delta(z)$, the system uncertainty as the only path by which user input can influence the diagnostic residual. Since the nominal

system has the same response to user input as the model of the system, this block diagram is equivalent to that shown in Figure 4.4. Note that in this simplified block diagram, u, n, and f are combined, after filtering, to form y', which is the only input to the diagnostic filter.

In the diagrams shown in Figures 4.4 and 4.5, it is assumed that the modeling uncertainty only affects the system's reponse to user input, u. In general, the actual system response to noise and fault signals will not match the model perfectly, either. Since the fault and noise signals cannot be subtracted out of the observer the way user input can, the percentage error due to neglecting modeling uncertainty for the noise and fault signals will be much smaller than it is if modeling uncertainty is neglected for user input. Additionally, in cases where the noise is predominantly output sensor noise, or the fault is an output sensor fault, these signals will be largely independent of modeling uncertainty.

4.3.1 Parametric Model Uncertainty

In many cases, the uncertainty in the system model is not in the form of a $\Delta(z)$ block, but rather a set of tolerances on various parameters within the model. For example, in the case of the model of P1, most of the vehicle parameters, such as mass, mass distribution, or tire cornering stiffness, will vary over a small range during normal operation, just due differences in who is driving, whether or not there is a passenger or additional cargo, the temperature of the tires, etc. In order to apply the techniques presented in this chapter to such as system, it is necessary to first find an equivalent $\Delta(z)$ representation of these modeling uncertainties.

One very simple way to accomplish this is by discretization of the uncertainty space and the frequency axis. The transfer function of the system response to user input is simply evaluated a fixed number of frequencies, as each parameter is varied over a fixed number of values within its nominal range. At each frequency, the maximum singular value of the transfer matrix of the perturbed system model minus the nominal system model is recorded. The provides a discretized envelope of worst-case system response due to modeling uncertainty, which can be used as the $\Delta_{wc}(\omega)$

block. Specifically, the following can be used to find an approximate value for $\Delta_{wc}(\omega)$:

$$\Delta_{wc}(\omega) = \sup_{p \in P} ||G'_u(z) - G_u(z)||_\infty \quad \forall \omega \in \Omega \tag{4.12}$$

where Ω is a discrete set of frequencies in the range of 0 to π and p denotes a particular element from P, the finite (but possibly quite large) space of all possible combinations parametric deviations:

$$P = P_1 \times P_2 \times P_3 \times \cdots \times P_n \tag{4.13}$$

where n is the number of parameters and P_i is the discrete set of all values at which the i^{th} parameter should be evaluated.

This is, of course, a computationally intensive approach. There is a natural trade-off between the accuracy of the worst-case bound and the time required to compute it. As the resolution with which the frequency axis and uncertainty space are sampled goes up, the likelihood diminishes that there will be a point somewhere between those evaluated that is actually worse than those surrounding it. The computational effort grows polynomially with respect to the sampling resolution, and exponentially with the number of uncertain parameters. Fortunately, this particular operation only needs to be performed once to generate a $\Delta_{wc}(\omega)$, which can then be used in the optimization of the residual filter design. For this reason, unless one is faced with a really large number of uncertain parameters, this direct approach is sufficient.

4.4 Optimization

With the cost function established, the next logical step is to maximize the capacity of the diagnostic channel, over all stable diagnostic filters. In order to have a meaningful optimization problem, the design space needs to be parameterized, such that there are a finite set of decision variables over which to optimize. In the previous chapter, there were several general classes of diagnostic filter: parameter estimation via recursive least-squares, steady-state Kalman filters, and simple open-loop models. The latter

two both fall under the more general category of Luenberger observers (the open-loop case simply being an observer with $L = 0$). We can easily parameterize all Luenberger observers of a fixed order by the observer gains, L, and the output gains, H. Here, $H \in \mathbb{R}^{1\times n}$ as the filter should always produce a single residual, and $L \in \mathbb{R}^{n\times m}$, where n is the order of the observer and m is the number of measurements available to the observer.

The diagnostic filter design process can be stated as the following optimization problem:

$$\begin{aligned} \text{maximize} \quad & \int_0^{2\pi} \log_2\left(1 + \frac{S(\omega)}{I(\omega)}\right) d\omega \\ \text{subject to} \quad & |\lambda_i(A - LC)| < \gamma, \end{aligned} \tag{4.14}$$

where the parameter γ, which is strictly less than 1, establishes a buffer against creating diagnostic filters that are only marginally stable.

As will be discussed in greater detail in the next chapter, this optimization problem is not necessarily convex. The results presented in this chapter were obtained using a gradient search method, starting with an arbitrary feasible initial point. This approach unfortunately cannot guarantee global optimality of the resulting design, but the performance guarantee obtained for a particular solution is still valid over all possible values of $\Delta(z)$, regardless of whether that solution is the global optimum.

4.5 Design of a Diagnostic Filter for a Steer-by-Wire Vehicle

This section presents the design of a filter for use with the a diagnostic system for a steer-by-wire vehicle. The particular filter is designed around a model of the vehicle dynamics, with steering angles, δ_ℓ and δ_r, as inputs and vehicle yaw rate, r, and lateral acceleration, a_y, as outputs. This model is given by (2.8) and (2.9). The structure of this filter is shown in Figure 4.6. Note that this is only one filter of many that would be necessary to thoroughly diagnose such a system, as discussed in the

preceding chapter.

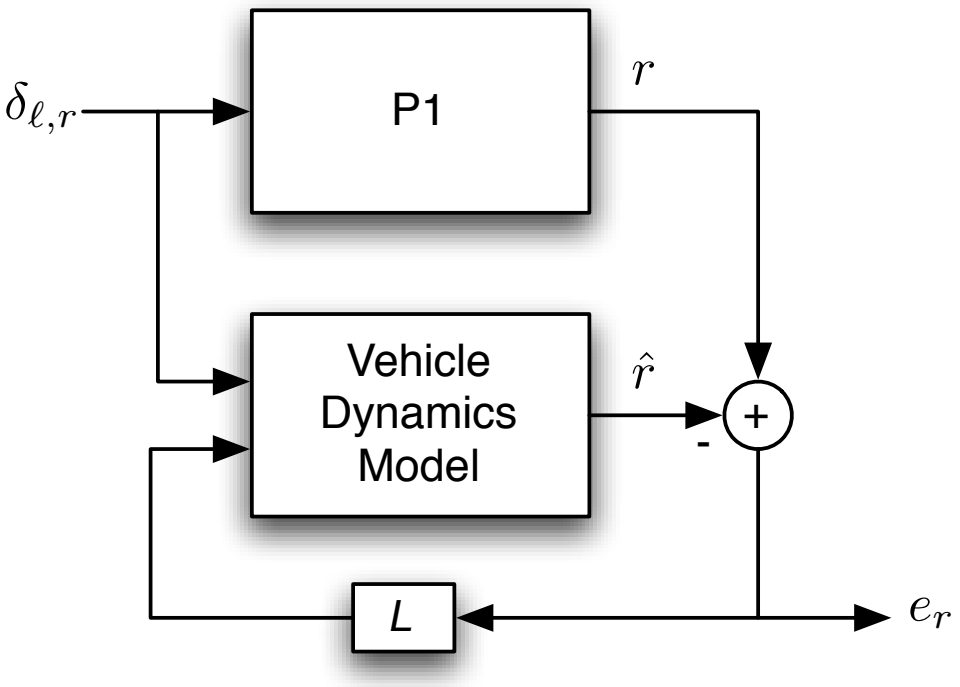

Figure 4.6: Luenberger observer as a diagnostic filter for steer-by-wire system

4.5.1 Simulation

With all of the system model components established, the only design step is to evaluate the optimization problem in (4.14). The following figures illustrate the characteristics of the resulting filter. Figure 4.7 shows $S(\omega)$ and $I(\omega)$ for a system with precisely nominal parameters, i.e. $\Delta(z) = 0$. It also shows a line representing the integrand of (4.7), which is an indicator of which portions of the frequency spectrum are providing the most useful information about the fault signal. In this nominal case, the information about the fault is even pretty evenly spread across the frequency spectrum, with slightly more information coming through at low frequencies.

Figure 4.8 shows the same information only now the simulated system has some modeling errors. Specifically, the simulated vehicle is traveling at 14 m/s, instead of

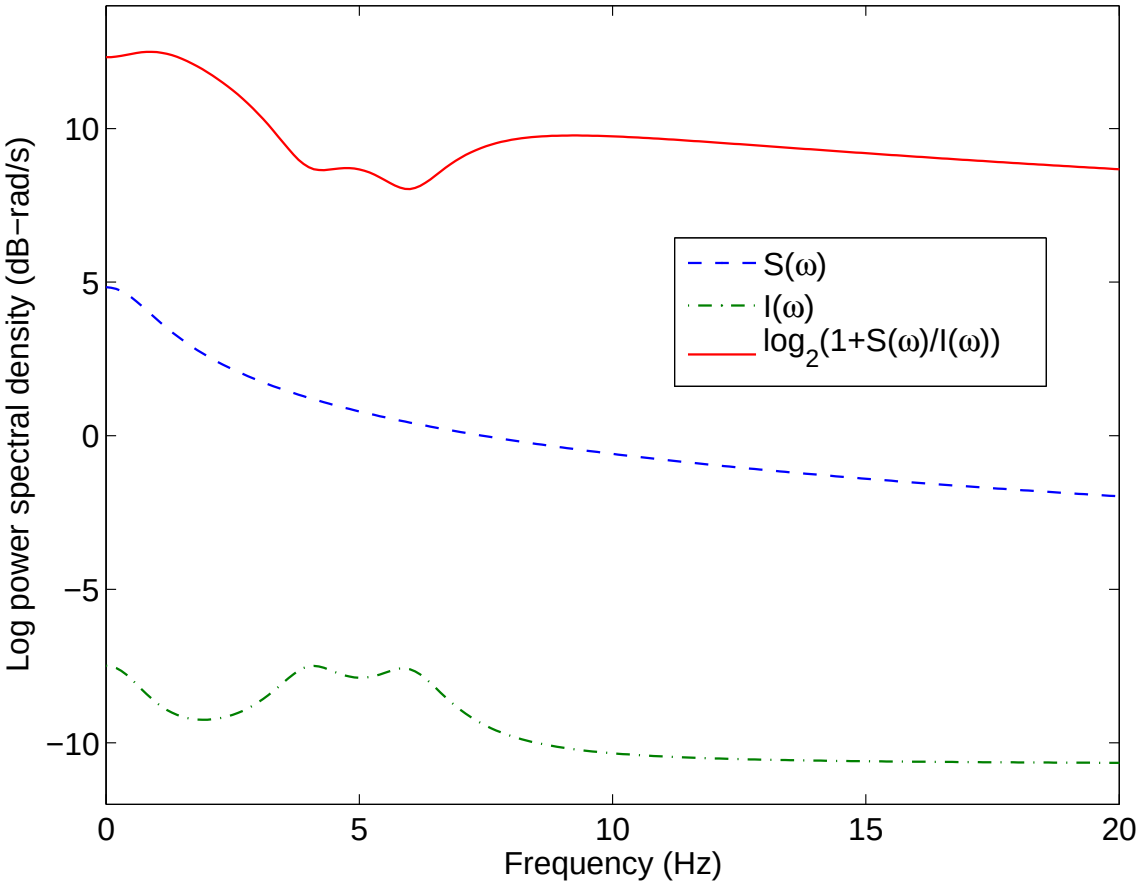

Figure 4.7: Simulated Channel Capacity by Frequency for a Nominal System

16 m/s, and has a front left tire cornering stiffness of only 43,000 N/rad, instead of 45,000 N/rad. Now the effect of the driver input signal showing up in the residual can be seen, and the residual now has significantly less useful information at low frequencies. At higher frequencies, the information content in the residual is largely unaffected by the modeling errors, due to the lack of high-frequency content in the driver signal.

Figure 4.9 shows the simulated time-domain response of the diagnostic filter to the sudden introduction of a 3° bias on the measurement of the left steer angle, δ_ℓ. The simulated driver is executing a 1 Hz slalom maneuver at an amplitude of 3° at the road wheels. Throughout the simulation the vehicle is traveling at constant speed

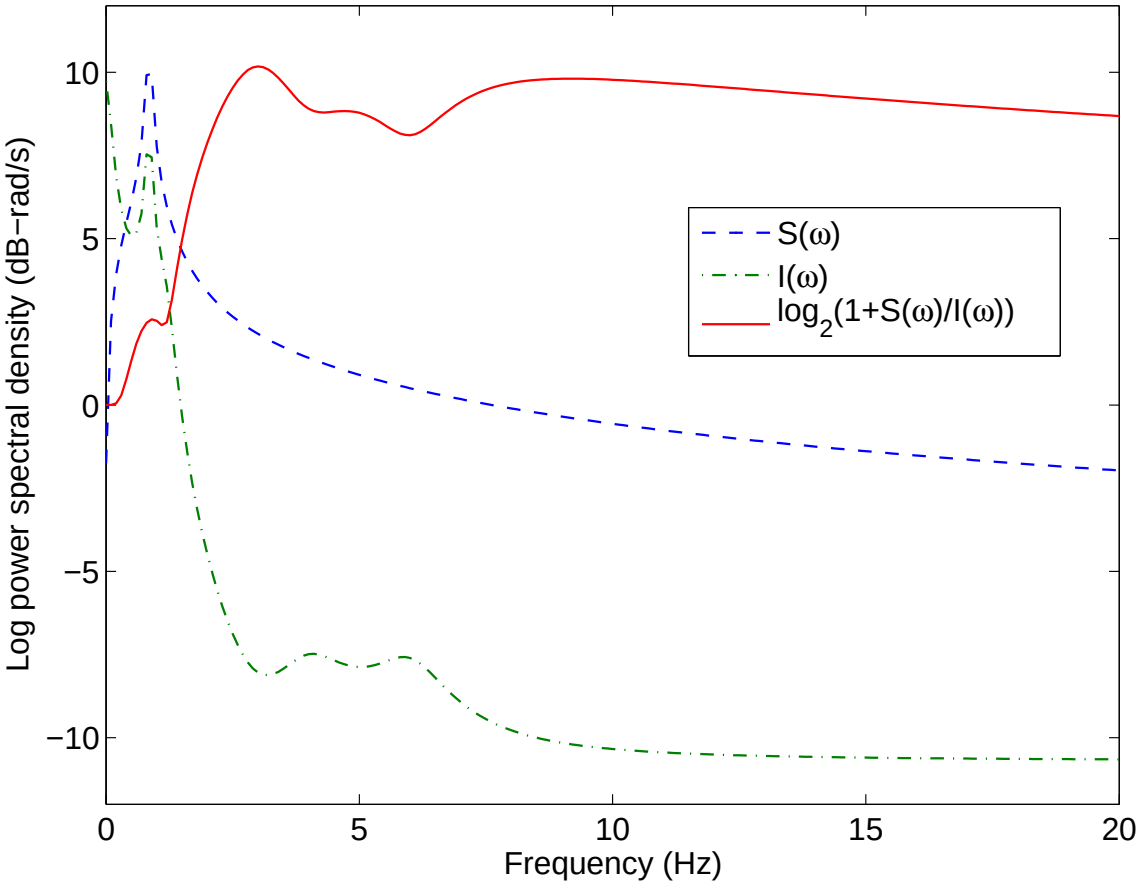

Figure 4.8: Simulated Channel Capacity by Frequency for a System with Modeling Error

of 14 m/s, and the left front tire cornering stiffness is reduced to 43,000 N/rad, as before. These discrepancies between the nominal model used to design the diagnostic filter and the actual model used for the simulated vehicle cause a small portion of the driver command to show up in the residual, as expected.

4.5.2 Experimental Results

Experimental fault testing was performed on an unused airfield ramp to provide ample space to safely accommodate unexpected vehicle response to steering system faults. The particular fault presented here is the same as the one used in simulation in the

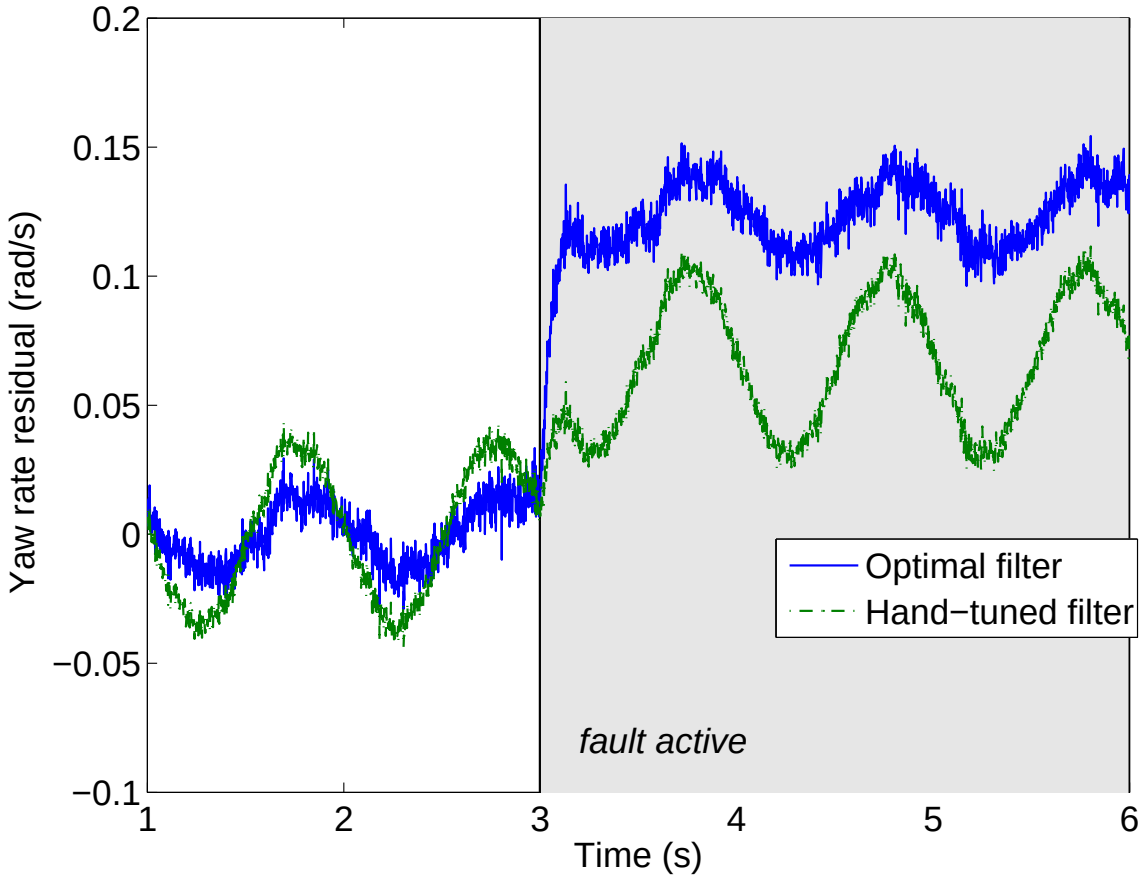

Figure 4.9: Simulated Response of Residual to a 3° Steer Angle Sensor Bias

preceding section, a sudden 3° bias error on the left steer angle sensor. During this experiment, the driver executed a 1-Hz slalom maneuver, traveling at speeds ranging between 15 m/s and 20 m/s. Figure 4.10 shows the actual response of the diagnostic filter to the fault, which was injected at approximately 52.7 s into the experiment. The exact tire cornering stiffness is, of course, not known, but is in the vicinity of its nominal value of 45,000 N/rad. The diagnostic filter used here is exactly the same filter used in the simulation.

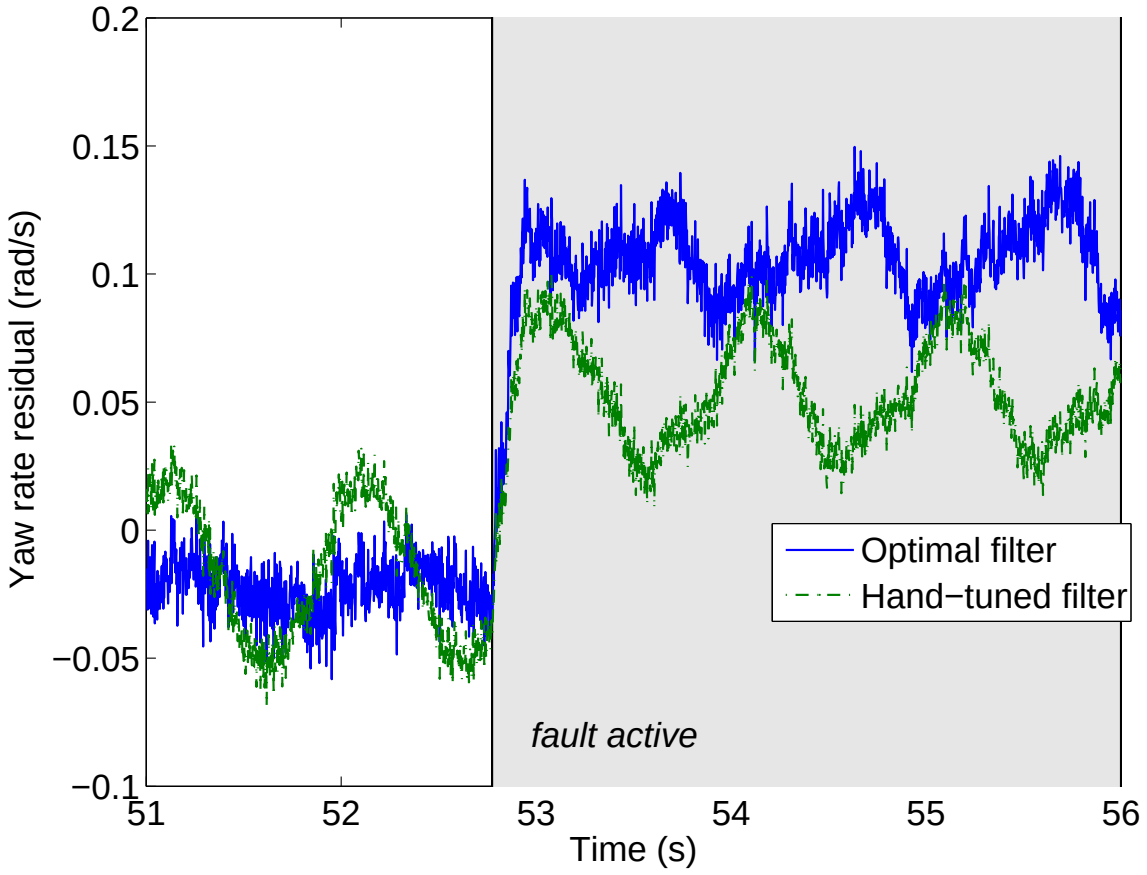

Figure 4.10: Experimental Response of Residual to a 3° Steer Angle Sensor Bias

4.6 Conclusion

This chapter presented an optimal fault detection filter design approach based on a cost function that regards the path from fault to residual as a communication channel whose capacity is to be maximized. Unlike existing cost functions, this cost function implicitly favors designs providing good spectral separation, ensuring that signal power and noise power will, to maximum extent possible, occupy separate frequence ranges. Modeling uncertainty is accounted for through the use of an additive uncertainty block. By optimizing the filter design against the worst-case additive uncertainty, the method is robust to bounded modeling uncertainty. This chapter concluded with an example of this technique applied to the design of one of the

diagnostic filters discussed in the previous chapter. Here, however, the design process required no hand-tuning, resulting in comparable performance without relying on a skilled designer.

Chapter 5

Some Properties of Channel Capacity as Diagnostic Cost Function

5.1 Introduction

This chapter describes some of the properties of channel capacity as a diagnostic performance metric, and the impact these have on its use in designing diagnostic filters. The first section focuses on some interesting invariance properties of channel capacity. In particular, the channel capacity of a diagnostic residual is invariant under linear filtering, a property which decouples the design of a diagnostic filter from the design of post-processing filters. Additionally, the channel capacity of a diagnostic residual based on a Luenberger observer is invariant over all choices of observer gain when the observer only has access to a single measurement of the system.

The second section examines the convexity properties of channel capacity. Due to the well-developed theory regarding optimization problems with convex cost functions, convexity is naturally a desirable property to have in a cost function. Unfortunately, the channel capacity of a diagnostic filter is, in general, neither convex nor quasi-convex.

5.2 Invariance Properties

5.2.1 Linear Filtering

It is well beyond the scope of this thesis to discuss all the methods by which a residual or set of residuals can be processed to produce a diagnosis, but there is one simple form of post-processing that merits a closer examination. Since channel capacity when used as a diagnostic cost function leads to residuals with good spectral separation of fault information from noise and interference, it seems only reasonable to want to apply a linear filter to the resulting residual, to suppress frequency ranges where noise dominates the fault signal. The following theorem considers the effect of linear filtering on the diagnostic capacity of a residual.

Theorem 1 *The diagnostic capacity of a residual is invariant under filtering by an LTI system, provided the filter has a countable number of zeros.*

Proof. The application of an LTI filter, H, to a given diagnostic residual will scale $S(\omega)$ and $I(\omega)$ by the same amount:

$$H(z)G(z) = [\ H(z)G_n(z)\ \ H(z)G_f(z)\ \ H(z)G_u(z)\ ] \tag{5.1}$$

$$\begin{aligned} S'(\omega) &= H(z)S(\omega)H^*(z)\big|_{z=e^{j\omega}} \\ &= \left|H(e^{j\omega})\right|^2 S(\omega) \qquad (5.2) \\ I'(\omega) &= H(z)I(\omega)H^*(z)\big|_{z=e^{j\omega}} \\ &= \left|H(e^{j\omega})\right|^2 I(\omega) \qquad (5.3) \end{aligned}$$

$$\begin{aligned} \log_2\left(1+\frac{S'(\omega)}{I'(\omega)}\right) &= \log_2\left(1+\frac{\left|H(e^{j\omega})\right|^2 S(\omega)}{\left|H(e^{j\omega})\right|^2 I(\omega)}\right) \\ &= \log_2\left(1+\frac{S(\omega)}{I(\omega)}\right) \qquad (5.4) \end{aligned}$$

This leaves the integrand unchanged after filtering, except at values of ω where

$H(e^{j\omega}) = 0$, where the integrand becomes undefined. At frequencies where the residual has no dependence on the fault, there is no useful information available, so we must regard these undefined cases to be identically zero. Provided there are no continuous regions of the frequency spectrum where $H(e^{j\omega})$ is zero, the value of the integral will be unaffected. Note that this technical condition on H only eliminates physically unrealizable filters and the trivial filter, $H(z) = 0$. $\square$

An important consequence of Theorem 1 is that linear post-processing of a residual will not affect the overall capacity of a diagnostic filter. This decouples the design of the filter that produces the residual from the design of any additional filters that may be applied to the residual. Depending on the technique used for fault detection (fixed/adaptive/fuzzy thresholds, Bayesian networks, neural networks, etc.) it may still be desirable to have such post-processing filters, but Theorem 1 establishes that these additional filters will neither increase nor decrease the maximum rate at which usable fault information can show up in the residual.

5.2.2 Luenberger Observers

Another form of invariance that presents itself when using channel capacity as a cost function is invariance over the descision variables themselves. In cases when this occurs, there is no change in performance regardless of how the filter is tuned. Somewhat surprisingly, this occurs for a broad class of diagnostic filter structures, namely, all Luenberger observers based on a single measurement of system output.

Corollary 1 *The diagnostic capacity of Luenberger observer is invariant over all choices of observer gains, L, and output gains, H, if $L \in \mathbb{R}^{n\times 1}$ and $H \neq 0$.*

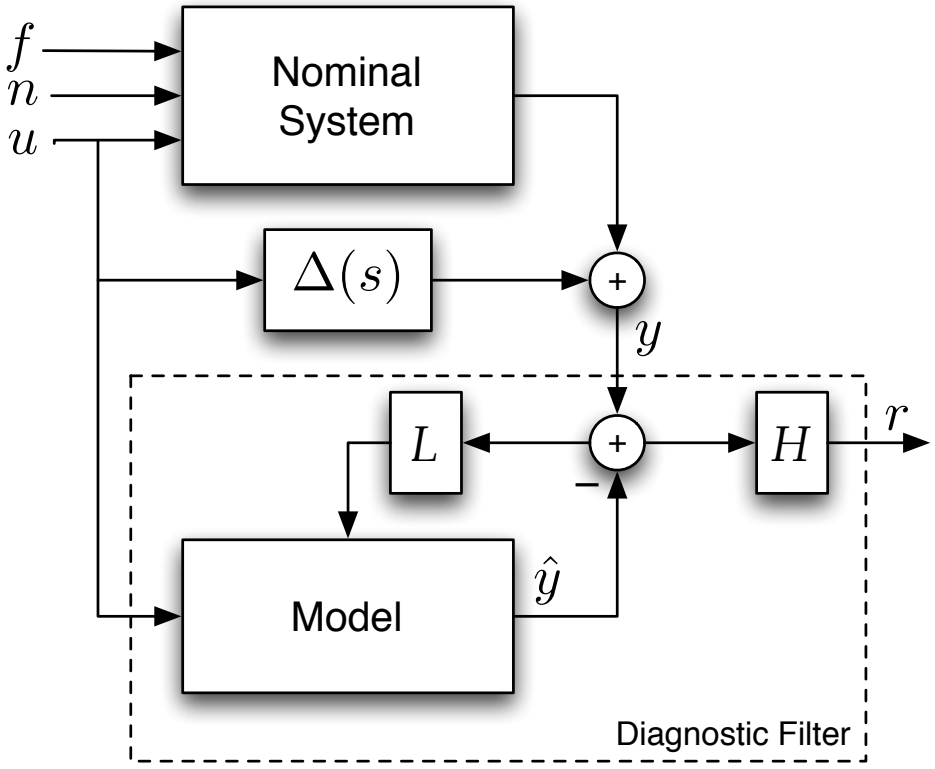

Figure 5.1: Block diagram of system with additive uncertainty

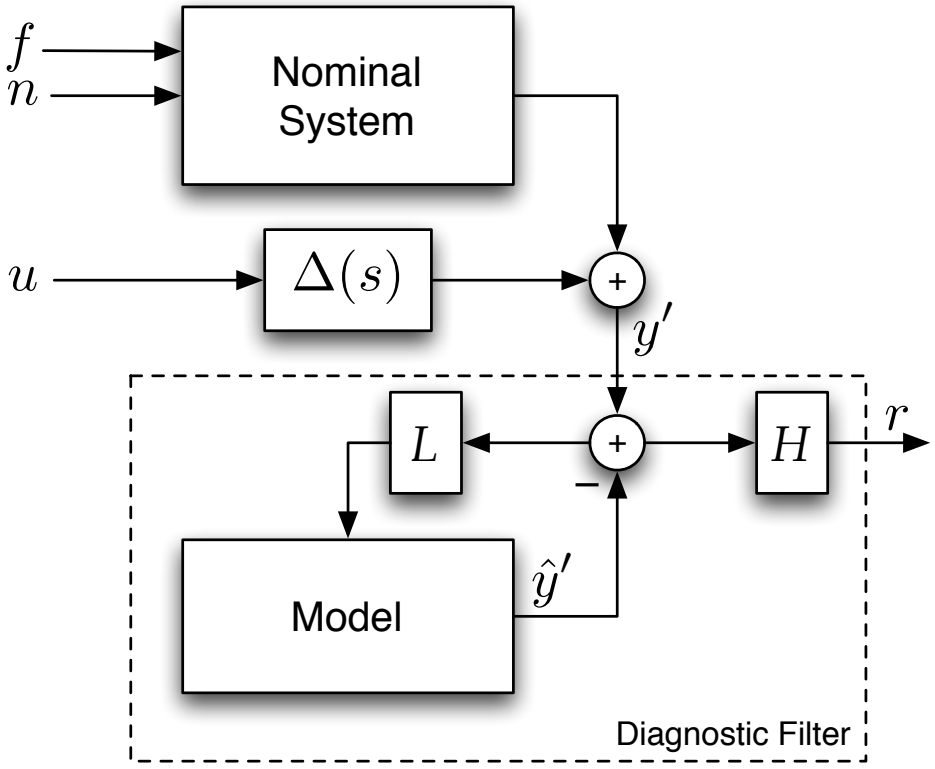

Figure 5.2: Simplifed block diagram of system with additive uncertainty

Proof. The diagnostic observer and system shown in Figure 5.1 are described by the following:

$$\begin{aligned} y &= P(u, f, n, 0) + \Delta(u) && (5.5)\\ \hat{y} &= P(u, 0, 0, L(y - \hat{y})) && (5.6)\\ r &= H(y - \hat{y}) && (5.7) \end{aligned}$$

where P is the nomial system model. Since P is a linear system, superposition holds, allowing us to write:

$$\begin{aligned} y &= y' + P(u, 0, 0, 0) && (5.8)\\ \hat{y} &= \hat{y}' + P(u, 0, 0, 0) && (5.9) \end{aligned}$$

where

$$\begin{aligned} y' &= P(0, f, n, 0) + \Delta(u) && (5.10)\\ \hat{y}' &= P(0, 0, 0, L(y - \hat{y})). && (5.11) \end{aligned}$$

Since $y - \hat{y} = y' - \hat{y}'$ we can write:

$$\begin{aligned} r &= H(y' - \hat{y}') && (5.12)\\ \hat{y}' &= P(0, 0, 0, L(y' - \hat{y}')) && (5.13) \end{aligned}$$

This establishes the equivalence of the block diagrams shown in Figures 5.1 and 5.2.

Since $L \in \mathbb{R}^{n\times 1}$, it has a width of 1, hence the observer shown in Figure 5.2 has a single scalar input, y'. As the observer also has a single scalar output, r, by application of Theorem 1, the diagnostic capacity of r is always equal to that of y', provided $H \neq 0$. Since y' is unaffected by the choice of H or L, the diagnostic capacity of r is also unaffected. □

Note, that in this case we can relax the linearity restriction on the Δ block. Here it is defined to be precisely the difference between the model of the system and the

actual system. This means there is no loss of generality in assuming that any system coupled to a Luenberger observer can be represented by the diagram in Figure 5.2. As the steady-state Kalman filter is simply a specific choice of gains for a Luenberger observer, this result applies equally well to steady-state Kalman filters.

Corollary 1 establishes the triviality of single-measurement observer design for diagnostic systems, something which is not immediately obvious when trying to tune such an observer by hand. This result is not saying that every filter tuning will result in the same residual, only that every residual will have the same diagnostic capacity. Further, no residual will differ from any other by more than the application of linear filtering operation.

This is not to suggest that single-measurement observers are of no use in diagnostic systems, only that there is no benefit to the use of a particular set of observer gains over any other. In particular, the special case of $L = 0$, where the observer becomes just the simple comparison of an open-loop model with the measured output, such as the residual R_r presented in Chapter 3, will provide no less diagnostic capacity than any other observer gain choice.

5.3 Convexity

In the previous chapter, a simple gradient search method was used to find locally optimal filter designs. This provides no assurance that the particular design is globally optimal, unless we can additionally show that channel capacity is a quasi-concave function of the design variables and that the feasible set is convex. Unfortunately, neither of these conditions are met.

The feasible set for this problem is the set of all stable observers gains:

$$\{L : |\lambda_i(A - LC)| < 1\}. \tag{5.14}$$

Figure 5.3 shows a slice of the stable set of observer gains for the following example

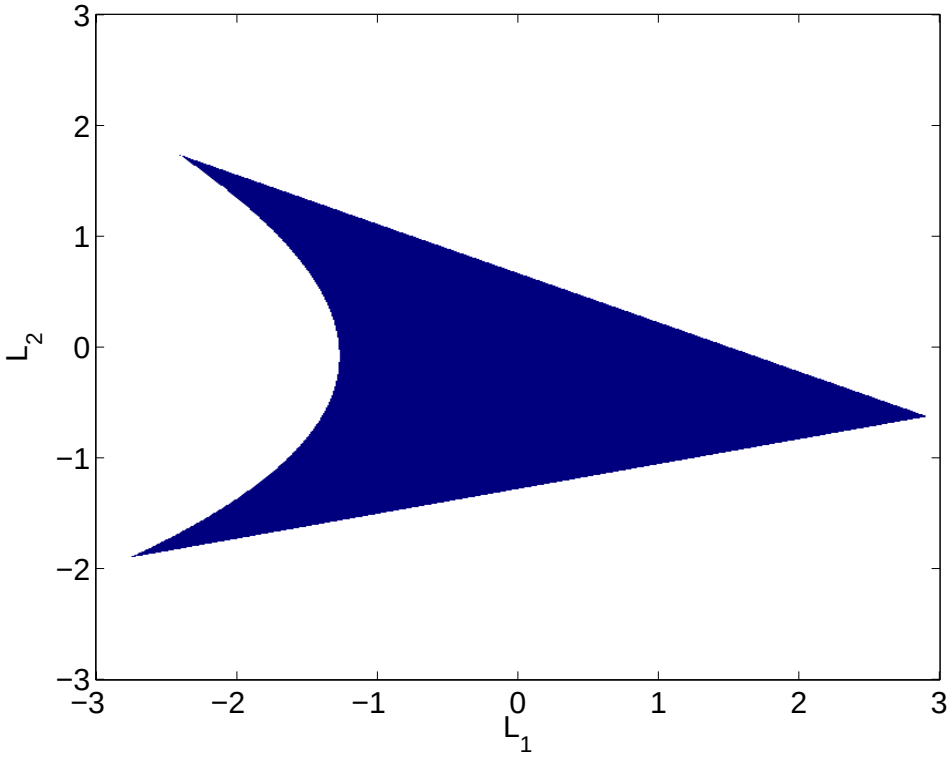

Figure 5.3: $L_3 = 0$ slice of the set of stable observer gains for an example system.

system:

$$x_{k+1} = Ax_k \tag{5.15}$$

$$y_k = Cx_k \tag{5.16}$$

$$A = \begin{bmatrix} -0.25 & 0 & 1.5 \\ -0.5 & -0.5 & 0 \\ -0.25 & -0.25 & 0.25 \end{bmatrix} \tag{5.17}$$

$$C = \begin{bmatrix} 0 & 1 & -0.25 \end{bmatrix}. \tag{5.18}$$

Since an observer for a 3$^{\text{rd}}$ system has three gains, the feasible set lies in $\mathbb{R}^3$, but for plotting convenience only the $L_3 = 0$ slice of that set is shown. In this example, the set is clearly not convex, hence we cannot rely on the set of stable observers being a convex set.

Additionally, channel capacity is not a quasi-concave function of the observer gains and output gains. Note that since we seek to maximize channel capacity, rather than minimize it, concavity is the desirable property for it to have, not convexity as is typically the case. Figure 5.4 shows how the channel capacity of an example diagnostic filter varies as a function of the two output gains, H_1 and H_2. It clearly illustrates not only a lack of concavity, but two distinct "ridges" that are each local maxima. This suggests that gradient search algorithms will, on occasion, find locally optimal designs that are inferior to the globally optimal solution.

While unfortunate, these properties do not mean there exists no computationally efficient way to find the globally optimal solution, only that existing convex optimization algorithms cannot be applied directly. For relatively small systems, such as those studied in this thesis, even exhaustive search techniques are still practical, so computationally efficiency is not as important as it might be for larger-scale systems. Fortunately, many systems are well described by models on the same scale or even smaller than those studied here, so these techniques can be applied to a variety of diagnostic problems without encountering computational limitations, even in the absence of a computationally efficient algorithm for optimizing the diagnostic capacity of a residual.

5.4 Conclusion

This chapter presented some of the properties of channel capacity as a diagnostic cost function. The channel capacity of a diagnostic residual is unaffected by linear filtering. This separates the problem of residual filter design from the problem of post-processing filter design, and leads to directly the result that the channel capacity of single-measurement Luenberger observers is invariant over all choices of observer gain. This chapter also established that optimizing the channel capacity of a residual based on a Luenberger observer is not a convex problem and may prove to be computationally challenging for large-scale systems.

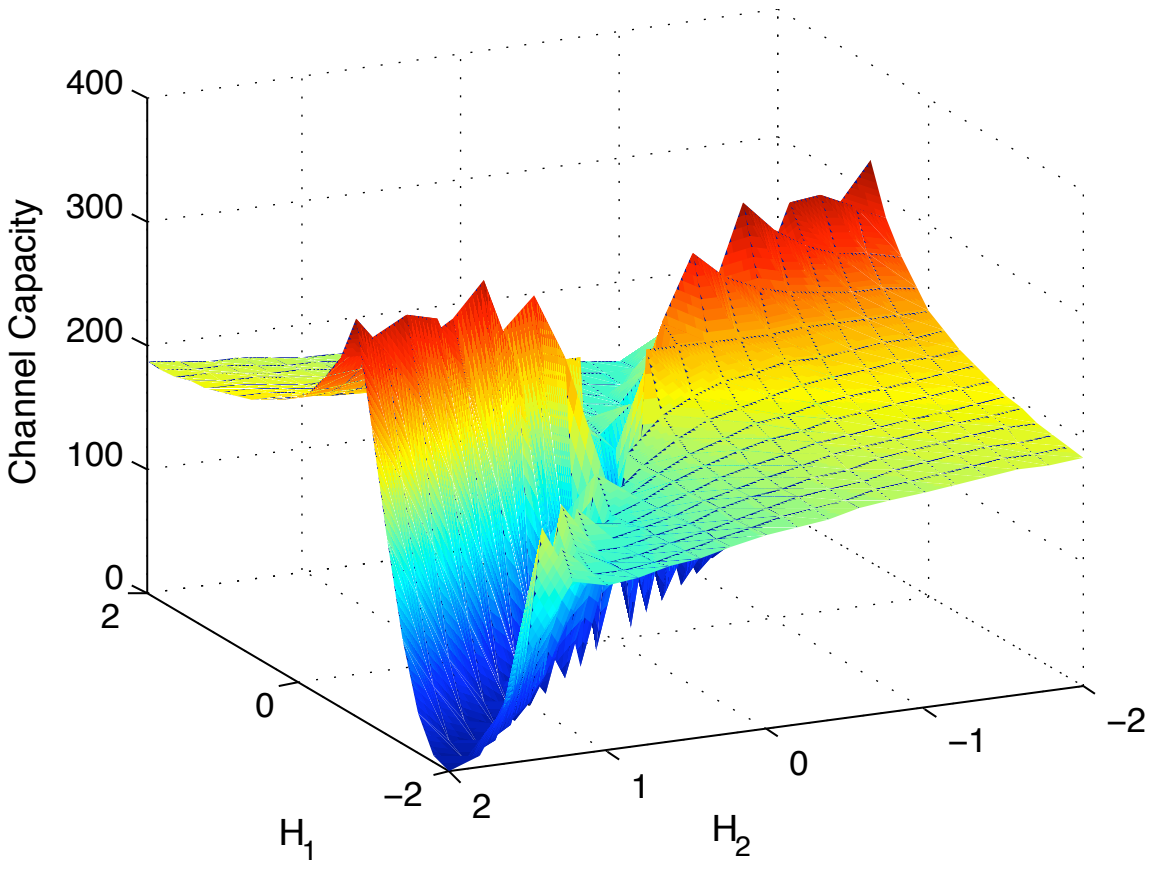

Figure 5.4: Channel capacity as a function of output gains, H_1 and H_2

Chapter 6

Conclusion

This thesis presents an important step towards bringing safe and practical steer-by-wire vehicles to the road. The results here show how a model-based diagnostic system can detect and isolate a wide range of steering system faults in real-time, providing the information necessary to know when to switch over to a backup component. The use of model-based diagnostic techniques avoids the expense of triply-redundant sensors, and extends the range of faults that can be detected and identified. This provides a solution that has the potential to be both more reliable and more cost-effective than a conventional steering system.

This thesis also describes a novel diagnostic filter performance metric: the capacity of the communication channel between the fault signal and the diagnostic residual signal, as established by the system and diagnostic filter. Rather than focusing on ease of optimization, this cost function tries to measure the rate at which useable information about the fault condition is being made available in the residual, providing a more relevant measure of diagnostic performance. The resulting filters have a guaranteed level of performance, explicitly accounting for modeling uncertainty as well as stochastic sources of disturbance to system being diagnosed.

6.1 Future Work

The vehicle model presented here neglected longitudinal tire forces, as well as operation in the non-linear region of handling and the effects of vehicle roll. Considering the small amount of time a vehicle spends in the non-linear handling region, it arguable whether or not a steering diagnostic system needs to be able to operate in the non-linear region, but it certainly an interesting area for further study. The effects of longitudinal tire forces and vehicle roll, however, are both areas where the current vehicle model could benefit from additional work.

Another avenue for further study is automating the process of determining which filters should be sensitive to which faults. The results presented in Chapter 4 show how to take a particular filter and optimize its design, assuming it is known to which fault or faults it should be sensitive, and what sensors or input signal it should use. The designer is still left with the burden of determining how best to partition the system for diagnosis. In the case of relatively small systems, such as the steer-by-wire system studied here, this process is relatively simple. For larger, more complex systems, such as aircraft, however, this manual partitioning task could be impractical.

Using channel capacity as a cost function has a number of advantages, in particular how it favors designs that provide good spectral separation of fault from noise, but a major disadvantage is its non-convexity, as demonstrated in the previous chapter. Strictly speaking, most diagnostic cost functions are non-convex, but can either rewritten as an equivalent convex problem, or still be solved efficiently through the solution of a series of convex problems. It remains to be determined whether or not there exists a computationally efficient algorithm for finding the optimum value of the cost function used in this thesis. For the results presented here, a simple gradient search method was used, but there may be much better heuristics for selecting a design, such a semi-definite relaxation technique. It should also be possible to establish a loose upper bound on the maximum possible filter performance, thereby loosely bounding the amount of "lost" performance due to the inability to solve for the global optimal solution.

Lastly, at a practical level, the techniques presented here need to be combined with

complimentary diagnostic techniques (to convert residuals to a diagnosis) along with fault-tolerant and/or fault-accommodating control designs, to produce a complete steer-by-wire system. Presumably, early designs will include a complete conventional backup steering system for matters of legal liability and driver peace-of-mind. Ultimately such backup systems will become unnecessary, once steer-by-wire has proven itself to be safer and more reliable than conventional steering systems of today.

Appendix A

Proof of Shannon's Limit on Channel Capacity

This appendix presents a proof of Shannon's limit on the capacity of a linear communication channel corrupted by a Gaussian noise source. This proof was originally published in 1949 by Claude Shannon[51]. It is paraphrased here for completeness, as Chapters 4 and 5 rely on the concept of channel capacity.

Since any band-limited signal can be uniquely represented by its samples at the Nyquist rate of $W/2$, it suffices to know just $2TW$ values to uniquely specify any signal that can be transmitted over a channel of bandwidth W in a period of time T. Thus, any band-limited signal of finite duration can be considered to be a single point, x, in a $2TW$- dimensional vector space. The encoding process maps the particular message we wish to communicate to a particular point in this vector space, hopefully in such a fashion that it can be correctly decoded on the receiving end. The question is what is the maximum number of possible messages, M, can be sent, error-free, over a given channel. The rate of information transfer in bits per second is then given by:

$$C = \frac{\log_2 M}{T} \tag{A.1}$$

There is an upper bound, P, on the average power in the signal to be transmitted,

$f(t)$:

$$\int_{-\infty}^{\infty} f(t)^2 dt = ||x||^2 < PT \tag{A.2}$$

During transmission through the channel, the signal is corrupted by additive zero-mean, white Gaussian noise of variance $\sigma^2 = N$. This means that while the transmitter sends a signal, x, the receiver must decode a signal $y = x + d$, where, d is the error introduced by the noise. The distribution of d is given by:

$$\begin{aligned} p(d) &= \prod_{n=1}^{2TW} \frac{1}{\sqrt{2\pi 2TWN}} \exp\left(-\frac{d_n^2}{2TWN}\right) && \text{(A.3)} \\ &= \frac{1}{(2\pi 2TWN)^{TW}} \exp\left(-\frac{1}{2TWN} \sum_{n=1}^{2TW} d_n^2\right) && \text{(A.4)} \\ &= \frac{1}{(2\pi 2TWN)^{TW}} \exp\left(-\frac{1}{2TWN} ||d||^2\right). && \text{(A.5)} \end{aligned}$$

Since this distribution only depends on the magnitude of d, not its orientation, it is a spherical disturbance to the original signal, x. Furthermore, as the dimensionality of the space, $2TW$, increases, the boundary of this distribution becomes increasingly sharp, with a radius of $\sqrt{2TWN}$. The received signal, y, has an average power of $P+N$, and therefore lies very close to the surface of a sphere of radius $\sqrt{2TW(P+N)}$. When the received signals are always distinct, that is with no overlap, then error-free communication is possible. We can easily place an upper bound on the number of possible messages that can be sent, by simply dividing the volume of a sphere of radius $\sqrt{2TW(P+N)}$ by the volume of sphere of radius $\sqrt{2TWN}$:

$$V = \frac{\pi^{n/2}}{(\frac{n}{2})!} r^n \tag{A.6}$$

$$V_y = \frac{\pi^{TW}}{(TW)!}(2TW(P+N))^{TW} \tag{A.7}$$

$$V_d = \frac{\pi^{TW}}{(TW)!}(2TWN)^{TW} \tag{A.8}$$

$$M < \frac{V_y}{V_d} = \frac{(2TW(P+N))^{TW}}{(2TWN)^{TW}} = \left(\frac{P+N}{N}\right)^{TW} \tag{A.9}$$

$$\tag{A.10}$$

This can be rearranged:

$$\log_2 M < TW \log_2 \left(\frac{P+N}{N}\right) \tag{A.11}$$

$$\frac{\log_2 M}{T} < W \log_2 \left(\frac{P+N}{N}\right) \tag{A.12}$$

$$C < W \log_2 \left(\frac{P+N}{N}\right) \tag{A.13}$$

It now remains to show that this bound is tight, that there exists a mapping between message and signal which actually achieves this rate of communication with an arbitrary small probability of error, ϵ. Somewhat surprisingly, when the set signals are chosen at random from the points within a sphere of radius $\sqrt{2TWP}$, the mapping is optimal. The design of the encoder consists of selecting M possible signals. If we consider the average probability of a communication error over all possible selections of M signals, we can show that this probability can be made arbitrarily low. Since it is the average probability, there will exist both mappings that perform better than the average as well as mappings that perform worse. Hence for any desired probability of error, ϵ, there exists a mapping which will result in a lower probability of error.

When the receiver sets about to decode a given signal, y, there is a small volume of possible signals, x, that could have resulted in y. The volume of the set of possible transmitted signals is conservatively enclosed by a sphere of radius $\sqrt{2TW\frac{PN}{P+N}}$. If, in the particular mapping used, there is only one possible signal that lies in that region, then a correct decoding will occur. We are therefore concerned with the probability that a second possible signal also lies in that volume. Since our mapping scheme was to choose possible signals at random, the probability that any given possible signal

lies in that volume is:

$$\left(\frac{\sqrt{2TW\frac{PN}{P+N}}}{\sqrt{2TWP}}\right)^{2TW} = \left(\frac{N}{P+N}\right)^{TW}. \tag{A.14}$$

Since we have M possible signals, the probability that no other signal lies within that volume is:

$$\left[1-\left(\frac{N}{P+N}\right)^{TW}\right]^{M-1}, \tag{A.15}$$

which we require to be greater than $1-\epsilon$.

Since M-1 is positive,

$$\left[1-\left(\frac{N}{P+N}\right)^{TW}\right]^{M-1} > 1-(M-1)\left(\frac{N}{P+N}\right)^{TW}. \tag{A.16}$$

This gives the requirement:

$$1-(M-1)\left(\frac{N}{P+N}\right)^{TW} > 1-\epsilon, \tag{A.17}$$

which can be rearranged as:

$$(M-1) < \epsilon\left(\frac{P+N}{N}\right)^{TW}, \tag{A.18}$$

or

$$\frac{\log_2(M-1)}{T} < W\log_2\frac{P+N}{N} + \frac{\log_2\epsilon}{T} \tag{A.19}$$

So for any arbitrary probability of error, ϵ, we can always choose a T large enough that this equation will be satisfied. This establishes that with a random selection of possible signals, we can obtain an arbitrarily low probability of error and transmit at a rate arbitrarily close to:

$$W\log_2\frac{P+N}{N}. \tag{A.20}$$

This completes the proof.

Appendix B

Derivation of Recursive Least-Squares Algorithm

Suppose we have a set of measurements that are well suited to a least-squares data fitting algorithm. Assume these measurements are becoming available in a real-time fashion and that we wish to re-solve the least-squares problem after each time step. Additionally, we want to impose an exponential weighting filter, characterized by a "forgetting factor" λ, so that older measurements are de-emphasized as compared to more recent ones. Thus at the i^{th} time step we wish to choose $x_i \in \mathbb{R}^n$ so as to minimize $||A_i x_i - b_i||_2$, where $A_i \in \mathbb{R}^{i \times n}$ and $b_i \in \mathbb{R}^i$ contain the all of the measurements since the first time step:

$$A_i = \begin{bmatrix} \lambda^{i-1} a_1^T \\ \lambda^{i-2} a_2^T \\ \vdots \\ a_i^T \end{bmatrix} \quad b_i = \begin{bmatrix} \lambda^{i-1} d_1 \\ \lambda^{i-2} d_2 \\ \vdots \\ d_i \end{bmatrix} \tag{B.1}$$

The traditional solution to the least-squares problem, $x_i = (A_i^T A_i)^{-1} A_i^T b_i$, is impractical for solving this real-time problem as its computational complexity and memory requirements will grow linearly with time. The recursive least-squares algorithm achieves the same mathematical result with constant computational complexity and

memory requirements. We will start our derivation of the recursive algorithm by defining the following symbols:

$$\begin{aligned} P_i &= (A_i^T A_i)^{-1} \\ \psi_i &= A_i^T b_i \end{aligned}$$

Note that $x_i = P_i \psi_i$. Now we write P_i in terms of P_{i-1}:

$$\begin{aligned} P_i &= (\lambda A_{i-1}^T A_{i-1} + a_i a_i^T)^{-1} \\ &= (\lambda P_{i-1}^{-1} + a_i a_i^T)^{-1} \end{aligned}$$

Using the matrix inversion lemma (see Section B.1) this can be written as:

$$\begin{aligned} P_i &= \frac{1}{\lambda} P_{i-1} - \frac{P_{i-1} a_i a_i^T P_{i-1}}{\lambda^2 + \lambda a_i^T P_{i-1} a_i} \\ &= \frac{1}{\lambda}(I - k_i a_i^T) P_{i-1} \end{aligned}$$

where we define k_i as follows:

$$k_i = \frac{P_{i-1} a_i}{\lambda + a_i^T P_{i-1} a_i} \tag{B.2}$$

This formula allows us to compute the value of P_i given only the value of P_{i-1} and the most recent set of measurements, a_i. Next we need to write ψ_i in terms of ψ_{i-1}:

$$\begin{aligned} \psi_i &= \lambda A_{i-1}^T b_{i-1} + a_i d_i \\ &= \lambda \psi_{i-1} + a_i d_i \end{aligned}$$

With this we can find an expression for x_i in terms of x_{i-1}:

$$\begin{aligned}
x_i &= P_i(\lambda\psi_{i-1} + a_i d_i) \\
&= \frac{1}{\lambda}(I - k_i a_i^T)P_{i-1}(\lambda\psi_{i-1} + a_i d_i) \\
&= (I - k_i a_i^T)P_{i-1}\psi_{i-1} + \frac{1}{\lambda}(I - k_i a_i^T)P_{i-1}a_i d_i \\
&= (I - k_i a_i^T)x_{i-1} + \frac{1}{\lambda}\left(I - \frac{P_{i-1}a_i a_i^T}{\lambda + a_i^T P_{i-1}a_i}\right)P_{i-1}a_i d_i \\
&= (I - k_i a_i^T)x_{i-1} + \frac{\lambda + a_i^T P_{i-1}a_i - P_{i-1}a_i a_i^T}{\lambda(\lambda + a_i^T P_{i-1}a_i)}P_{i-1}a_i d_i \\
&= (I - k_i a_i^T)x_{i-1} + \frac{\lambda P_{i-1}a_i + P_{i-1}a_i a_i^T P_{i-1}a_i - P_{i-1}a_i a_i^T P_{i-1}a_i}{\lambda(\lambda + a_i^T P_{i-1}a_i)}d_i \\
&= (I - k_i a_i^T)x_{i-1} + \frac{P_{i-1}a_i}{\lambda + a_i^T P_{i-1}a_i}d_i \\
&= (I - k_i a_i^T)x_{i-1} + k_i d_i \\
&= x_{i-1} + k_i(d_i - a_i^T x_{i-1})
\end{aligned}$$

Thus at the i^{th} time step we only need the values of P_{i-1} and x_{i-1}, and the new measurements, a_i and d_i, in order to compute the new least-squares solution, x_i. To summarize, at each time step, we compute the following:

$$\boxed{\begin{aligned}
k_i &= \frac{P_{i-1}a_i}{\lambda + a_i^T P_{i-1}a_i} \\
P_i &= \frac{1}{\lambda}(I - k_i a_i^T)P_{i-1} \\
x_i &= x_{i-1} + k_i(d_i - a_i^T x_{i-1})
\end{aligned}}$$

The algorithm also needs initial values for P_0 and x_0. The mathematically rigorous approach is to collect data until $\mathbf{rank}(A_i) = n$, then let $P_i = (A_i^T A_i)^{-1}$ and $x_i = P_i A_i^T b_i$, and start using the recursive algorithm. From a numerical perspective, simply testing the rank of A_i is impractical, so an alternative is to continue collecting data until the condition number of A_i is suitably small, then initialize the recursive algorithm as above. These approaches will yield a result which is mathematically

equivalent to solving the least-squares problem using the traditional formula, but will not produce any output until enough data has been collected to satisfy the rank or condition number criteria.

The forgetting factor λ makes older measurements less important than recent measurements, and similarly older values of P and x are less important than recent ones. This means for many applications an exact initialization of P and x is unnecessary. In the case when there is some estimate of what the elements of x should be, this can be used to set x_0. When no prior information about x is available, x_0 is typically set to zero. For P_0, any positive definite initial value will work. In general, the larger the singular values of P_0, the faster x will converge, but at the cost of greater initial sensitivity to measurement noise. These approximate intialization techniques are easier to implement and will converge to the same results as the exact initialization techniques, but will give different initial results.

B.1 Matrix Inversion Lemma

Given an invertible matrix A and any compatibly-sized matrices B and C,

$$(A + BC)^{-1} = A^{-1} - A^{-1}B(I + CA^{-1}B)^{-1}CA^{-1}. \tag{B.3}$$

Proof Start with $A^{-1} - A^{-1}B(I + CA^{-1}B)^{-1}CA^{-1}$ and left multiply $A + BC$:

$$\begin{aligned}
&[A^{-1} - A^{-1}B(I + CA^{-1}B)^{-1}CA^{-1}](A + BC) \\
&A^{-1}A + A^{-1}BC - A^{-1}B(I + CA^{-1}B)^{-1}(CA^{-1}A + CA^{-1}BC) \\
&I + A^{-1}BC - A^{-1}B(I + CA^{-1}B)^{-1}(I + CA^{-1}B)C \\
&I + A^{-1}BC - A^{-1}BC \\
&I
\end{aligned} \tag{B.4}$$

Next take $A^{-1} - A^{-1}B(I + CA^{-1}B)^{-1}CA^{-1}$ and right multiply $A + BC$:

$$\begin{aligned}
&(A + BC)[A^{-1} - A^{-1}B(I + CA^{-1}B)^{-1}CA^{-1}] \\
&AA^{-1} + BCA^{-1} - (AA^{-1}B + BCA^{-1}B)(I + CA^{-1}B)^{-1}CA^{-1} \\
&I + BCA^{-1} - B(I + CA^{-1}B)(I + CA^{-1}B)^{-1}CA^{-1} \\
&I + BCA^{-1} - BCA^{-1} \\
&I
\end{aligned} \tag{B.5}$$

which concludes the proof of this lemma.

Bibliography

[1] ZF-Aktivlenkung für pkw der mittel- und oberklasse. URL http://www.zf-lenksysteme.com/upload/edit_2/2305_34276/Aktivlenkung_D.pdf.

[2] A. Alessandri. Fault diagnosis for nonlinear systems using a bank of neural estimators. *Comput. Ind.*, 52(3):271–289, 2003. ISSN 0166-3615. doi: http://dx.doi.org/10.1016/S0166-3615(03)00131-3.

[3] P. Amann, J. M. Perronne, G. L. Gissinger, and P. M. Frank. Identification of fuzzy relational models for fault detection. *Control Engineering Practice*, 9(5): 555–562, 2001.

[4] J. Andreasson, C. Knobel, and T. Bünte. On road vehicle motion control - striving towards synergy. In *Proceedings of 8th International Symposium on Advanced Vehicle Control*, 2006.

[5] R. V. Beard. *Failure accommodation in Linear Systems through Self-reorganization*. PhD thesis, MIT, 1971.

[6] Carrie G. Bobier, Shad M. Laws, and J. Christian Gerdes. Transient responses of alternative vehicle configurations: A theoretical and experimental study on the effects of atypical moments of inertia. In *Proceedings of 2008 American Control Conference*, June 2008.

[7] Stephen Boyd and Lieven Vandenberghe. *Convex Optimization*. Cambridge University Press, 2004.

[8] E.A. Bretz. By-wire cars turn the corner. *Spectrum, IEEE*, 38(4):68–73, Apr 2001. ISSN 0018-9235. doi: 10.1109/6.915192.

[9] Christopher R. Carlson and J. Christian Gerdes. Optimal rollover prevention with steer bywire and differential braking. In *Proceedings of IMECE 2003 ASME Int. Mechanical Engineering Congress and Exposition*, 2003.

[10] Jie Chen and Ron J. Patton. *Robust Model-Based Fault Diagnosis for Dynamic Systems*. Kluwer Academic Publisher, 1999.

[11] Edward Y. Chow and Alan S. Willsky. Analytical redundancy and the design of robust failure detection systems. *IEEE Transactions on Automatic Control*, AC-29(7):603–614, July 1984.

[12] D. C. Fosth Clark, R. N., and V. M. Walton. Detection instrument malfunctions in control systems. *IEEE Transactions on Aerospace Electronic Systems*, pages 465–473, 1975.

[13] S. X. Ding, T. Jeinsch, P. M. Frank, and E. L. Ding. A unified approach to the optimization of fault detection systems. *International Journal of Adaptive Control and Signal Processing*, 14(7):725–745, 2000.

[14] X. Ding and L. Guo. Observer based optimal fault detector. In *Proceedings of the 13th IFAC World Congress*, pages 187–192, 1996.

[15] A. Emami-Naeini, M.M. Akhter, and S.M. Rock. Effect of model uncertainty on failure detection: the threshold selector. *Automatic Control, IEEE Transactions on*, 33(12):1106–1115, Dec 1988. ISSN 0018-9286. doi: 10.1109/9.14432.

[16] Abbas Emami-Naeini and Stephen M. Rock. Robust detection, isolation, and accommodation for sensor failures. Technical Report NASA CR-174825, NASA, 1986.

[17] Charles M. Farmer. Effects of electronic stability control: an update. *Traffic Injury Prevention*, 7(4):319–324, December 2006.

[18] Paul M. Frank. Fault diagnosis in dynamic systems using analytical and knowledge-based redundancy—a survey and some new results. 26(4):459–474, 1990.

[19] Thomas Fuehrer and Anton Schedl. The steer-by-wire prototype implementation: Realizing time triggered system design, fail silence behavior and active replication with fault-tolerance support. *SAE World Congress*, 1999. 1999-01-0400.

[20] Christopher D. Gadda, Paul Yih, and J. Christian Gerdes. Incorporating a model of vehicle dynamics in a diagnostic system for steer-by-wire vehicles. In *Proceedings of AVEC*, pages 779–784, 2004.

[21] Christopher D. Gadda, Shad M. Laws, and J. Christian Gerdes. Eliminating the need for sensor redundancy in diagnostic systems for steer-by-wire vehicles. In *Proceedings of AVEC*, 2006.

[22] Christopher D. Gadda, Shad M. Laws, and J. Christian Gerdes. Generating diagnostic residuals for steer-by-wire vehicles. *IEEE Transactions on Control Systems Technology*, 15(3):529–540, May 2007.

[23] Christopher D. Gadda, Shad M. Laws, and J. Christian Gerdes. Robust fault detection filter design with applications to steer-by-wire vehicles. In *Proceedings of IMECE 2007*, 2007.

[24] R. C. Hammett and P. S. Babcock. Achieving 10^{-9} dependability with drive-by-wire systems. *SAE World Congress*, 2003.

[25] D. W. Harless and G. E. Hoffer. The antilock braking system anomaly: a drinking driver problem? *Accident Analysis and Prevention*, 34(3):333–341, May 2002.

[26] Werner Harter, Wolfgang Pfeiffer, Peter Dominke, Gerhard Ruck, and Peter Blessing. Future electrical steering systems: Realizations with safety requirements. *SAE World Congress*, 2000. 2000-01-0822.

[27] R.A. Hess and A. Modjtahedzadeh. A control theoretic model of driver steering behavior. *Control Systems Magazine, IEEE*, 10(5):3–8, Aug 1990. ISSN 0272-1708. doi: 10.1109/37.60415.

[28] T. Hofling and Rolf Isermann. Fault detection based on adaptive parity equations and single-parameter tracking. *Control Engineering Practice*, 4(10):1361–1369, Oct 1996.

[29] Kunsoo Huh, Chanwon Seo, Joonyoung Kim, and Daegun Hong. Active steering control based on the estimated tire forces. *Proceedings of the 1999 American Control Conference*, 1:729–733, 1999. doi: 10.1109/ACC.1999.782923.

[30] Rolf Isermann. Diagnosis methods for electronic controlled vehicles. *5th International Symposium on Advanced Vehicle Control*, 2000.

[31] Rolf Isermann. *Fault-Diagnosis Systems*. Springer, 2006.

[32] Rolf Isermann. Process fault detection based on modeling and estimation methods—a survey. *Automatica*, 20(4):387–404, Jul 1984.

[33] Rolf Isermann. Fault diagnosis of machines via parameter estimation and knowledge processing–tutorial paper. *Automatica*, 29(4):815–835, 1993.

[34] Rolf Isermann and P. Ballé. Trends in the application of model based fault detection and diagnosis of technical processes. *In Proc. of IFAC 13th Triennial World Conference*, 1996.

[35] H. L. Jones. *Failure detection in linear systems*. PhD thesis, MIT, 1973.

[36] Nagarajan Kandasamy, John P. Hayes, and Brian T. Murray. Time-constrained failure diagnosis in distributed embedded systems: Application to actuator diagnosis. *IEEE Transactions on Parallel and Distributed Systems*, 16(3):258–270, Mar 2005.

[37] Ji-Hoon Kim and Jae-Bok Song. Control logic for an electric power steering. *Mechatronics*, 12(3):447–459, April 2002.

[38] U. Kramer and G. Rohr. A model of driver behavior. *Ergonomics*, 25(10): 891–907, 1982.

[39] Shad M. Laws, Christopher D. Gadda, Scott Kohn, Paul Yih, J. Christian Gerdes, and J. Craig Milroy. Steer-by-wire suspension and steering design for controllability and observability. In *Proceedings of IFAC World Congress*, 2005.

[40] A. Modjtahedzadeh and R. A. Hess. A model of driver steering control behavior for use in assessing vehicle handling qualities. *Journal of Dynamic Systems, Measurement, and Control*, 115(3):456–464, 1993.

[41] Olaf Moseler and Rolf Isermann. Application of model-based fault detection to a brushless dc motor. *IEEE Transactions on Industrial Electronics*, 47(5): 1015–1020, Oct 2000.

[42] Simon Oblak, Igor Škrjanc, and Sašo Blaič. Brief paper: Fault detection for nonlinear systems with uncertain parameters based on the interval fuzzy model. *Eng. Appl. Artif. Intell.*, 20(4):503–510, 2007. ISSN 0952-1976. doi: http://dx.doi.org/10.1016/j.engappai.2006.08.002.

[43] T. G. Park, J. S. Ryu, and K. S. Lee. Actuator fault estimation with disturbance decoupling. *IEEE Proceedings-Control Theory and Applications*, 147(5):501–508, Sept 2000.

[44] R.J. Patton, J. Chen, and T.M. Siew. Fault diagnosis in nonlinear dynamic systems via neural networks. *Control, 1994. Control '94. Volume 2., International Conference on*, pages 1346–1351 vol.2, March 1994.

[45] Ron J. Patton, Paul M. Frank, and Robert N. Clark, editors. *Issues of Fault Diagnosis for Dynamic Systems*. Springer, 2000.

[46] Pierluigi Pisu, Andrea Serrani, Song You, and Laci Jalics. Adaptive threshold based diagnostics for steer-by-wire systems. *Journal of Dynamic Systems, Measurement, and Control*, 128(2):428–435, June 2006.

[47] Mike Lind Rank and Henrik Niemann. Norm based design of fault detectors. *International Journal of Control*, 72(9):773–783, 1999.

[48] Matthew L. Schwall. *Dynamic Integration of Probabilistic Information for Diagnostics and Decisions*. PhD thesis, Stanford University, September 2005.

[49] Matthew L. Schwall and J. Christian Gerdes. Multi-modal diagnostics for vehicle fault detection. In *Proceedings of IMECE 2001*, 2001. DSC-24600.

[50] Matthew L. Schwall and J. Christian Gerdes. A probabilistic approach to residual processing for vehicle fault detection. In *Proceedings of ACC 2002*, pages 2552–2557, 2002.

[51] Claude Elwood Shannon. Communication in the presence of noise. *Proceedings of the IRE*, 37(1):10–21, January 1949.

[52] Joshua P. Switkes. *Handwheel force feedback with lanekeeping assistance: combined dynamics, stability and bounding*. PhD thesis, Stanford University, 2007.

[53] M.L. Tyler and M. Morari. Optimal and robust design of integrated control and diagnostic modules. In *Proceedings of the American Control Conference*, volume 2, pages 2060–2064, June-1 July 1994. doi: 10.1109/ACC.1994.752439.

[54] Miguel A. Vilaplana, Douglas J. Leith, and William E. Leithead. Control of sideslip and yaw rate in cars equipped with 4-wheel steer-by-wire. *SAE World Congress*, 2004. 2004-01-2076.

[55] Jian Liang Wang, Guang-Hong Yang, and Jian Liu. An LMI approach to $\mathcal{H}_-$ index and mixed $\mathcal{H}_-/\mathcal{H}_\infty$ fault detection observer design. *Automatica*, 43:1656–1665, 2007.

[56] Alan S. Willsky. A survey of design methods for failure detection in dynamic systems. *Automatica*, 12:601–611, 1976.

[57] P. Yih and J.C. Gerdes. Steer-by-wire for vehicle state estimation and control. *Proceedings of AVEC*, pages 785–790, 2004.

[58] P. Yih, J. Ryu, and J.C. Gerdes. Modification of vehicle handling characteristics via steer-by-wire. *Proceedings of the American Control Conference*, 2003.

[59] Paul Yih. *Steer-by-Wire: Implications for Vehicle Handling and Safety*. PhD thesis, Stanford University, 2005.

[60] M. Yoshimura, P. M. Frank, and X. Ding. Survey of robust residual generation and evaluation methods in observer-based fault detection systems. *Journal of Process Control*, 7(6):403–424, December 1997.

[61] Xiaodong Zhang, M.M. Polycarpou, and T. Parisini. A robust detection and isolation scheme for abrupt and incipient faults in nonlinear systems. *Automatic Control, IEEE Transactions on*, 47(4):576–593, Apr 2002. ISSN 0018-9286. doi: 10.1109/9.995036.

[62] Maiying Zhong, Steven X. Ding, James Lam, and Haibo Wang. An LMI approach to design robust fault detection filter for uncertain LTI systems. *Automatica*, 39: 543–550, 2003.